LOCALIZATION OF MOBILE ROBOTS FOR PRECISION MANUFACTURING

A TECHNICAL REPORT SUBMITTED TO AUCKLAND UNIVERSITY OF TECHNOLOGY
IN PARTIAL FULFILMENT OF THE REQUIREMENTS FOR THE DEGREE OF
DOCTOR OF PHILOSOPHY

Antonius Franciscus Maria Paijens

30 July 2021

School of Engineering, Computer and Mathematical Sciences
Auckland University of Technology

Abstract

"To manufacture a bigger part, you need a larger machine!"

This paradigm is going to be broken through the development of mobile robots that can move around a part and apply a manufacturing operation to it, instead of having to envelop it. Monument size machines will be replaced by a mobile appliance that can do great things. In almost any perspective, mobile appliances outperform big stationary machines sitting in a workshop. The size of the parts that can be produced with a mobile appliance is not constrained by the machine size. It is more flexible in its deployment. A mobile appliance does not take up workshop space permanently but can be used "on site" where the materials are and the part manufactured is needed. It can be taken to a workshop for maintenance and repair. As a consequence the cost of ownership of a mobile appliance is lower than the cost of ownership of a stationary machine. It will make processing of large parts accessible to a wider audience of makers and contribute to the democratization of manufacturing.

To enable a mobile robot to perform precision manufacturing operations, it has to be able to position itself accurately, within tolerances that match the allowable dimensional tolerances of the part to be manufactured by a certain margin. And in order to position itself accurately it has to measure its own location and orientation even more accurately. This challenge is made tangible by focusing on laser cutting as the manufacturing operation in the present research. Within the scope of laser cutting operations a benchmark is defined based on criteria for adoption of a mobile platform for precision manufacturing, derived from manufacturing practices in industries that apply laser cutting in their production. The benchmark states that the allowable manufacturing tolerance of a part to be cut is 0.1% of its maximum dimension. The mobile platform carrying the laser cutter will have to localize itself with a better accuracy by some margin to be able to cut a part within this tolerance. This benchmark defines a measurable target for allowable manufacturing tolerances of parts produced with laser cutting, against which the accuracy of the localization of a mobile robot for precision manufacturing can be evaluated.

The present research project aims to develop a system that can localize a mobile platform within the limits set by the benchmark. Optical flow sensors are selected for incremental odometry of the mobile platform and a laser lighthouse system to measure its absolute location and orientation. Optical flow sensors used to measure the movement of computer mice are very accurate in measuring displacement, but accumulate measurement errors in the course of time. An important source of systematic errors when applying multiple optical flow sensors is the absence of synchronization of the data acquisition by the sensors.

The measurement of a location and orientation in an absolute reference system with a laser lighthouse compensates for the accumulation of random errors generated by the optical flow sensors. The laser lighthouse is a single landmark beacon, emitting rotating light sheets generated with a laser, similar to a lighthouse. A mobile platform to be localized carries light sensors in known locations, that record timestamps when the light sheet from the lighthouse passes over a sensor. The timestamps from at least three sensors on the mobile platform allow for calculation of a planar location and orientation of the platform relative to the lighthouse when it sweeps a light sheet in one orientation. With light sheets swept in two orientations by the lighthouse, a spatial location and orientation can be established for a mobile platform with at least three light sensors.

In the computations for the incremental odometry, the sensitivity of the optical flow sensors and their position and orientation on the mobile platform are cardinal parameters. For the determination of an absolute location and orientation with a laser lighthouse, the location of the light sensors on the mobile platform is the key parameter. Inaccuracies in these parameters will generate a systematic error in the calculated position and orientation of the mobile platform and prevent it from meeting the criteria for adoption of the platform for precision manufacturing.

The present research focuses on experimental methods to establish accurate values for the sensitivity and the location and orientation of the optical flow sensors as well as the location of the light sensors on the mobile platform. Direct measurement of these parameters is difficult and produces uncertain results as for instance the location of the "focal point" of a light sensors with a surface area of several square millimeters can only be established by measurement with the sensor itself. This is exactly what the designed experiments intend to do: measure the magnitude of the cardinal parameters for the localization of the mobile platform with the sensors itself to eliminate systematic errors.

The experiments designed force the mobile platform to travel a constrained motion around a fixed ”anchor point”. The constrain imposed establishes a relationship between the movement the platform and the path traveled by the sensors that allows determination of the location and orientation of the sensors from their recordings while traveling the path in an experiment. Comparison of a reconstruction of the path using the sensor recordings and their measured position in the frame with the constrained motion confirms the efficacy of this approach:

- The computed location of the mobile platform deviated 0.16% of the total distance traveled by the platform (6.7 meter). This is a significant improvement over the next best result of an accuracy of 0.28% published in the open literature.
- After measuring the sensor locations on the experimental mobile platform with the experiments designed, the relative error of the location of the mobile platform established with one lighthouse base station, dropped from over 0.3% to below 0.2% (meter error per meter distance) for a slow moving platform.

The experiments demonstrate that when the mobile platform is stationary, the precision of localization of a mobile platform with the HTC-Vive laser lighthouse base station is an order of magnitude better than the benchmark of 0.1%. When the platform is moving however, the accuracy of the laser lighthouse method is insufficient to locate the mobile platform within the required tolerances set by the benchmark.

At the same time the present research has identified many leads for further reduction of systematic errors in the localization of a mobile platform to make precision manufacturing a feasible option.

As the result of the exploration performed to write this thesis, the following original research contribution were made:

- Analysis of the propagation of the error in the sensor sensitivity of optical flow sensors into the location of a mobile platform derived from the sensor data.
- Design of a data acquisition system that executes the data collection with the optical flow sensors in a schedule of strict coincidence.
- Design of a simple experiment to measure sensitivities of optical flow sensors.
- Design of an experiment to measure and validate location and orientation of the optical flow sensors on the mobile platform using readings from the sensors itself.
- Analysis of the propagation of errors in the location of the light sensors into the location of a mobile platform derived from the sensor data.
- Design of an experiment to measure and validate the location of light sensors on the mobile platform through the application of camera calibration techniques, using readings from the sensors itself.

Contents

List of Tables

List of Figures

Attestation of Authorship

I hereby declare that this submission is my own work and that, to the best of my knowledge and belief, it contains no material previously published or written by another person nor material which to a substantial extent has been accepted for the qualification of any other degree or diploma of a university or other institution of higher learning.

Signature of candidate

Acknowledgements

In the first place I want to thank my wife Karen for her patience with me and my PhD, her sustained support and enthusiasm as much as her (gentle) push to get on with it.
I also want to express my gratitude to the following persons at Auckland University of Technology that have provided essential support to this project:

- **Loulin Huang**
  my primary supervisor, for his knowledgeable guidance and relentless encouragement on the long journey of my PhD research.
- **Ahmed Al-Jumaily**
  my second supervisor for his support and lifting the mood when the long journey seemed to be going nowhere.
- **John Collins**
  for his hands on help in setting up the experiments with the lighthouse system and the subsequent processing of the data. John's support gave me the confidence that I had reached the point where we were actually producing science in this project. (And John allowed me to maintain the washer in place, glued in the center of the round table in his room, for a very long time. The washer was instrumental in all experiments as shown in Figures 3.3 and 4.7).
- **Jian Huang**
  for his support in building and preparing the setup used in this research project. And for teaching me that I can do most thing myself!
- **Akhil Anand**
  for coding the I^2C interface between the optical flow sensor boards and the Raspberry Pi. It has served me flawlessly!

Chapter 1

Introduction

1.1 From CAD/CAM to Digital Desktop Manufacturing

The manufacturing industry is experiencing a silent revolution in the upcoming of Digital Desktop Manufacturing Technology (DDMT) [1]. DDMT comprises highly integrated, compact (desktop size) machines that are computer controlled in order to manufacture parts and products with minimal human intervention. 3D printers, laser cutters and micro milling (CNC) machines are examples of this technology that is moving Computer Aided Manufacturing (CAM) from the workshop to the desktop. DDMT will change manufacturing in a comparable way the laser printer changed the printing business, but more profound, as manufacturing is everywhere. CAD/CAM has been around for more than five decades now, but only CAD (Computer Aided Design) has matured to a level that it has become accessible for a broader audience than industrial specialists. CAD tools, even the ones that are freely available on the Internet, allow for the creation of highly sophisticated designs with relatively little training. CAD has become a versatile tool that allows the designer to concentrate on the implementation of his imagination in a design. The skills in designing with CAD have shifted from maintaining and managing the tool to using it as a display for our imagination. Consequently, creativity has overtaken operator skills in the design process. CAM has been lagging in this development but is catching up at high pace, thanks to Digital Desktop Manufacturing Technology. Especially the 3D printer is a valuable contribution to CAM technology as it allows for direct manufacturing of CAD

designs with minimal human intervention. This development is going to have deep impact on the manufacturing industry. It will change from a capital intensive industry for mass production to an industry for small to medium size companies and even individuals that are enabled to manufacture custom made parts and products at a modest investment [2]. Management and maintenance of the machine park no longer require a professional engineering staff but can be managed by the user. Products are desktop manufactured on a piece by piece basis, allowing for flexible production runs of products with different designs without retooling. This flexibility strengthens a manufacturers position in a market demanding for more individualized and bespoke products; "Personalized products" as Yoram Koren calls them [3]. Products will distinguish themselves more through their design than their plain functionality. Creativity is going to be of equal importance as functional engineering in the design of products. Desktop manufacturing enables people with good, creative ideas for products to produce them on the spot [4]. As industry analysts already stated: desktop manufacturing is the next technological revolution, which will democratize the manufacturing industry [1]. It brings back manufacturing from parties with money to people with imagination and ideas.

1.2 Development of Digital Desktop Manufacturing Technology (DDMT)

Although the development of DDMT has yielded machines of impressive quality, usability, and versatility, there are still limitations to be overcome in the manufacturing of parts with this technology. A serious limitation of digital desktop manufacturing machines is the small size in which parts can be produced. Parts must be manufactured within the operating space of the machine which is limited to the volume spanned by the combined operating range of the gantries and rotating arms to perform machining operations within the machine. For a desktop size machine, this space is typically small. There is a clear demand for manufacturing of larger parts and not only in the heavy industries. Interior architects, window dressers, carpenters, furniture and boat builders, sail makers, the fashion industry, sculptors and creative artists all work with parts in sizes that exceed the working volume of a desktop machine. The requirement to apply

a large machine to produce large parts deprives professionals and semi-professionals in these fields of many benefits of desktop manufacturing equipment: compared to compact machines, large machines are over-proportionally more expensive, harder to maintain and operate, require a larger workshop and are never big enough as there is always a larger part to process. The solution is development of compact (desktop size) machines with the ability to move around while carrying and applying their tools: a mobile platform for manufacturing operations. These machines push the limit of desktop manufacturing of parts to infinite size, dramatically increasing the versatility of desktop manufacturing technology. Cutting of sheet material, 3D printing of large (concrete) structures, applying surface treatments (cleaning, coating, marking, painting) of large objects all benefit from the versatility of a mobile platform to do the job. Moreover, a mobile platform has the potential of a more flexible deployment, on site where the parts are to be processed, instead of in a distant workshop for instance. Whereas these advantages have been recognized by many in the manufacturing industries and acknowledged in the conclusions of a literature review commissioned by the American National Institute of Standards and Technology (NIST) in 2015, the technology to support manufacturing operations by mobile platforms is still lacking in accuracy, precision and flexibility [5]. The NIST review by Shneier and Bostelman demonstrates that although solutions for localization of mobile platforms exist, these are either too inaccurate or cumbersome to operate with manufacturing tools. The present research intends to contribute to the development of a localization system to enable mobile platforms to complement the digital desktop manufacturing tool set. As the markets for Desktop Manufacturing Devices have only just started to take off and are expected to grow at double digit rate for decades to come, there are good opportunities to apply the results of this research in marketable products, contributing to New Zealand's high tech industry sector and economy.

1.3 A paradigm shift: moving away from large stationary machines to intelligent mobile machines.

Conventional and contemporary machines for manufacturing are stationary contraptions that envelope the operating space where the parts are being produced. From a (mechanical) engineering

perspective there are good reasons to constrain a manufacturing operation to a stationary volume within the operating space of gantries, spindles and rotating arms that carry the toolhead. The position of the toolhead translates directly into dimensions of the part processed. The motion of gantries, spindles and rotating arms allow for accurate positioning of a toolhead without actual measurement of its position. As a consequence of the shape closed design of the parts that control the motions, such as gears and belt transmissions and ball and lead screws, the position of the toolhead is kinematically fully determined by the position of the constituent parts of the mechanism. Positions of gantries, spindles and/or rotating arms can be measured relatively easy by position encoders. State of the art x-y gantries can be positioned with a resolution as low as 10 micron. What this means for the positioning accuracy of the toolhead is unclear however as manufacturers of CNC hardware shy away from giving hard figures on the positioning accuracy of the toolhead. This is somewhat understandable as the actual manufacturing tolerance of parts made in a CNC machine are dominated by backlash and flexure and wagging of the beams in the machine, more than the resolution of the controlling servo and stepper motors. Basic mechanical considerations make evident that positioning the toolhead on a gantry within certain tolerances, becomes increasingly harder and costly with increasing sizes of the machine. These "mechanical" tolerances as a consequence of slack space and beam flexure and wagging can be reduced through proper design and construction of the manufacturing machines. There is a limit to what can be achieved within given cost constraints, however. Deflections of beams under load are proportional to the length of the beam to the power of three for example [6], making control of the tolerances in a manufacturing machine increasingly more challenging with increasing size of the machines. Since this is a kind of recursive curse (a recurse ?), as making the parts for a bigger machine already requires a machine of bigger size, it can be expected that both magnitude of the manufacturing tolerances realized in large machines and the costs to control them escalates exponentially with size.

This "mechanical" scale factor does not apply to an intelligent mobile platform as it can not rely on form closed mechanisms to (pre-)determine its position but has to measure and adjust it by feedback motion control. The dimensional accuracy of parts processed by tools on mobile platforms depend directly on the measurement and control of its position. This

represent a paradigm shift from controlling manufacturing tolerances of parts by design and construction of the manufacturing machine, to intelligent control of the manufacturing machine by means of algorithms. The advantages are prevalent as a mobile platform does not suffer from exponentially growing scale effects on processing accuracy in the way stationary machines do. The mobile platform does not have to be bigger and more expensive for it to process larger parts. As its design and construction are independent of the size of the part to be processed, any effect of the scale of the part to be manufactured on the manufacturing tolerances is due to scale effect in the error of the position measurement of the mobile platform. Since these measurements are based on (tri-)angulation, the error in positioning is expected to scale proportionally with the linear dimensions of the part. Hence the manufacturing accuracy of increasingly larger parts could very well benefit from the deployment of mobile platforms over stationary manufacturing machines where the positioning error of the toolhead scales with the part size to the power of three!

Of course a machine using a form closed mechanism to control the positioning of its toolhead can be equipped with toolhead positioning feedback control comprising a localization system to enjoy the benefits of improved accuracy for the cutting process. It beats the purpose however as the greater flexibility and versatility of a mobile platform with a feedback controlled positioning system remains untapped as long as the machine is still stationary, while pushing its price upward with the new features.

Nonetheless, positioning a mobile platform with resolution of 10 micron is not in the (commercial) picture yet according to Schneier and Bostelman as the best performing robot in their review has a positioning accuracy of 5 mm. They conclude that the development of mobile robots for manufacturing needs more focused research on the development of an accurate localization system [5]. This is exactly what the present research intends to contribute to.

1.4 Thesis overview

1.4.1 Scope, aims and objectives

In perspective of the development of DDMT outlined in the previous section, the aim of this thesis is to develop a localization method for a mobile platform that enables automatic/autonomous/robotic manufacturing of parts that exceed the size of a desktop machine. This scope of work still envelopes a vast field of manufacturing applications that each has specific requirements. To formulate relevant criteria for adoption of a localization system, laser cutting and engraving of sheet material is chosen as the application of focus. Laser cutting and engraving has characteristics that facilitate application of a mobile platform: it is essentially a 2D operation that does not generate reaction forces. Laser cutting and engraving has gained popularity and market share fast in many industry sectors, replacing more traditional operations like mechanical (knife) cutting and machining. Laser cutting is applied to process fabrics, plastics, composites and other synthetic materials in sheets and to cut and engrave wood panels, plywood/wood composites, medium density fiber (MDF) boards and sheet metal for a wide range of applications. It is a mature operation that is currently overtaken by newer cutting methods like plasma and water-jet cutting for certain materials and applications. In its present implementation a laser cutter is a stationary machine with a flat horizontal cutting bed (flatbed) to support the sheets being cut. The flatbed has to be of a size that it can support the complete sheet of material to be processed. The bed is spanned widthwise by a gantry. The gantry moves on rails mounted lengthwise on each side of the flatbed. The toolhead is suspended on a bracket mounted on rails over the gantry. The bracket on the gantry is height adjustable to enable focusing of the laser beam on the sheet material under it. This setup enables the laser cutting toolhead to traverse the full planar space over flatbed. The laser ray is generated in the stationary base of the laser cutter under or adjacent to the flatbed and beamed into the toolhead with mirrors. As a consequence the laser cutting toolhead is very lightweight comprising merely a mirror and lens. The absence of reaction forces on the toolhead, allows the gantry beams of a laser cutter/engraver to be relatively skinny. The mechanical power requirements to drive the system are modest as a consequence. Nevertheless a state of the art laser cutter relying on a gantry to traverse the toolhead is a big

machine for stationary setup in a workshop. Transformation of this functionality into a setup comprising a mobile appliance and a foldable bed structure to support the sheet material, that can be transported for use on-site will be groundbreaking.

Within this scope, the present research aims to develop a localization method for a mobile platform for laser cutting and engraving. The objectives for the research are derived from the ”criteria for adoption” for a mobile platform to operate as a laser cutting and engraving machine. The performance of actual flatbed laser cutters presents a point of reference here, although application of the mobile platform is not intended to completely overlap with the application of a flatbed machine. Competition between mobile and fixed machines is to be expected in similar applications and in the same application markets as a consequence. This means that the ”criteria for adoption” have to include the attributes of fixed bed machines that have made it popular with manufacturers and makers. The attributes overlapping between a mobile platform and a fixed bed machine apply to the quality of the products produces. The paramount quality measure of laser cut products are the ”manufacturing tolerances” of the product which are obviously governed by the accuracy and precision of the positioning of the toolhead of the laser cutter. Hence the easiest way to define design objectives for the development of the localization method would be to use the performance specifications of flatbed laser cutters for toolhead positioning as targets for the mobile platform. This approach is dismissed however for the following reasons:

- The field of application of flatbed laser cutters is very diverse in terms of materials and sizes of parts that can be processed. Deriving performance specifications requires further narrowing down of the application field for which no selection criteria are developed at this stage.
- Vendors of flatbed laser cutters do not provide hard figures for absolute manufacturing tolerances that can be realized with their machines.
- The experience using a flatbed laser cutter to cut parts for a mobile platform to experiment with was unsatisfactory as is explained below.

Instead, criteria for adoption are derived from design and manufacturing practices in a number of industries. The practices specify limits for tolerances of the dimensions of parts made from

sheet material. These limits enable formulation of performance targets for the accuracy and precision of the manufacturing process. The limits on tolerances defined by the manufacturing practices are not futile. In the course of the present research it appeared that the industrial grade flatbed laser cutter used to produce parts for the experimental setup, did not comply. The localization results acquired in experiments with the setup exposed consistent systematic deviations of unexpected magnitude. Hand measurement of the dimensions of parts of the setup manufactured on the laser cutter revealed that they were essentially off-spec. This presented a problem as the locations of certain features in the mobile platform could not be assumed to be in the (CAD) locations they were designed to be. Since especially the location of the sensors on the platform is critical for its localization this introduced an unforeseen new requirement: measurement of the location of the sensors in the mobile platform coordinate system. This was a decisive revelation for the course of the research as it forged the awareness that measurement of the location of optical sensors is required for any mobile platform equipped with multiple sensors for the purpose of localization, even when the platform is produced using CAD-CAM. The location of the sensors in the mobile platform coordinate frame is a pivotal parameter in the localization of the platform and has to be established by measurement. Calculation of the mobile platform location leverages on the sensor locations in the platform coordinate frame. As a consequence there is amplification of errors in the dimensional coordinates of the sensor location into the dimensional coordinates of the location of the mobile platform, equal to the ratio of these absolute dimensions. Moreover, this error is amplified further by the mathematical and numerical methods used to compute the platform location. As a consequence measurement of sensor locations and the propagation of errors in the locations of sensors moved into focal position of the research towards a localization method with the objective to design a method that enables a mobile platform for laser cutting and engraving to comply with the manufacturing practices of the targeted industries.

1.4.2 Structure of the thesis

- Chapter 2 reports on the results of a literature review of criteria for adoption of a mobile platform for laser cutting in a number of industries. A quantitative benchmark is derived

from the criteria for adoption that provides a handle to estimate the feasibility of the development of a localization method. A conceptual design for a mobile platform is presented to understand how it can meet the criteria for adoption. For localization, the platform relies on incremental odometry and absolute location measurement. Based on previous experiences reported in the open literature a choice is made for optical technologies for incremental odometry and absolute location measurement to implement the localization method. The available information on the performance of the optical technologies is reviewed and used to compile a list of topics to research.

- Chapter 3 elaborates the list of research topics for the incremental odometry using optical flow sensors. The topics are propagation of errors in the sensitivity of the sensors and design of an experiment to measure and validate the location and orientation of optical flow sensors in the coordinate system of the mobile platform

- Chapter 4 works out the list of research topics for the absolute location measurement using a laser lighthouse. After an introduction into the computation of a location using a laser lighthouse, an analysis is made of the propagation of errors in the location of light sensors on the mobile platform into the location of the platform computed from the sensor measurements. To mitigate the errors an experimental design is presented, tested and validated to measure the sensor locations on the mobile platform.

- Chapter 5 concludes this thesis by collecting and discussing the findings of the present research and evaluating the feasibility of the development of a localization system for mobile platforms. The thesis is completed with a listing of opportunities for future research that the present projects has opened.

1.4.3 Summary of Publications and Contributions

The research reported in the present thesis comprises the following scientific contributions and associated papers:

1. Review and analysis of the original laser lighthouse concept for localization of a vehicle in a planar space as proposed and patented by Tsumara et al. in 1984. The review

is published in: A. Paijens, L. Huang, and A. Al-Jumaily, "Mobile robot positioning system for precision manufacturing: The laser lighthouse revisited", 2017 3rd International Conference on Control, Automation and Robotics (ICCAR) IEEE, Apr 2017, http://dx.doi.org/10.1109/iccar.2017.7942666

2. An analysis is made of the propagation of errors in the time stamping of sweeps with a light sheet emitted by a laser lighthouse into the calculated location of a mobile platform. The error propagation is compared for multiple sensor arrangements on the mobile platform resulting in the recommendation to include the analysis in an algorithm to select the best combination of sensors to compute the location of the platform in any pose. The analysis is published in: A. Paijens, L. Huang, and A. Al-Jumaily, "Analysis of sensor arrangements to localize mobile robots with one laser lighthouse," 2017 24th International Conference on Mechatronics and Machine Vision in Practice (M2VIP). IEEE, Nov 2017, http://dx.doi.org/10.1109/m2vip.2017.8211469

3. The use of optical flow sensors for incremental odometry of a mobile platform is reviewed and several improvements are proposed to the approaches presented in earlier papers on this subject. A software configuration to synchronize the data acquisition of multiple optical flow sensors is worked out as well as a new method to measure the location and orientation of the optical flow sensors in the mobile platform coordinate system with the sensors themselves. The design of the experiment that is part of the measurement method enables experimental validation of the location and orientation of the optical flow sensors. The validation demonstrates the best results for accuracy and precision of the measurement of displacement of a mobile platform reported in the open literature. The research is published in: A. Paijens, L. Huang, and A. Al-Jumaily, "Implementation and calibration of an odometry system for mobile robots, based on optical computer mouse sensors," Sensors and Actuators A: Physical, vol. 301, p. 111731, Jan 2020, http://dx.doi.org/10.1016/j.sna.2019.111731

4. For the 3D localization of a mobile platform with a spatial version of a laser lighthouse the locations of the light sensors in the mobile platform coordinate system are parameters

of paramount importance as demonstrated by the error propagation analysis performed. Measurement of the sensor locations is required to obtain accurate results with the localization. As it is hard to obtain locations of the light sensors by direct measurement with external instruments, a method is designed to find the location with the sensors themselves. An experiment is designed that is similar in execution to the experiment to measure the location and orientation of optical flow sensors. Likewise the design of the experiment enables experimental validation of the location of the light sensors. The validation demonstrates significant improvement of the localization results after measurement of the sensor locations with the method designed. The research is reported in: A. Paijens, L. Huang, and A. Al-Jumaily, "Measurement of the positions of light sensors on a mobile platform being tracked with a lighthouse localization system", Sensors and Actuators A: Physical, p. 112979, Jul 2021, http://dx.doi.org/10.1016/j.sna.2021.112979

Overall, the research conducted for this thesis produced two peer-reviewed journal publications, and two peer-reviewed conference papers.

Chapter 2

Literature Review

2.1 Introduction

The literature review covers the following topics:

- Section 2.2 elaborates the criteria for adoption of a mobile platform for laser cutting and engraving. The feasibility of the present research project are assessed according to the ability of the localization system under development to meet these criteria for adoption. In manufacturing practices the main measure of quality for parts that are manufactured by cutting sheet material can be categorized as "allowable manufacturing tolerances". Section 2.2 lists the results of a survey of engineering practices in different industries to formulate a benchmark for "allowable manufacturing tolerances" to serve as criteria for acceptance. It is assumed that the criteria for laser cutting cover the criteria for laser engraving as well.

- Section 2.3 presents a concept for a mobile platform as a guideline for the literature survey and the subsequent research. The concept outlines an implementation for the suspension of the toolhead that enables translation of the allowable manufacturing tolerances into requirements for the positioning of the mobile platform and the toolhead of the laser cutter. A qualitative analysis of the process to control the dimensional accuracy of a laser cut part, comparing suspension of the toolhead on a gantry based flatbed laser cutter with suspension on a mobile platform, puts the focus strongly on localization of the mobile

platform as the subject of interest. At the same time the analysis shows the advantages of a mobile platform compared to a gantry based suspension of the toolhead at increasing size of parts to be cut from sheet material.

- Section 2.4 explains how localization requirements compare to the positioning of a mobile platform when multiple measurement systems are being used.
- Sections 2.5 and 2.6 focus on the core subject of the thesis: measurement of the location of the platform by means of odometry and absolute location measurement respectively. Building on previous surveys of localization technologies, each section reports on the scouting for mature and new technologies for localization of mobile platforms. Optical methods appear to be the most suitable to achieve the desired level of accuracy out of the technologies reviewed. A combination of optical flow sensing for odometry and laser lighthouse localization is selected as the best fitting solution to localize a mobile platform for laser cutting and engraving. For each systems an overview is presented of the available information on their operation and performance as well as sources of errors.

The present chapter concludes with a list of observations from the review of open literature that are relevant to the benchmark for feasibility defined in Section 2.2. The list is supplemented by an overview of gaps in the knowledge of optical flow sensing for odometry and laser lighthouse localization that need to be filled by additional research and analysis.

2.2 Criteria for adoption of a mobile platform for laser cutting and engraving

As has been set out in Section 1.4.1 the scope of the thesis is the development of a localization system for a mobile platform for laser cutting and engraving of parts from sheet material. The choice for laser cutting and engraving over other machining operations is motivated by the fact that laser cutting is a purely 2D operation that does not generate reaction forces, making the process relatively easy to control. For the same reasons, laser cutting has gained popularity and market share fast in many industry sectors, replacing more traditional operations like engraving

and metal cutting. Laser cutting is applied to cut fabrics, plastics, composites and other synthetic materials in sheets, wood panels, plywood/wood composites, MDF board and it is a non-contact sheet metal technique for a wide range of applications.

The main criteria for adoption for a mobile platform for laser cutting and engraving concern the ability to produce parts of acceptable quality. The quality of a part cut from sheet material is assessed by the extent to which its dimensions comply with the design dimensions of the part as specified in the input file for the cutting machine. This compliance with the specified dimensions of a part can be considered the “manufacturing accuracy”. It is the direct consequence of the accuracy with which the toolhead aiming the laser beam is targeting its intended position on the sheet material.

"Accuracy" is defined by the Joint Committee for Guides in Metrology (JCGM) in the context of measurement as "the closeness of agreement between a measured quantity value and a true quantity value of a measurand" [7]. It can be understood as the rate of absence of systematic errors in the measurement result.
Accuracy has to be distinguished from "precision", which according to the JCGM is defined as: "the closeness of agreement between indications or measured quantity values obtained by replicate measurements on the same or similar objects under specified conditions" [7]. Precision is therefore often referred to as "repeatability", reflecting random (non-systematic) errors and expressed as the variance or standard deviation of repeated measurements.

In a manufacturing context where parts are cut from sheet material, "true quantity value" is easy to interpret: the true (quantity) value of the dimension of a part to be manufactured is the value that is assigned to it by design. In present day engineering practices that is the value specified in the CAD file of the part. Consequently, the manufacturing accuracy of a sheet cutting process is "the closeness of agreement of the dimensions of the cut part with the dimensions specified in the CAD file". In quantitative terms, the accuracy of a laser cutting process is the agreement between the design value of the dimensions of a part and the mean value of those dimensions of the parts produced. Likewise the manufacturing precision can be defined as "the closeness of agreement between the dimensions obtained from replicate parts", which is expressed in the variance or standard deviation of the dimensions of the parts manufactured.

For the quality of the parts manufactured by a laser cutter, the implication of accuracy and precision of the cutting process is limited. Most parts cut on a laser cutter can be considered parts of a puzzle for which it does not matter what the accuracy and precision of the cutting machine is, as long as the pieces of the puzzle fit together "nicely". This quality is quantified by the "manufacturing tolerance" which is defined as the margin between the highest and lowest value of a dimension of a part, measured over a relevant sample of replicates manufactured in the process. To fit "nicely" the manufacturing tolerance of parts should not exceed a maximum value as expressed by the "allowable manufacturing tolerance", beyond which a part is considered "off spec" and has to be reworked or disposed of. Generally the allowable manufacturing tolerance is specified as a tolerance around the value of the dimension specified in the design of the part. For a mature manufacturing process where the systematic errors have been ironed out, the allowable manufacturing tolerance can be associated with a rejection rate of the parts produced, of for instance 5% or < 1% rejection due to excessive manufacturing tolerances.

The aim of the present research is the development of a localization system that allows a form closed mechanism to be replaced by a mobile platform to suspend the toolhead in a laser cutting process. The success of the adoption of the replacement is determined by the accuracy and precision with which the mobile platform and the toolhead can be positioned as this translates into the manufacturing tolerances of the parts produced. To set a criterion for feasibility that covers the criteria for adoption it is proposed to define a benchmark for the allowable manufacturing tolerance at the 5% rejection level. This benchmark is to be viewed as a target for the manufacturing tolerance for the application of a mobile platform in laser cutting, to make it competitive to the existing laser cutting machines. Expressed mathematically for a part with a dimension d_d according to its design, the benchmark is:

$$d_d - \frac{\Delta_{max}}{2} \leqslant \mu_d - 2\sigma_d \leqslant \mu_d + 2\sigma_d \leqslant d_d + \frac{\Delta_{max}}{2}$$

or

$$\|d_d - \mu_d\| + 2\sigma_d \leqslant \frac{\Delta_{max}}{2}$$

where Δ_{max} is the allowable manufacturing tolerance, μ_d and σ_d are respectively the mean value and standard deviation of the dimension of the parts produced. The absolute difference

Table 2.1: *Allowable manufacturing tolerances for miscellaneous parts made from sheet material.*

Parts made from sheet material	**Allowable tolerance**	**Reference**
Stainless steel sheet (4' x 8') over 2 mm thick for tank manufacturing. Gaps up to 2 mm can easily be closed by manual welding. Robot welding closes gaps up to 1 mm without problems.	2 mm	Previous personal industry experience
Metal bulkheads for ships (8' x 20' sheets).	5 mm	[8]
Plywood parts for boat building. (4' x 8' sheets).	3 mm	[9]
Parts for carpentry, furniture making (2' x 4' to 4' x 8').	3 mm	[10]
Parts for architectural woodwork from (2' x 4' to 4' x 8').	2 mm	[10]

between d_d and μ_d is the systematic error of the manufacturing process. Figures for allowable manufacturing tolerances Δ_{max} can be obtained from applications of laser cut sheets. Flat parts from sheet material are utilized in manufacturing of tanks and industrial cabinets and enclosures, car manufacturing, ship and boat building, carpentry and furniture making, architectural metal and woodwork and interior design, amongst others. Where fabrics and thin metal sheet can be obtained on rolls, more rigid materials are processed in panels. The most popular sheet size for panels is 4 x 8 foot. Metal sheets are available in standard sizes up to 8 x 20 foot, mainly for the heavy industries. The applications of the parts can provide some clues on the allowable manufacturing tolerances of the cutting operation. Table 2.1 lists some allowable dimensional tolerances of parts for typical applications. Although the information in the table has a basis in design recommendations and engineering practices, it is more indicative than exhaustive and should not be considered as representative for the complete manufacturing industry. Nevertheless, it can be observed that there are manufacturing operations in carpentry, furniture making, architectural woodwork and interior design for example, where the dimensional tolerances of parts are expressed in millimeters rather than microns. Formulated as a ball park figure, a dimensionless tolerance ϵ_{max} of 0.1% of the parts' maximum dimension d_{max} is allowable for the manufacturing of parts from sheet material for boat building, carpentry and furniture making,

architectural metal and woodwork and interior design:

$$\epsilon_{max} = \frac{\Delta_{max}}{d_{max}} = 0.1\% \tag{2.1}$$

2.3 Mobile platform for manufacturing

As was indicated in Section 1.3 and elaborated in the previous section, the development of a mobile platform that can replace the gantry in a laser cutter focuses on accuracy and precision of the positioning of platform and toolhead. This comprises both a measurement and control problem of which the measurement part has the highest priority. Without measurement of the location of the mobile platform with the required accuracy and precision, control of the toolhead position within the required manufacturing tolerances is impossible. To further analyze the performance of positioning a toolhead with a mobile platform and make a comparison with a flatbed machine with a gantry, an outline of the operating conditions that are relevant to the positioning of the mobile platform is given below:

- The mobile platform moves on top of a sheet of material to be processed with a laser cutter. Its operating space is a horizontal planar space of 4 x 8 feet over the sheet of material.
- The sheet material is smooth and free of course particular matter on which the mobile platform could slip. The floor is visibly, but not necessarily perfectly horizontal.
- The sheet of material is supported on a bed that carries the sheet plus the mobile platform without causing it to deflect in vertical direction and without causing parts cut off to drop away from the sheet. (It is common practice not to cut parts fully loose from the sheet, but to leave them attached to the sheet through small “bridges” that have to be removed manually [11].)
- The mobile platform localizes itself using one or more beacons located next to the bed supporting the sheet of material

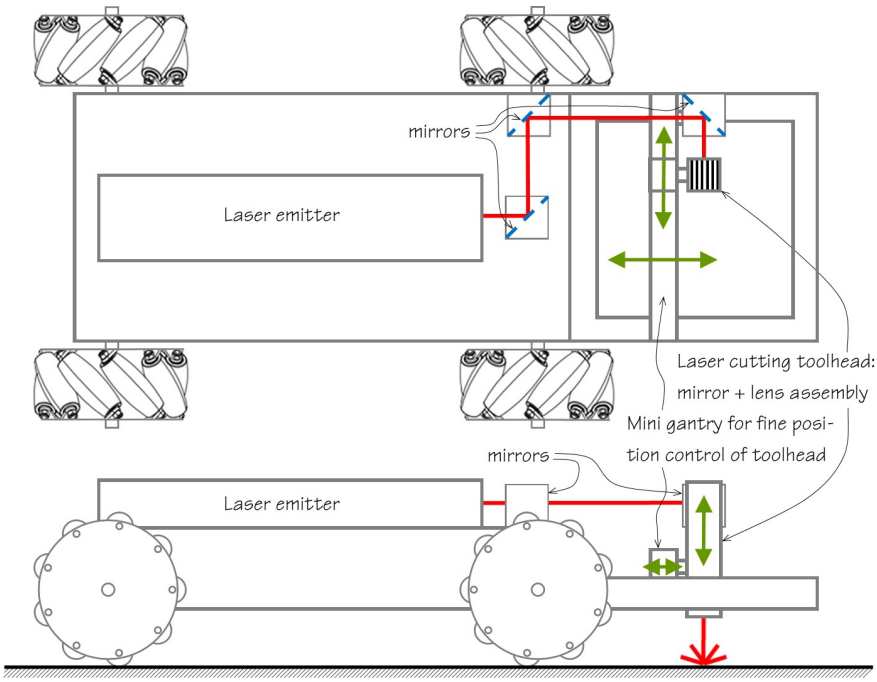

Figure 2.1: *Sketch of a concept of a mobile platform for laser cutting.*

- The wheels of the mobile platform are of such size that it can cross the kerf cut by the laser, without disturbance of its motion. As the kerf width of a properly operated laser cutter does not exceed 0.5 mm this should not pose any problem for a mobile platform with a wheel diameter over 50 mm.
- The mobile platform operates under minimal cover protecting it against strong drafts, precipitation and exposure of the operating space to direct sunlight. For the purpose of vehicle navigation the environment is to be considered as "indoor".
- The cutting speed ranges between 1 and 100 mm/sec

For the definition of an engineering design, the specification of the operating conditions have to be extended with constraints to ensure that the operation of the mobile platform is well controlled and safe. This is considered not within the scope of the present research however.

Figure 2.1 presents a sketch of a concept for a mobile platform for low power (non-metal) laser cutting applications that operates at the conditions listed above. It features mecanum wheels for agile maneuverability while driving over the sheet to be processed. A solid state laser

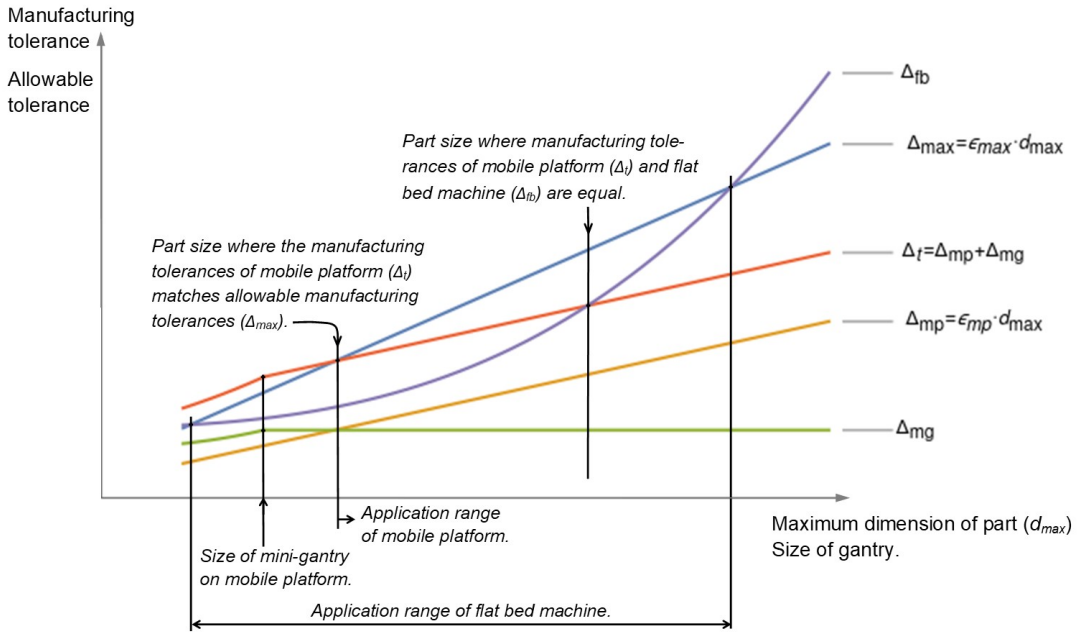

Figure 2.2: *A qualitative comparison of manufacturing tolerances generated by a laser cutter on a flatbed machine and on a mobile platform.*

emitter is preferred as it is smaller than a CO_2 tube and available in lower power ratings that can be powered by an on board battery more easily. Air assist to the laser cutting can be added by means of an air blower mounted on the platform with an air tube connected to a nozzle on the toolhead. The setup on the platform is similar to the setup of a conventional flatbed laser cutting machine: the toolhead is a lightweight mirror + lens assembly where the laser ray is beamed into from the laser emitter by means of mirrors. The toolhead is suspended on a mini-gantry for fine positioning. The location of the mobile platform is measured whereas the mini-gantry operates without measurement feedback, relying on its form closed design to position the toolhead.

Using the build up of the mobile platform shown in Figure 2.1 a qualitative comparison can be made between the performance in terms of accuracy between a flatbed laser cutter and a laser cutter on a mobile platform. The comparison is illustrated by the graphs in Figure 2.2, plotting manufacturing tolerances and the allowable manufacturing tolerance against the maximum dimension of the part. The line tagged Δ_{max} ($= \epsilon_{max} \cdot d_{max}$) represents the allowable manufacturing tolerance as defined in Equation (2.1). As proposed in Section 2.2, ϵ_{max} is set to 0.1% as benchmark for the feasibility of the deployment of a mobile platform.

For a flatbed laser cutter the maximum dimension of the part fixes the size of the sheet that

has to be processed which determines the size of the machine that is used. The graph tagged Δ_{fb} represents the manufacturing tolerance of a flatbed laser cutter of a particular design and construction, with a gantry that envelopes the sheet processed. The curvature of the graph reflects the exponential growth of the tolerance with the size of the sheet processed, as a result of mechanical scale effects as flexure and wagging of the constituent beams on top of backlash in the drive mechanism of the gantry. Consequently there is an upper limit to the size of a part that can be manufactured within chosen allowable manufacturing tolerance with a flatbed laser cutter of a particular design and/or construction. To extend the application range of the flatbed laser cutter indicated in Figure 2.2 its design and or construction has to be upgraded.

The graph of the manufacturing tolerances for a laser cutter on a mobile platform tagged Δ_t is the accumulation of tolerances caused by the errors in the measurement of the mobile platform's location Δ_{mp} and the positioning of the laser cutting toolhead with the mini-gantry tagged Δ_{mg}: $\Delta_t = \Delta_{mp} + \Delta_{mg}$. Δ_{mp} and Δ_{mg} have separate graphs in Figure 2.2. Δ_{mg} grows exponentially with the size of the part similar to Δ_{fb}. The difference with Δ_{fb} is that the mini-gantry is small, smaller than the part to be cut, which caps Δ_{mg} to a maximum value determined by the size of the mini-gantry. For parts larger than the size of the mini-gantry, Δ_{mg} does not exceed this maximum. The line representing the error in the measurement of the mobile platform's location Δ_{mp} reflects the expectation that it is proportional with the distance between the beacons for triangulation and the mobile platform as argued in Section 1.3. With the beacons surrounding the sheet of material, the distance is proportional with the size of the sheet to be processed.

Overlooking the graphs in Figure 2.2 it can be observed that the manufacturing tolerance Δ_t of a laser cutting process on a mobile platform beats the the manufacturing tolerance Δ_{fb} of a flatbed laser cutter at some scale as the consequence of the exponential growth of Δ_{fb} compared to the linear growth of Δ_t with the size of the part being cut. Δ_t grows linearly with the part size as a consequence of the linear growth of Δ_{mp} which can be expressed in a dimensionless figure ϵ_{mp} as a fraction of the maximum dimension d_{max} of the part being cut:

$$\epsilon_{mp} = \frac{\Delta_{mp}}{d_{max}} \tag{2.2}$$

In order to meet allowable manufacturing tolerances for parts with maximum dimensions over a size d_{mmin}, the errors in the measurement of the mobile platform's location have to be limited to $\epsilon_{mp} < \epsilon_{max}$:

$$\Delta_t \leqslant \epsilon_{max}\, d_{mmin}$$

which is expanded to:

$$\Delta_{mp} + \Delta_{mg} \leqslant \epsilon_{max}\, d_{mmin}$$

Inserting Equation (2.2) for $d_{max} = d_{mmin}$ and rearranging the terms:

$$d_{mmin} \geqslant \frac{\Delta_{mg}}{\epsilon_{max} - \epsilon_{mp}}$$

This result emphasizes that the key to competitive deployment of a mobile platform is the accuracy and precision of the location measurement (localization) of the mobile platform.

2.4 Localization of a mobile platform

Localization of a mobile platform is a combination of estimation of the displacement from the previous location with on-board sensors for direction and distance (odometry) corrected by periodic measurement of the absolute location of the platform [12–14]. Odometric sensors can measure displacements with resolutions matching those of gantry positioning when measuring incremental displacement. Accumulating these incremental displacements to calculate a location inevitably leads to errors, no matter how high the resolution is. Location measurements in an absolute reference frame are needed to recalibrate the odometric measurements periodically [12]. To put it in perspective of the definitions presented in Section 2.2: odometry can be precise, but is in principal never accurate as the error in the estimated location grows unconstrained in the absence of an absolute reference frame. Adding a location measurement in an absolute reference frame allows both measurements to be "fused" into an improved location by application of a Kalman filter, provided the localizing errors have a Gaussian probability density distribution. A Kalman filter applies a "weight" to the available location information to estimate an improved location by means of a weighing factor known as the "Kalman gain" k_k. For two sources of location information, for instance a model estimate (source 1) and a measurement (source 2), k_k

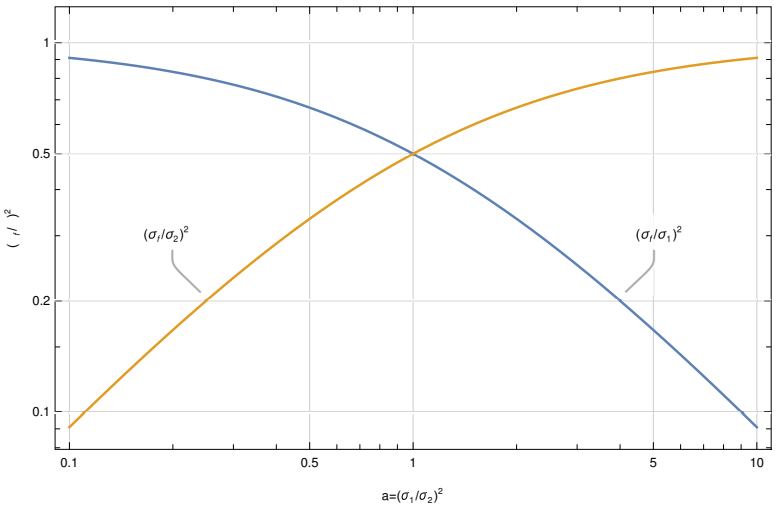

Figure 2.3: *Ratio of the fused variance σ_f, to the variances σ_1 and σ_2 with which σ_f is calculated by application of a Kalman filter.*

is expressed as:

$$k_k = \frac{\sigma_1^2}{\sigma_1^2 + \sigma_2^2}$$

The fused location μ_f and variance σ_f^2 are computed from mean locations μ_1 and μ_2 and location variances σ_1^2 and σ_2^2 from the two sources of location information, as [15]:

$$\begin{aligned} \mu_f &= \mu_1 + (\mu_2 - \mu_1)\, k_k \\ \sigma_f^2 &= k_k\, \sigma_2^2 = (1 - k_k)\, \sigma_1^2 = \frac{\sigma_1^2\, \sigma_2^2}{\sigma_1^2 + \sigma_2^2} \end{aligned} \tag{2.3}$$

Figure 2.3 shows plots of $(\sigma_f/\sigma_2)^2 = k_k$ and $(\sigma_f/\sigma_1)^2 = 1 - k_k$ against the ratio $a = (\sigma_1/\sigma_2)^2$. Obviously, σ_f^2 is always smaller than the largest of σ_2^2 and σ_1^2: the noisiest of the measurements is improved by the presence of a less noisy measurement method. However the least noisy measurement only improves by the presence of the second measurement method by any significance, if the variances of both measurements as expressed by the ratio $a = (\sigma_1/\sigma_2)^2$, do not differ more than one order of magnitude. Figure 2.3 illustrates that if $a \gg 1$, k_k approaches 1, σ_f^2 converges to σ_2^2 and μ_f converges to μ_2 according to Equations (2.3). Vice versa, if $a \ll 1$, k_k approaches 0, $1 - k_k$ approaches 1, σ_f^2 converges to σ_1^2 and μ_f will converge to μ_1. The use of an additional independent measurement method is most effective if the ratio of the variances of the location measurements is 1, which causes the variance of the fused location to be half of the variance of the separate locations. In the context where a mobile platform is

used to manufacture parts within allowable dimensional tolerances, the accuracy of its location will have to be better than these tolerances. If the location is established as the result of a combined measurement with an odometric and an absolute localizing system and both systems meet this criteria separately, the fused location effectively adds to the necessary margin between the accuracy of the location of the mobile platform and the manufacturing tolerances.

2.5 Odometry

Odometry is measurement of the displacement of a mobile platform (vehicle) in an incremental way, relative to its previous location [12–14]. It is a field of mature solutions dominated by incremental wheel shaft encoder reading [16]. The encoders measure the incremental rotation of the wheels of a vehicle and convert this into a displacement of the vehicle frame by means of a kinematic model, relating the rotation of the wheels to a displacement of the platform over the floor [5].

With encoders available that can measure thousands of steps in one shaft rotation, high resolutions are possible, at relatively at modest cost [16]. Unfortunately, there are quite a few sources of errors in odometry using rotary encoders, preventing proper translation of the encoder signal into an accurate displacement, such as slippage of the wheels, presence of particles on the surface and unknown or inaccurate parameters in the kinematic model [5, 14, 17, 18]. Borenstein developed a method to properly measure values for the wheel diameter and width of the wheel base of a robot, which are cardinal parameters in the kinematic model [19, 20].

2.5.1 Optical flow sensors

Alternative to measuring the rotation of the wheels with a rotary encoder, several researchers have looked into indoor application of optical flow sensors as used in computer mice, to measure the displacement of mobile platforms. Optical flow sensors in computer mice evaluate their displacement by photographing a small patch of the surface they are moving on at low resolution, typically between 16 x 16 and 30 x 30 pixels at frame rates that can vary between 500 and 12000 fps[1]. The displacement is computed by measurement of the change in location of features in the

subsequent images. This yields a translation of the sensor in pixels in the image plane directly. Since these optical flow sensors measure $x - y$ translations only, a minimum of two sensors in different locations on the mobile platform is required to obtain values for all three kinematic parameters for translation and rotation of the platform in a planar displacement [21, 22]. As a consequence of their non-tactile operation, optical flow sensors avoid errors caused by slippage of the wheels or particles on the surface. Moreover, optical flow sensors are cheaper than rotary encoders and have the specifications to perform odometry at high resolution. State of the art, off the shelf optical mice for office computers scan the surface they are moved over at a resolution of 1600 dpi or close to 15 micron. Optical flow sensors for gaming mice scan at a resolutions up to 16000 dpi[1], matching the 10 micron resolution offered by gantries easily. Sekimori and Miyazaki demonstrated how a robot controlled by feedback of its displacement measured by four optical flow sensors far outperforms the same robot equipped with rotary encoders on the wheel shafts in terms of accuracy of the odometry, as long as the maximum velocity at which the sensors can scan the surface is not exceeded [23]. Other examples of successful application of optical flow sensors in odometry have been published by Tresanchez et al. [24], Ng [21], Cooney et al. [25], Jackson et al. [26] and more recently by Yi et al. [27].

Although promising, the operation of an optical flow sensor as a displacement sensor is not without limitations. The sensitivity of an optical flow sensor tends to be inconsistent and dependent on the distance between the sensor aperture and the floor surface as well as the optical properties of the surface such as reflectiveness and transparency and on properties of the sensor's motion trajectory such as velocity and curvature. Ng noted that the distance between the sensor and the surface it is moved on, is critical for the accuracy of the measurement [21] and that the sensor has speed limitations when measuring vibrations [28]. Minoni, and Signorini [29] reported that their optical flow sensor exhibited reduced sensitivity when installed at greater height from the surface, resulting in underestimation of the distance traveled. Palacin et al. argued that the field of view of the optical flow sensor covers a larger area on the surface when mounted higher, resulting in under reporting of the displacement [30]. Palacin further found dependencies on the angle of the direction in which the sensor was moved, of the calibration factor between distance measured and traveled. Finally he observed a consistent discrepancy in distance measured along a curved and along a straight path for the sensor that he used.

2.5.2 Odometry with optical flow sensors

The optical flow sensor used in a computer mouse can measure its linear displacement only, leaving its rotational angle (angular displacement) undecided. Therefore a mobile platform with three degrees of freedom requires at least two sensors at different locations to compute the full planar (linear and angular) motion. With two or more optical flow sensors in place, the displacement data measured is redundant and allows for calculation of the mobile platform motion by means of least squares linear regression [31].

Ping-Lin Wu et al. elaborated a non-linear approach, that takes into account higher order effects of the rotation of the mobile platform on the displacements of the sensors [32]. The displacement of the platform has to be solved in an iterative procedure at considerable increased computing cost. Comparison of the accuracy of the calculated orientation in an experiment with optical flow sensors traveling a windy path, Ping-Lin Wu et al. produced better results with the non-linear approach than with the linearized method elaborated in Chapter 3, that is used by most researchers.

2.5.3 Precision and error propagation in odometry with optical flow sensors

The precision of the estimation of the displacement of a mobile platform using optical flow sensors depends on the sensitivity, location and orientation of the sensors and on the timing of the sensor measurements.

1. **Sensor sensitivity**

   The sensitivity f of an optical flow sensor for application in a computer mouse, is the ratio between the reading of a displacement from the optical sensor in pixels Δo_p to the dimensional displacement Δo that the sensor has traveled in the displacement:

   $$f = \frac{\Delta o_p}{\Delta o}$$

   Although no analysis of the propagation of errors in the sensitivity into the estimated location of a mobile platform has been found in the open literature, several remedies have been published to mitigate the effects of errors in the sensitivity of the sensors and limit propagation of the error:

- Since it has been observed that the sensitivity of optical flow sensors is dependent on the optical properties of the floor surface such as reflectiveness and transparency it is highly advisable to repeat measurement of the sensors sensitivity on each new surface that they are applied to.
- Yi et al. proposed modifications to the optics of optical flow sensors to mitigate the dependency of its image acquisition system on the height of its aperture over the floor surface [33]. By addition of an extra lens to the optics, capturing images of the floor surface is made a-focal, reducing the sensitivity of the displacement measured over surfaces that are not flat.

  Hyun et al. described a setup in which pairs of optical flow sensors each acquire an image of the same spot on the floor from a different distance [34]. The sensors difference in distance to the floor is fixed which allows calculation of the distance traveled by comparison of the distance traveled in the images of each sensor of the pairs separately. This setup requires extensive hardware modifications to the standard packaging of optical flow sensors for computer mice.
- Addition of extra sensors to the set of sensors mounted on the mobile platform. The presence of redundant sensors using identical or alternative measurement principles dilute the effect of errors in the sensitivity in one of them [27, 30, 35, 36]. Hu et al. refined this approach for a set of identical optical flow sensors, by calculating the displacement of the mobile platform from measurement data of each pair of sensors in the set. The data of sensors that produce outliers in the distribution of mobile platform displacements calculated from all sensor pairs is removed from the final calculation of the platform displacement [37].
- An optimal number of (redundant) optical flow sensors has not been established, but more sensors produce a more accurate estimate of the displacement of the mobile platform. Sekimori and Miyazaki [23] used arrays of two and four optical flow sensors on a mobile platform measuring their own displacement from which the displacement of the platform was estimated by least square regression. In their test, a robot controlled by feedback of its location estimated with the optical flow sensors,

the odometry based on four optical flow sensors outperformed the odometry based on two optical flow sensors by a significant margin in terms of location accuracy. The experimental results from Kim and Kim [38] also indicated that more sensors result in a better estimate of the robot location as the variance of the solution of the robot displacement is inversely proportional to the number of sensors used. This observation complies with Equation (2.3) for the fusion of measurement data from two sensors. When sensors 1 and 2 are identical, implying that $\sigma_1 = \sigma_2 = \sigma$, σ_f^2 becomes: $\sigma_f^2 = \sigma^2/2$. Further extension to the variance of the measurement data of a set of n sensors σ_n can be achieved by simple induction, through addition of an identical sensor to a set of $n-1$ sensors with variance $\sigma_{n-1}^2 = \sigma^2/(n-1)$:

$$\sigma_n^2 = \frac{\sigma^2\sigma_{n-1}^2}{\sigma^2 + \sigma_{n-1}^2} = \frac{\sigma^2\sigma^2/(n-1)}{\sigma^2 + \sigma^2/(n-1)} = \frac{\sigma^2}{n} \tag{2.4}$$

2. **Sensor location and orientation**

The odometry system using the optical flow sensors has it highest sensibility when small displacement and rotations of the mobile platform translate into displacements of the sensors as large as possible. This enables the system to properly detect small movements of the platform. At the same time propagation of errors in the displacement measured by the optical flow sensors into errors of the estimated displacement and rotation of the mobile platform has to be mitigated as much as possible. Cimino and Pagilla as well as Kim and Kim have proposed algorithms to balance maximization of the sensibility and minimization of the relative condition number to reduce error propagation with similar results for the best location of the sensors: furthest away from the geometrical center of the platform [31]. The best distribution of the sensors is in a regular polygonal arrangement around the geometrical center of the mobile platform [31, 39–41]. The orientation of the sensors has no consequences for the sensibility the odometry system with the optical flow sensors. If less intuitive locations for the sensors are sought when the conditions for the best arrangement are in conflict with each other as the consequence of the geometry of the mobile platform or constraints to the location of installation of sensors, the algorithms

identify optimal arrangements within these constraints. The algorithm of Kim and Kim offers an additional degree of freedom to find the optimal locations for the sensors by allowing the geometrical center of the sensor arrangement to deviate from the geometrical center of the mobile platform [31].

The actual location and orientation at which each sensor is mounted in the mobile platform can be hard to establish in a setup using optical flow sensors, as the location and orientation of the small apertures of the sensors are difficult to measure and the location of the sensors in the mobile platform coordinate system might not coincide with their design value, due to manufacturing tolerances of the platform.

Kim and Kim proposed to determine sensor locations through a one-time calibration measurement of the robot displacement using a separate highly accurate calibration system [38]. The calibration measurements reveal the deviation in the robot's displacement as measured by the optical flow sensors. Through its relation with the errors in the sensors' locations, the deviation can then be traced back to improve the accuracy of the sensor locations established. The method does not evaluate the sensors orientations but assumes them to be aligned with the mobile platform coordinate system.

In the approach published by Hu et al. a robot is moved over an arbitrary homogeneous path comprising of a line or an arc, recorded by the optical flow sensors on the robot frame [37]. The recorded displacements of the separate sensors are coupled by the kinematics of the robot, in which the location and orientation of the sensors in the robot frame are parameters. These parameters are estimated by minimization of the difference between the displacement derived from the kinematic model and the displacement as recorded by the sensors. The method still requires an accurate figure for the distance between at least two sensors on the robot, which is difficult to obtain. The calculation of the sensor locations and orientations is a brute force computation solving all parameters for all sensors in one minimization operation, while reconstructing the path of the robot at the same time. The calibration method is validated in an additional experiment by moving the robot in a closed circular path, measuring the distance and orientation from the end

location as measured by the sensors, to the starting location of the path. Hu et al. reported a satisfactory accuracy of the measurement of the displacement after the calibration.

3. **Timing of sensor readings**

   The linear regression model used to relate the displacements of the optical flow sensors to the translation and rotation of the mobile platform, is purely static. This condition presumes synchronization of the acquisition of displacement data from the sensors in a schedule of strict coincidence. Uncertainty about the times at which the displacement was recorded by the different sensors translates into uncertainty of the calculated location and orientation of the mobile platform. Notwithstanding this prerequisite, previous papers using the same regression model have completely omitted the aspect of synchronicity in data collection from different sensors or disregard explanation on the design and implementation of a scheduled data acquisition system [32, 35, 37, 38].

2.6 Absolute location measurement

Whereas the research cited in Section 2.5.1 demonstrates that optical flow sensors can be applied for odometry to measure displacement of a mobile platform with resolutions matching those of gantry locations, these sensors can gauge incremental displacement only. Addition of these incremental displacements to calculate a location for the mobile platform inevitably leads to errors, no matter how high the resolution. Therefore locations based on odometric estimates or "dead reckoning" have to be complemented with location measurements in an absolute reference frame to correct or calibrate the odometric measurements [12].

Scouting for an absolute localization system for a mobile platform that can meet the accuracy requirements, the subsequent overviews by Borenstein et al. in 1996 [12], Liu et al. in 2007 [42], Mautz in 2012 [43] and Mainetti et al. in 2014 [44] provide good oversight over the developments of systems for indoor localization. The systems can be distinguished by the combination of physical phenomenon and method that is used as to measure and transmit the location information: Radio Frequency, Acoustics, Optics/Computer Vision, Optics/Angulation/Lateration and Optics/Lighthouse.

- **Radio Frequency**

  The development of radio frequency (RF) for communication has had considerable off spin into its use for location measurement, using lateration and angulation of electromagnetic waves in the RF spectrum. It is interesting to see in the overview articles of localization systems, that the accuracy of systems based on lateration and/or angulation, implemented in a technology like radio frequency and networking communication, has not improved very much over a 20 years time span, in spite of tremendous developments in these technologies for communication [12, 42–44]. Apparently there are physical limits that prevent localization using RF technologies to reach below certain (centimeter scale) resolutions [45].

- **Acoustic**

  Although acoustic signals travel much slower than radio waves which allows for more accurate lateration, acoustics are plagued by a large amounts of noise as the consequence of the very high frequencies needed to create the necessary sharp sound pulses [46]. These high frequency pulses reflect strongly on the surrounding surfaces, introducing lots of echoes in the acoustic signal. Moreover the sound speed is temperature dependent and influenced by motion of the air in the workspace, which makes the accuracy of the measurements hard to predict [47].

- **Optical/Computer Vision**

  Computer vision systems based on digital camera's are the runners up in the race for localization systems. With state of the art, off the shelf camera sensors now featuring resolutions of 16 Mpixel (4920×3264 pixels) and higher, it is theoretically possible to observe displacements even smaller than 1 mm on a 4 by 8 foot (1220×2440 mm) workspace, if the camera is positioned such that it is facing the planar working space perpendicularly. This requires a rig that allows to mount the camera overhead of the working space however, which impedes the ease of deployability of the mobile platform setup. For camera's positioned in other locations relative to the workspace, Horaud et al. and DeMenthon have presented algorithms to reconstruct location and orientation relative

to the camera in three dimensions from digital images of an object carrying markers on known locations on the object. Horaud elaborated a solution for four markers on the object and DeMenthon has developed an approximate method that uses three points [48, 49]. Eberli et al. used a circular mark on their micro aerial vehicle (MAV) to reconstruct its position from the projection of the circle on the projection plane of a camera [50]. The methods are elegant, but computationally intensive and in the end still limited in accuracy by the resolution of the camera. The camera has to be pointed at the object moreover, which requires an additional feedback control loop and a measurement system to control the pose of the camera to monitor the position of the moving platform.

- **Optical/Angulation**

  Application of angulation to optical/visual observations is the oldest method to establish a location of a mobile platform and is still widely practiced in marine navigation to locate ships in the planar working space at the water surface [51]. Applications of lasers has enabled the measurement of angles using light sensors. This has paved the way for localization systems that read bearings in multiple directions directly into computers. The Minnesota scanner developed by Sorensen et al. [52] sweeps two sheets of laser induced light around two separate vertical axes and another sheet around a horizontal axis. The locations and orientations of all axes are known as well as the rotation frequency of the light sheets. From the time difference between time stamps recorded at the passing of the light sheets over a light sensor in a fixed, known reference location and any other light sensor, the location of the latter sensor can be estimated. The Minnesota scanner has been successfully used to track the movement of the human body in locomotion. Using a similar setup with laser induced sweeping light sheets around fixed axes in known locations and orientations, the Nikon iGPS system reportedly has a sub-millimeter accuracy over an area of an impressive 10 x 10 x 2 m., at equally impressive expenditure, though [53]. The system needs at least four laser transmitters to obtain the sub-millimeter accuracy. Much simpler experimental setups relying solely on angulation, have been reported to locate mobile platforms with accuracies below 7 mm over a 3 by 3 meter workspace by Simi [54] and well below 1 mm in a 60 x 20 x 20 cm workspace by Linga

[55]. Alenya et al. performed experiments in which the localization of a mobile robot by means of angulation with two stationary laser beams is compared with localization through location calculations using a camera on the robot observing patterns on the walls surrounding the workspace [56]. The triangulation with laser beams manages to locate the robot under stationary conditions with deviations between 0.25 and 1.75 mm in a 4 by 6 m workspace. Using computer vision on a moving mobile robot the deviations jump to 100 mm. As the experiments by Alenya illustrate, for location measurement in an unobstructed planar space, lateration and/or angulation using laser beams provides the highest accuracy [43, 57], surely when expressed per unit of cost. Laser beams are limited in their deployment, because of the requirement for a line of sight (LoS) between the emitter and the sensor, but this does not hamper the deployment in a planar workspace occupied by a sheet of material lying flat on the floor. The laser emitters can be installed adjacent to the workspace, facilitating flexible deployment. Looking at the solutions available and researched for localization by angulation with laser beams it can be observed that they depend on multiple stationary landmarks and in some cases on light sensors in fixed location [58–61]. The accuracy of localization of the mobile platforms depends directly on the accuracy with which the location of these landmarks and sensors is known. For a stationary setup in a workshop this is not a problem as the locations of the landmarks and fixed sensors can be established by a one time measurement using high accuracy tools and methods. The stationary setup of landmarks and sensors is a huge obstacle in the flexible deployment of the mobile platform however, for instance on a construction site.

- **Optical/Lighthouse**

  A localization system introduced in a paper in 1982 and patented in 1984 by Tsumura and collaborators has the potential to overcome the limitations of the optical/angulation method mentioned above [62–65]. Tsumura introduced a 2D vehicle localization system based on a single landmark beacon, emitting a rotating light sheet generated with a laser, similar to a lighthouse. For this reason the setup is referred to as the "laser lighthouse". The vehicle carries three light sensors in known locations, that record time stamps when

the light sheet passes over a sensor. From the time difference between the time stamps the difference in angle of arrival of the light sheet can be calculated. With two differences in angle of arrival between two pairs out of three sensors, the location of the light house in the coordinate frame of the vehicle can be established. If one additional measurement is made to establish an absolute angle of arrival of one of the sensors relative to the lighthouse in the global coordinate system (of the lighthouse), the location of the lighthouse relative to the vehicle can be transformed into the location of the vehicle relative to the laser lighthouse in global coordinates. Romanik filed a patent in 1998 extending Tsumara's approach to determining a location in three dimensions, using a second light sheet rotating in a vertical plane [66]. Hernandez et al. developed and patented a setup comparable to Tsumara's, in 2012 [67]. Apparently unfamiliar with the work of Tsumara and Romanik, Hernandez claimed that his setup is the first using only one landmark with a sweeping light sheet. His system uses an array of light sensors covering the perimeter of a cylinder mounted vertically on top of the vehicle to be located. The sensors take time stamps of the passing of the light sheet, similar to Tsumara's system. Measurement of the angle at which the lighthouse is sounded from the vehicle occurs through identification of the sensor on the cylindrical array that is illuminated first by the light sheet swiped around by the lighthouse. The distance to the lighthouse is determined by the angle between the first and the last sensor on the cylindrical array that is illuminated by the light sheet swiped around. The method overcomes the problems occurring when landmarks or sensors line up in triangulation [68]. Hernandez indicates a locating accuracy of 5 cm and a heading accuracy of 1 degree for the system over a 20 x 20 meter workspace.

In a more recent development a collaboration between the Taiwanese company HTC and the American computer games developer Valve Corporation has applied the lighthouse concept for virtual reality (VR) computer gaming and other VR applications. For this purpose HTC-Valve developed pose trackers equipped with multiple light sensors and a lighthouse system that sweeps light sheets to excite the light sensors on the trackers, similar to the way Tsumara's lighthouse operates in a planar space. The light sheets are generated by diffusion of a laser ray through a cylindrical lens. The HTC-Valve lighthouses emit two

rotating light sheets that rotate with a 180° phase shift around perpendicular axes, similar to Romanik's approach [66]. Moreover, the lighthouse generates an omni-directional light flash at a fixed phase point between the sweeps of the lighthouse as a synchronization pulse. The sync pulse is encoded by its length of time, as to identify the direction of the next light sheet[2]. From the time difference between the light sensor registering the sync pulse and the passing of a sweep of the light sheet over the sensor, an absolute value for the angle of incidence of the light sheet can be calculated. With these angles of incidence measured in two sweep directions for each sensor in a set of at least three sensors in known locations on a (rigid) mobile platform, the spatial location of the sensors and the platform can be calculated. The HTC-Valve VR-kit was introduced in the market in June 2016 under the name "HTC-Vive" at a price level of USD 800[3]. The complete kit comes with two lighthouse "base stations" that each sweeps the two perpendicular light sheets, a head mounted display (HMD) comprising a tracker measuring the pose of the users' head and two hand-held controllers acting as pose trackers for each hand. The lighthouses are also equipped with light sensors and calibrate their relative locations and orientations themselves. Although a spatial location and orientation of a tracker can be obtained with one lighthouse base station, the use of at least two base stations secures that a 3D location and orientation of the trackers can be established when the user's body is blocking a line of sight between the tracker and one of the lighthouses. For the same reason, to maintain a line of sight, the user instructions recommend to position the lighthouses at a height of at least 2 meter over the floor at two different edges of the playing field[4]. The size of the playing field of the first generation Vive VR-kit is set by the recommendation to put the lighthouses no more than 5 meter apart and more forcefully by the 5 meter long cable connecting the HMD of the first generation of the VR-kit to the graphics card in a computer. In addition to 31 light sensor on the HMD and 24 sensors on each controller, each tracker carries an inertial measurement unit (IMU) to complement the laser lighthouse measurements with incremental spatial displacement estimates. HTC has not released any details on the fusion of the measurements from the different sensors, nor about the fusion of the measurements from the two lighthouses. Several updates of

the VR-kit and its components have emerged, mainly to improve user friendliness and expand the play area. The operating space can be extended with extra lighthouses. A separate tracker with 22 light sensors has been introduced that can be placed on top of any (movable) object to track its spatial location and orientation. Impromptu testing by Kreylos[5] shortly after introduction of the HTC-Vive VR kit indicated a performance level of the implementation of the lighthouse concept in the HTC-Vive kit that approaches the level of Nikon's iGPS system[6] mentioned above, that is commercially available at a price level two orders of magnitude higher than the HTC-Vive kit [43].

The lighthouse concept as elaborated by Tsumara [64], Romanik [66], Hernandez [67] and HTC[2], provides a robot localization system that requires a minimum of only one active landmark in the form of a laser lighthouse. This makes deployment of these systems easier than any other system described in the open literature. The stationary lighthouse carries the laser emitter, which has the advantage of not exposing it to motions and vibrations as equipment mounted on a vehicle is. No calibration measurement have to be performed to set up a single lighthouse system and no additional data communication is required between the lighthouse and the mobile platform to be tracked. The platforms to be tracked can record time stamps from light sensors on known locations on the platform and process the timing information "on board" of the mobile platform, into a location of the platform in the global (lighthouse) coordinate system . Hence the "laser lighthouse" is the most versatile concept to provide absolute location measurements to a mobile platform localization system.

2.6.1 Accuracy and error propagation of locations measured with a laser lighthouse

The interest in the application of a laser lighthouse to locate mobile platforms is reflected in the number of papers issued in the relative short time span since the emergence of the HTC Vive system, on the subject of the accuracy of a location and orientation measured with the Vive system [69–78]. Unfortunately there has not yet been defined a unified method with criteria to measure and rate the accuracy of the location and orientation of a mobile platform. As a

consequence there are as many tests and outcomes as there are researchers working on this subject which makes the results hard to compare.

Kreylos indicated that with a single base station from the HTC-Vive VR kit, the location of HMD in a space between two lighthouses at 4 m distance of each other can be established with a precision 2.1 mm in direction of the line of sight between the lighthouse and the controller and a precision of 0.3 mm in lateral direction (perpendicular to the line of sight). The accuracy of a location of a controller established with two lighthouses has an RMS value below 2 mm[5]. Kreylos also noted that by principle the lighthouse system can never excite the sensors on a mobile platform coincidentally. If the tracked platform moves, the sensors move during the sweep of the light sheet and their calculated location becomes inaccurate.

Greiff et al. researched the performance of the multiple HTC Vive system base stations to locate micro unmanned aerial vehicles (MUAV's) with two light sensors, in a 3 m cubical operating range [73]. Greiff et al. propose a dynamic model and the use of a Kalman filter to locate a moving MUAV. From their experiments Greiff et al. conclude that the measured values for the horizontal and vertical bearing angles are approximately Gaussian in their distribution with a standard deviation of approximately 3 $[10^{-5}$ rad$]$. Based on the observed noise in the measurement Greiff et al. estimate sub-millimeter precision for their application for the location of a tracker in a stationary position obtained with at least two lighthouses.

Kilberg et al. triangulated the location of a single light sensor with two HTC Vive lighthouses and report errors of a few centimeters within a 1 meter working range [75]. Niehorster et al. have found deviations of the same centimeter order of magnitude while operating two HTC Vive lighthouses to locate the HMD of the HTC Vive VR-kit in operating ranges occupying a workspace of 8, 6 and 4 meters wide by 4 meters length [71]. Niehorster et al. establish a mean sample RMS jitter in x, y and z direction over these operating ranges, of well below 1 cm. Moreover Niehorster et al. observed a systematic error in the measured elevation of the tracker in locations over a real world horizontal plane. The plane appeared slanted in the measurements, as confirmed in experiments by Luckett and Bauer et al. [72, 76].

In a highly conditioned measurement facility for the calibration of localization instruments, Bauer et al. established the noise in the bearings taken from a HTC Vive HMD, controller and

tracker in different locations in a horizontal planar space, using one second generation HTC Vive lighthouse base station. The standard deviation of the noise in x-y location in the planar space measured at a distance of 1.8 [m] from the lighthouse at unknown elevation over the planar space, ranged between 0.1 - 0.5 [mm], which corresponds to a standard deviation of noise in the measured bearing angle in the range $5.5 – 27.8$ $[10^{-5}$ rad$]$ [76]. The measurements by Bauer et al. enabled four more relevant observations:

1. The noise measured is non-isotropic and is strongest in the direction of the line of sight between the lighthouse and the tracked object. In the direction perpendicular to the line of sight, the magnitude of the noise is two to three times smaller, which corresponds to the notion that movements of objects perpendicular to the line of sight are easier to spot than movements in the direction of the line of sight.

2. Application of a second lighthouse in a setup where the lines of sight of the two lighthouses intersect at angles in the range of $\pi/4 – 3\pi/4$ [rad] over the tracked objects, effectively eliminates the anisotropy of the noise in the bearings taken from the objects. Operation with two lighthouses reduces the standard deviation to the lowest level of noise observed using one lighthouse, which is the noise in the direction perpendicular to the line of sight between lighthouse and tracked object.

3. The magnitude of noise in the x-y location in the planar space established with one lighthouse is proportional with the distance to the lighthouse base station. This implies that the noise in the measured bearing angle is independent from the distance to the lighthouse. For the Vive tracker Bauer et al. measure noise levels at 3.2 $[10^{-4}$ rad$]$ in the direction of the line of sight when using one lighthouse and 2 $[10^{-5}$ rad$]$ in perpendicular direction. Using two lighthouses the noise level measured by Bauer et al. ranges between $2 – 12$ $[10^{-6}$ rad$]$. This is in good agreement with the estimate from Greiff [73].

4. The noise level correlates inversely to the number of light sensors mounted on the tracked object. The standard deviation of the noise in the measured bearing angle increases when using a tracker with 22 light sensors instead of the HMD unit with 31 sensors. The set of experimental data for different trackers is too sparse to characterize the correlation, but in

principle the standard deviation should be inversely proportional to the number of sensors on the tracker as expressed by Equation (2.4).

Using a single lighthouse base station from the Vive-kit to locate a Vive tracker, Bauer et al. measured a mean accuracy of 5.4 mm over an operating range of about 4×4 meter centered 4 meter ahead of the lighthouse at unknown elevation. Adding a second lighthouse in a location with a line of sight to the center of the operating range perpendicular to the line of sight of the other lighthouse, improves the accuracy to 3.5 mm [76].

Jansen et al. measured the location and orientation of two stationary lighthouse base stations separated by a distance between 1 and 4 meters, using their own tracker with 32 light sensors at a distance of 2 to 6 meter from the lighthouses [70]. Jansen et al. report a localization accuracy of a few cm and a precision around 1 cm. Sletten observed a localization accuracy at millimeter scale when using an unknown number of lighthouses while moving a HTV Vive hand tracker over a 300 mm distance at an unreported distance from the lighthouses [74].

2.7 Observations and conclusions from the literature review

In Section 1.4.1 the scope of the present research has been set around the localization of a mobile platform for laser cutting and engraving. The literature review conducted within this scope has three main topics of focus.

1. Formulation of criteria for adoption of a mobile platform for laser cutting and engraving
2. Odometry with optical flow sensors
3. Absolute location measurement with a laser lighthouse

The observations and conclusions below summarize the information found in the literature on each topic as well as the gaps in the knowledge that need to be filled by additional research and analysis.

1. **Formulation of criteria for adoption of a mobile platform for laser cutting and engraving**

   1.1. Criteria for adoption are derived to judge the feasibility of a localization system for a mobile platform for laser cutting and engraving. It is observed that the main measure of quality for parts that are cut from sheet material are "manufacturing tolerances" that should not exceed the "allowable manufacturing tolerances". After consultation of engineering practices in a number of industries a benchmark has been formulated for the "allowable manufacturing tolerances" at a ball park figure of 0.1% of the parts' maximum dimension, for the scope of the present research project.

   1.2. A concept for a design of a suspension of the toolhead on a mobile platform is outlined, that enables interpretation of the allowable manufacturing tolerances into requirements for the localization of the mobile platform and the toolhead of the laser cutter.

   1.3. A qualitative analysis is made of the relation between the make up of a laser cutter and the dimensional accuracy of a laser cut part, comparing suspension of the toolhead on a gantry based flatbed laser cutter with suspension on a mobile platform. The analysis allows for the following observations:

   - The analysis puts the focus strongly on localization of the mobile platform as the subject of interest. The key to competitive deployment of a mobile platform that supports the laser cutter to operate within the allowable manufacturing tolerances is the accuracy and precision of the measurement of location and orientation of the mobile platform.
   - A mobile platform with a localization system can have an advantage over a

gantry based flatbed machine in limiting manufacturing tolerances of parts cut from sheet material with increasing size of the sheets to be processed.

1.4. The proven practice to localize a mobile platform is the use of data fusion of displacement measurements and measurement of the absolute location of the platform. To enable a mobile platform to cut parts within specified dimensional tolerances using a similar localization system using a combination of multiple measurement systems, the accuracy of the location of the platform established with each measurement system separately has to be better than the specified tolerances.

2. **Odometry with optical flow sensors**

Complying with the proven practice to use a combination of odometry and absolute location measurement to establish location and orientation of the mobile platform for laser cutting, optical flow sensors as used in computer mice have been selected to measure the displacement of the platform, because of their potential as suitable, non-tactile, high resolution, low cost displacement sensors. Previous research of application of optical flow sensors for odometry has highlighted the following observations:

2.1. The sensitivity of state of the art optical flow sensors is at micron level, matching the resolution of wheel encoders[1].

2.2. The precision of the odometry of a mobile platform using optical flow sensors depends on the sensitivity of the sensors used and is inversely proportional to the number of sensors installed [Section 2.5.3].

2.3. The accuracy of the displacement of a mobile platform measured with optical flow sensors depends on the accuracy of the sensor location and the timing of the sensor measurements used to estimate the displacement of the mobile platform [Section 2.5.3].

2.4. The orientation of the sensors has no consequences for the sensibility the odometry system with optical flow sensors [39].

2.5. The best distribution of the sensors is in a regular polygonal arrangement around the geometrical center of mobile platform [31, 39].

The previous research has left the following gaps in the analysis of odometry with optical flow sensors that are addressed by the present research described in Chapter 3.

- No method to measure the sensitivity of optical flow sensors has been found in the open literature, neither any analysis of the propagation of errors in the sensitivity into the estimated location of a mobile platform.
- Timed (coincident) data acquisition using optical flow sensors has not received any attention at all.
- The previous approaches to measure the locations of optical flow sensors in a mobile platform are not satisfactory. The method proposed by Kim and Kim requires a separate highly accurate calibration system [38]. The method from Hu et al. entails an accurate figure for the distance between at least two sensors on the mobile platform, which is difficult to obtain without using metrological instruments [37].

3. **Absolute location measurement with a laser lighthouse**

   To measure the location and orientation of a mobile platform for laser cutting, a recent implementation of the laser lighthouse has been selected. In concept, the lighthouse system provides a localization system that requires a minimum of only one active landmark to enable a rigid body equipped with at least three light sensors in known locations on the body, to determine its own location and orientation relative to the lighthouse. The literature review of the laser lighthouse concept has produced the following observations:

   3.1. By principle the lighthouse system can never excite all sensors on a mobile platform coincidentally[5]. If the mobile platform is moving, the sensors on it move in the sweep of the light sheet too. As a consequence the location and orientation of the platform calculated from the measured locations of the light sensors become more inaccurate the faster the platform moves.

   3.2. Measurement tests indicate that the noise (jitter) in angular bearings of light sensors measured with one HTC-Vive lighthouse base station is in the range 5.5 – 27.8 $[10^{-5}$ rad$]$. The noise observed using one base station is non-isotropic and is strongest in the direction of the line of sight between the lighthouse and the

tracked object. In the direction perpendicular to the line of sight, the magnitude of the noise is two to three times smaller [76].

3.3. Application of a second lighthouse effectively eliminates the anisotropy of the noise in the bearings taken from the light sensors. Operation with two lighthouses reduces the noise to the lowest level observed using one lighthouse [76]. Independent analysis of the HTC Vive system yielded estimates for the angular noise of an order of magnitude of 3 $[10^{-5}$ rad$]$ when operating two lighthouses [73].

3.4. The highest accuracy obtained with a single base station lighthouse to locate a stationary HTC-Vive tracker using the software included in the HTC-Vive VR-Kit is 5.4 mm in a 4×4 meter workspace centered 4 meter ahead of the lighthouse [76]. The highest accuracy for two base stations in the same workspace is 3.5 mm [76] and below 2 mm in a workspace between two base stations at a distance of 4 m[5].

3.5. The angular noise is independent from the distance to the lighthouse [76].

3.6. The angular noise correlates inversely to the number of light sensors mounted on the tracked object [76]. According to the analysis made for optical flow sensors in Section 2.5.3, the angular noise level is expected to be inversely proportional to the number of sensors on the tracker as expressed by Equation (2.4).

The conclusions are very encouraging in perspective of the feasibility case presented in Section 2.2:

- Conclusion 3 indicates that the noise level of the location of a mobile platform obtained with a single lighthouse is below the maximum allowable manufacturing tolerance. This can be considered a necessary condition to any localization system for a mobile platform for manufacturing.
- Conclusion 5 indicates that an out of the box HTC-Vive kit already demonstrates an accuracy of the required order of magnitude: 5.4 mm in a workspace with a $4\sqrt{2}$m diagonal.
- Conclusion 6 supports the assumption made in Section 1.3, that the error of localizing a mobile platform is linear with the distance to the reference beacons for navigation.

For the lighthouse system this beacon is the lighthouse base station.

At the same time no analysis has yet been published on systematic errors in the lighthouse system and their propagation into the location obtained for a mobile platform using the system. This is the focus of Chapter 4.

Chapter 3

Odometry with optical flow sensors

3.1 Introduction

The literature review in Chapter 2 concluded with the observation that optical flow sensors as used in computer mice have potential as suitable, non-tactile, high resolution, low cost displacement sensors. For this reason optical flow sensors are selected for further research into their application to measure the displacement of a mobile platform. The research described in this chapter follows up on the gaps found in the previous research published in the open literature:

- It has been observed that the sensitivity of optical flow sensors is dependent on multiple factors including the height at which the sensor is mounted over the floor sensor and the optical properties of the floor surface such as reflectiveness and transparency. For this reason it is highly advisable to measure the sensitivity of each sensor, on each new surface it is applied to. However, in spite of its simplicity, no method to measure the sensitivity of optical flow sensors has been found in the open literature, nor any analysis of the propagation of errors in the sensitivity into the estimated location of a mobile platform.
- Neither has any attention been given to the timing aspects of data acquisition with optical flow sensors in the open literature.

- Previous approaches to measure the locations of optical flow sensors on a mobile platform are not satisfactory as they rely on a separate calibration system or on a measurement of the distance between two optical flow sensors which is very difficult to obtain.

The sensitivities of the optical flow sensors and their orientation and location on the mobile platform are cardinal parameters in the kinematic model used to establish the displacement and rotation of the platform from the displacement measured by the sensors. The present chapter introduces new and improved methods to determine the magnitude of these parameters. The first experiment and only hand measurement that has to be performed is the setup of a path of a set length to measure the sensors' sensitivities. The sensitivities are required for the measurement of the orientation and location of all optical flow sensors on the mobile platform. The orientation and location of the sensors are measured by swiveling the mobile platform around a fixed anchor point, without any prior knowledge of the location of the sensors or the anchor point. By forcing the platform to travel over arcs of constant radius, the orientation and location of the sensors can be derived directly from the displacement measured by each sensor, using a model of the kinematics of the swivel motion. Since the anchor point is stationary in each experiment, its displacement as calculated with the measured values of the parameters of the odometry system directly reflects the measurement error of the location and orientation of the mobile platform and can serve as a validation for the measurement.

This approach is innovative in the following four aspects:

1. It requires only one measurement to set the length of a straight path to calibrate the sensor sensitivities. Orientations and locations of the sensors on the mobile platform can be derived subsequently from the displacements measured by the optical flow sensors on the mobile platform in the swivel experiments. This makes design of the experiments highly suitable to be implemented as a self-calibration procedure.

2. Orientation of the sensors on the mobile platform is derived from the measurement data directly, independent of the determination of the location of the sensors on the platform. With the orientations resolved, the locations of sensors can be established from the same dataset. In the approach by Hu et al. all parameters are established in one brute force numerical root finding operation [37].

3. Validation of the measurements through calculation of the displacement of the anchor point can again use the same dataset acquired for the measurement of the sensor orientation and locations. The deviation of the anchor point calculated from this dataset defines an unambiguous measure to validate the previous measurements of the sensor locations and orientations. The use of an anchor point as reference point for validation can be extended to compare the performance of different mobile platforms and navigation systems.

4. The micro controller based measurement system developed for this project implements synchronization of the data acquisition by multiple optical flow sensors over a data bus (I^2C) without requiring additional hardware. No other sources elaborating the synchronization of the data collection by multiple optical flow sensors have been found in the open literature.

Chapter 3 is organized as follows: after an introduction to odometry with optical flow sensors in Section 3.2, comprising an analysis of precision and error propagation in the odometry, Section 3.3 elaborates the experimental designs for the measurement of the sensitivity of the sensors and their orientation and location in the mobile platform. Section 3.4 describes the experimental setup with which the measurement data are collected, including the measurement system that secures proper synchronization of the data acquisition from all optical flow sensors. Section 3.5 reports the execution of the experiments performed to collect the measurement data as well as the outcomes of the processing of the data: the sensitivity of the sensors and their orientation and location in the mobile platform. The outcomes are validated with calculations of the path of the mobile platform in Section 3.6. Section 3.7 completes Chapter 3 with a summary of the findings and improvements in the conclusions.

3.2 Odometry with optical flow sensors

The square in Fig. 3.1 referred to as "Frame B", represents the contour of a mobile platform with coordinate system ${}^{B}x - {}^{B}y$, with its origin B_o in the geometrical center of B and n optical flow sensors o_i with their apertures at locations ${}^{B}o_i = {}^{B}[o_{i,x}\ o_{i,y}]^T, i \in (1,..,n)$. Frame B moves in a fixed planar space referred to as Frame C, spanned by coordinate system ${}^{C}x - {}^{C}y$ with its

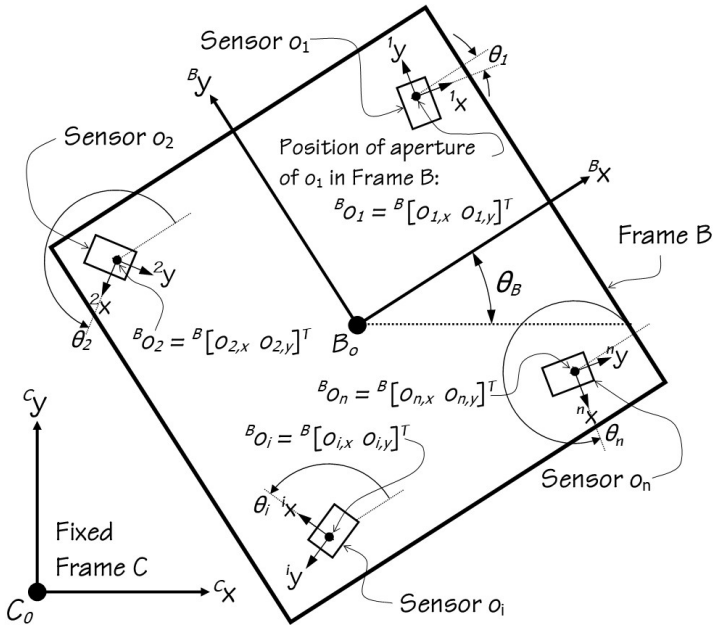

Figure 3.1: *Contour of a mobile platform (Frame B) with optical flow sensors and corresponding coordinate systems.*

origin C_o in a chosen location. The pose of Frame B in Frame C is determined by the location ${}^CB_o$ of origin B_o in Frame C and by the orientation of Frame B in Frame C, represented by θ_B, the angle between axes ${}^Bx$ and ${}^Cx$. Each optical flow sensor o_i has its own coordinate system ${}^ix - {}^iy$ with its origin in point ${}^Bo_i$ in the center of the aperture of the sensor. The orientation of the sensor in the mobile platform coordinate Frame B is represented by θ_i, the angle between ${}^ix$ and ${}^Bx$. Whereas the pose of a sensor in Frame B as expressed by ${}^Bo_i$ and θ_i is always fixed, the pose of Frame B in Frame C as expressed by ${}^CB_o$ and θ_B changes as the consequence of Frame B's motion. The motion of Frame B is computed as a translation of its origin $\Delta B_o = {}^B[\Delta B_{o,x}\ \Delta B_{o,y}]^T$ and a rotation of angle $\Delta\theta_B$ of the mobile platform around its center in origin B_o. This computation and the subsequent update of the pose of the Frame B in Frame C occurs at the end of each sampling time interval in which the optical flow sensors have recorded their displacements $\Delta^i o_i = {}^i[\Delta o_{i,x}\ \Delta o_{i,y}]^T$. During a sampling time interval the pose of the mobile platform is considered fixed. The relationship between the displacement of the optical flow sensors and the motion of Frame B is derived from the inverse kinematic relationship between the displacement of the sensors as a consequence of motion of Frame B. This relationship can be conveniently expressed in the coordinate system of Frame B as it is fixed

over the period of a sample time interval. The translation of Frame B translates sensor o_i on Frame B over an identical path: $\Delta^B o_i = \Delta B_o$. A rotation of Frame B over angle $\Delta\theta_B$ around its center B_o, causes sensor o_i to move from its location ${}^B o_i$ to location ${}^B o_i' = R_2^T(\Delta\theta_B)\,{}^B o_i$. The transpose matrix $R_2^T(\Delta\theta_B)$ is the transformation matrix for a planar rotation of an object over an angle $\Delta\theta_B$ in a fixed coordinate frame. R_2^T also is the inverse of the rotation matrix R_2 which transforms the coordinates of a fixed object when the coordinate system rotates over an angle θ:

$$R_2(\theta) = \begin{bmatrix} \cos(\theta) & \sin(\theta) \\ -\sin(\theta) & \cos(\theta) \end{bmatrix}$$

The displacement $\Delta^B o_i(\Delta\theta_B)$ of sensor o_i as the consequence of the rotation over angle $\Delta\theta_B$ is the difference in location $\Delta^B o_i$ before and after the rotation:

$${}^B o_i' - {}^B o_i = \left(R_2^T(\Delta\theta_B) - I_2\right){}^B o_i \tag{3.1}$$

Under the condition that $\Delta\theta_B$ is sufficiently small, the following first order approximations can be applied to Equation (3.1):

$$\lim_{\Delta\theta_B \to 0} \sin(\Delta\theta_B) = \Delta\theta_B \;,\; \lim_{\Delta\theta_B \to 0} \cos(\Delta\theta_B) = 1 \tag{3.2}$$

This simplifies Equation (3.1) for an infinitesimally small rotation $\Delta\theta_B$ to:

$$\lim_{\Delta\theta_B \to 0} \Delta^B o_i(\Delta\theta_B) = R_2(\text{-}\pi/2)\,{}^B o_i\,\Delta\theta_B$$

$R_2(\text{-}\pi/2)$ is the rotation matrix $R_2(\theta)$ for $\theta = \text{-}\pi/2$.

The total displacement $\Delta^B o_i$ of sensor o_i for any infinitesimally small displacement of Frame B, comprising a translation ΔB_o of the frame center B_o and a rotation $\Delta\theta_B$ around B_o is:

$$\Delta^B o_i = \Delta B_o + \Delta^B o_i(\Delta\theta_B) = \Delta B_o + \Delta\theta_B\, R_2(\text{-}\pi/2)\,{}^B o_i \tag{3.3}$$

The result can be expressed as a displacement $\Delta^i o_i$ in the sensor coordinate frame o_i by planar

space transformation:

$$\Delta^i o_i = R_2(\theta_i)\ \Delta^B o_i \tag{3.4}$$

Combining Equations (3.3) and (3.4) yields:

$$\Delta^i o_i = R_2(\theta_i)\ {}^B A_{o_i}\ \Delta^B \Theta_B \tag{3.5}$$

where

$$\Delta^B \Theta_B = [\Delta B_o \mid \Delta\theta_B]^T = {}^B[\Delta B_{o,x}\ \Delta B_{o,y}\ \Delta\theta_B]^T$$

and

$${}^B A_{o_i} \in \mathbb{R}^{2\times 3}, \quad {}^B A_{o_i} = [I_2 \mid R_2(\text{-}\pi/2)\ {}^B o_i]$$

Similarly, the sensor displacement in Frame o_i is related to the sensor displacement $\Delta^C \Theta_B = {}^C[\Delta B_{o,x}\ \Delta B_{o,y}\ \Delta\theta_B]^T$ in Frame C through:

$$\Delta^i o_i = R_2(\theta_B)\ R_2(\theta_i)\ {}^C A_{o_i}\ \Delta^C \Theta_B$$

where:

$${}^C A_{o_i} \in \mathbb{R}^{2\times 3}, \quad {}^C A_{o_i} = [\ I_2 \mid R_2(\text{-}\pi/2)\ R_2(\text{-}\theta_B)^B o_i\ ]$$

Since ${}^B A_{o_i}$ is independent of the orientation of Frame B in Frame C, Equation (3.5) is the preferred expression to be expanded into a system of n pairs of linear equations for n sensors. The superscript B is dropped in this expansion.

$$\Delta O_n = R_2(\theta_n)\ A_n\ \Delta\Theta_B \tag{3.6}$$

where $\Delta O_n \in \mathbb{R}^{2n}$ is the vector of displacements registered by all sensors in their own coordinate system, $A_n \in \mathbb{R}^{2n\times 3}$ the aggregation of all matrices A_{o_i} and $R_2(\theta_n)$ is the aggregation of the rotation matrices $R_2(\theta_i)$ of all sensors o_i in Frame B:

$$\Delta O_n = [\Delta^1 o_1 \mid .. \mid \Delta^i o_i \mid .. \mid \Delta^n o_n]^T$$

$$A_n = [A_{o_1} \mid .. \mid A_{o_i} \mid .. \mid A_{o_n}]^T$$

$$R_2(\theta_n) = \text{diag}(R_2(\theta_{o_1}) .. R_2(\theta_{o_n})) = \begin{pmatrix} R_2(\theta_{o_1}) & & 0 \\ & \ddots & \\ 0 & & R_2(\theta_{o_n}) \end{pmatrix}$$

Equation (3.6) can be used to calculate an ordinary least squared estimator $\Delta\widetilde{\Theta}_B$ for the displacement of Frame B in coordinate frame B, when at least three independent displacement figures, comprising $\Delta^i x$ and $\Delta^i y$ are available from the optical flow sensors. The resulting optimal (least squares) estimator for $\Delta\Theta_B$ can be calculated for coordinate frame B [79]:

$$\Delta\widetilde{\Theta}_B = A_n^+ R_2^T(\theta_n)\, \Delta O_n \tag{3.7}$$

A_n^+ is the pseudo inverse of A_n:

$$A_n^+ = (A_n^T A_n)^{-1} A_n^T$$

3.2.1 Precision and Error propagation in odometry with optical flow sensors

The precision of the estimation of the displacement according to Equation (3.7) depends on the three factors sensor sensitivity, sensor location and timing of the sensor measurements.

1. **Sensor sensitivity**

   As was mentioned in Section 2.5.1, it has been observed by several researchers that the sensitivity of optical flow sensors tends to be inconsistent. The sensitivity of sensor o_i, referred to as f_i is the ratio between the reading from the sensor in pixels $\Delta^i o_{p,i}$ when o_i travels over a dimensional distance $\Delta^i o_i$ in any direction[7]: $f_i = \Delta^i o_{p,i} / \Delta^i o_i$. Since the sensitivity depends on factors that can vary between the sensors, such as the distance between the sensor aperture and the floor surface, on the optical properties of the surface such as reflectiveness and transparency and on properties of the sensor's motion trajectory such as velocity and curvature, each sensor has its own sensitivity f_i and error δf_i in the

conversion from measured data in pixels $\Delta^i o_{p,i}$ to dimensional displacement $\Delta^i o_i$. The sensitivities of all sensors o_i, $i \in (1, .., n)$ on a mobile platform can be captured in a list f_O:

$$f_O = [f_1, .., f_n] = [\Delta^1 o_{p,1}/\Delta^1 o_1 \; .. \; \Delta^i o_{p,i}/\Delta^i o_i \; .. \; \Delta^n o_{p,n}/\Delta^n o_n]^T$$

the sensitivities are used to convert the measured displacements in pixels to dimensional displacement ΔO_n, through:

$$\Delta O_n = [\Delta^1 o_{p,1}/f_1 \; .. \; \Delta^i o_{p,i}/f_i \; .. \; \Delta^n o_{p,n}/f_n]^T \tag{3.8}$$

Defining a vector $\Delta O_{p,n}$, collecting the sensor readings in pixels $\Delta^i o_{p,i}$ for all n sensors,

$$\Delta O_{p,n} = [\Delta^1 o_{p,1} \; .. \; \Delta^i o_{p,i} \; .. \; \Delta^n o_{p,n}]^T$$

Equation (3.8) can be rewritten as:

$$\Delta O_n = \Delta O_{p,n} \; \mathrm{diag}(1/f_O) \tag{3.9}$$

with:

$$\mathrm{diag}[1/f_O] = \mathrm{diag}[1/f_1 \; .. \; 1/f_n]$$

The propagation of δf_i into the calculated displacement of the mobile platform $\Delta\widetilde{\Theta}_B$, is estimated by computation of a relative condition number $\kappa(\Delta\widetilde{\Theta}_B, f_O)$. $\kappa(\Delta\widetilde{\Theta}_B, f_O)$ is the ratio between norms of the relative errors of $\Delta\widetilde{\Theta}_B$, expressed as $\delta[\Delta\widetilde{\Theta}_B]/\Delta\widetilde{\Theta}_B$ and of f_O, expressed as $\delta f_O/f_O$ [80]. $\kappa(\Delta\widetilde{\Theta}_B, f_O)$ is derived from the relationship between $\Delta\widetilde{\Theta}_B$ and f_O, through:

$$\kappa(\Delta\widetilde{\Theta}_B, f_O) = \lim_{\epsilon \to 0} \sup_{\|\delta f_O\| \leqslant \epsilon} \frac{\|\delta[\Delta\widetilde{\Theta}_B]\|/\|\Delta\widetilde{\Theta}_B\|}{\|\delta f_O\|/\|f_O\|} = \frac{\|f_O\|}{\|\Delta\widetilde{\Theta}_B\|} \left\| \frac{\partial \Delta\widetilde{\Theta}_B}{\partial f_O} \right\| \tag{3.10}$$

Inserting Equation (3.9) in (3.7), the Jacobian $\partial\Delta\widetilde{\Theta}_B/\partial f_O$ in Equation (3.10), can be

elaborated into:

$$\frac{\partial \Delta\widetilde{\Theta}_B}{\partial f_O} = A_n^+ \, \Delta O_{p,n} \, \frac{\partial (1/f_O)}{\partial f_O} = A_n^+ \, \Delta O_{p,n} \, \mathrm{diag}(-1/f_O^2) = -\Delta\widetilde{\Theta}_B \, \mathrm{diag}(1/f_O) \quad (3.11)$$

From Equation (3.11) a constraint is derived for $\|\Delta\widetilde{\Theta}_B\|$:

$$\|\Delta\widetilde{\Theta}_B\| = \|-\Delta\widetilde{\Theta}_B\| = \|\frac{\partial \Delta\widetilde{\Theta}_B}{\partial f_O} \, \mathrm{diag}(f_O)\| \leqslant \|\frac{\partial \Delta\widetilde{\Theta}_B}{\partial f_O}\| \, \|\mathrm{diag}(f_O)\|$$

Consequently:

$$\kappa(\widetilde{\Delta^B\Theta_B}, f_O) \leqslant 1$$

Hence the propagation of a relative error in the sensitivity of the optical flow sensors is constrained to the same relative error in the calculated displacement of the mobile platform.

2. **Sensor location and orientation**

Additional analysis of matrix A_n in Equation (3.6) reveals consequences of the choice of the locations ${}^B o_i$, $i \in (1, .., n)$ of the optical flow sensors on Frame B for the odometry with the sensors. Matrix A_n defines the kinematic relationship between the displacement observed by the optical flow sensors s_i and the displacement and rotation of the center of Frame B. In order for the odometry system using the optical flow sensors to have maximum sensibility, small displacement and rotations of Frame B should translate into displacements of the sensors as large as possible, to enable the system to properly detect small movements of Frame B. This can be achieved by maximizing the norm of the product $R_2(\theta_n) \, A_n$ in Equation (3.6). The term $R_2(\theta_n)$ in this product is the aggregation of the rotation matrices of the sensors and does not change the norm of the product with matrix A_n. Physically this implies that the orientation of the sensors has no consequences for the sensibility the odometry system with the optical flow sensors. Their orientation can be determined by practical considerations which is assumed to be in alignment with the coordinate system of Frame B for computational convenience: $\theta_i = 0$, $i \in (1, .., n)$ and $R_2(\theta_n) = I_{2n}$. Hence the sensibility of the odometry system is determined by the norm $\|A_n\|$ of matrix A_n. $\|A_n\|$ is expressed by its largest singular value w_n. Inspection of the elements of matrix A_n in Equation (3.5) indicates that $\|A_n\|$ is governed by the

sensor locations ${}^{B}o_i, i \in (1,..,n)$. The choice of the sensor locations on Frame B allows to maximize w_n and the sensibility of the odometry system as a consequence.

Defining O_n as the vector of locations of the optical flow sensors ${}^{B}o_i, i \in (1,..,n)$, the relative condition number $\kappa({}^{B}\Theta_B, O_n)$ has to be observed to prevent strong propagation of errors $\delta\Delta O_n$ in the displacement ΔO_n measured by the optical flow sensors into errors $\delta\Delta{}^{B}\Theta_B$ in the calculated displacement and rotation $\Delta{}^{B}\Theta_B$ of Frame B. $\kappa({}^{B}\Theta_B, O_n)$ is derived from Equation (3.6) using the maximum singular value of the matrices again to represent the norm the matrices involved:

$$\kappa({}^{B}\Theta_B, O_n) = \frac{\|\delta\Delta{}^{B}\Theta_B\|}{\|\Delta{}^{B}\Theta_B\|} / \frac{\|\delta\Delta O_n\|}{\|\Delta O_n\|} = \frac{\|\Delta O_n\|}{\|\Delta{}^{B}\Theta_B\|} \frac{\|\delta\Delta{}^{B}\Theta_B\|}{\|\delta\Delta O_n\|} = \|A_n\|\|A_n^{-1}\| = \frac{w_n}{w_1}$$

where w_1 is the smallest singular value of matrix A_n and consequently w_1^{-1} is the largest singular value of matrix A_n^{-1}.

3.3 Measurements of sensor sensitivity, location and orientation

This section introduces an new approach to measure the location and orientation of an optical flow sensor in a mobile platform that can be implemented as a self calibration procedure. The measurement of the location and orientation of the sensor is preceded by the description of a simple procedure to measure the sensor sensitivity.

3.3.1 Experimental design for measurement of the sensor sensitivity

Sensitivity refers here to the ratio between the reading from the optical flow sensor (mostly referred to as "number of pixels") and the corresponding distance (in meters) it moves on the surface. Consequently its unit is "pixels per meter" (ppm).

It has been observed that the sensor sensitivity is strongly dependent on the height of the sensor relative to the surface [21, 29, 30]. The easiest way to measure the sensitivity of the optical sensors is illustrated in Fig. 3.2. The mobile platform with sensors is moved in a straight

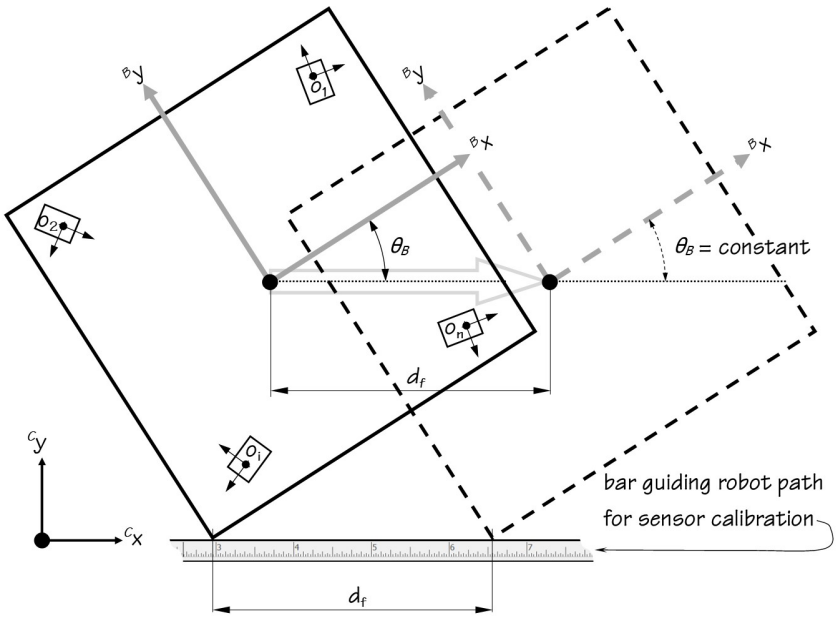

Figure 3.2: *Motion of the mobile platform to measure the sensor sensitivities* $f_i, i \in (1, 2, .., n)$.

line over a known distance d_f without rotating it, while recording the displacement in pixels $\Delta^i o_{p,i}$ as registered by the optical flow sensors o_i: $\Delta^i o_{p,i} = {}^i[\Delta o_{p,i,x}\ \Delta o_{p,i,y}]^T$.

The sensitivity f_i of the sensor o_i is given by

$$f_i = \frac{1}{d_f}\sqrt{(\Delta^i o_{p,i,x})^2 + (\Delta^i o_{p,i,y})^2} \tag{3.12}$$

Since it is independent to the motion direction of the sensor, according to the manufacturers specification[7], the solution of Equation (3.12) applies to any direction in which the sensor is moved, as long as it is in a straight line.

3.3.2 Experimental design for the measurement of the sensor location (location and orientation)

In this section it is assumed that the sensor sensitivities $f_i, i \in (1, 2, .., n)$ are available through the simple measurement procedure described in the previous Section 3.3.1 and that the sensors are mounted in alignment with Frame B: $\theta_i \approx 0$. No other information of the mobile platform or sensors is required.

The experimental procedure to determine the location ${}^B o_i$ of an optical flow sensor o_i

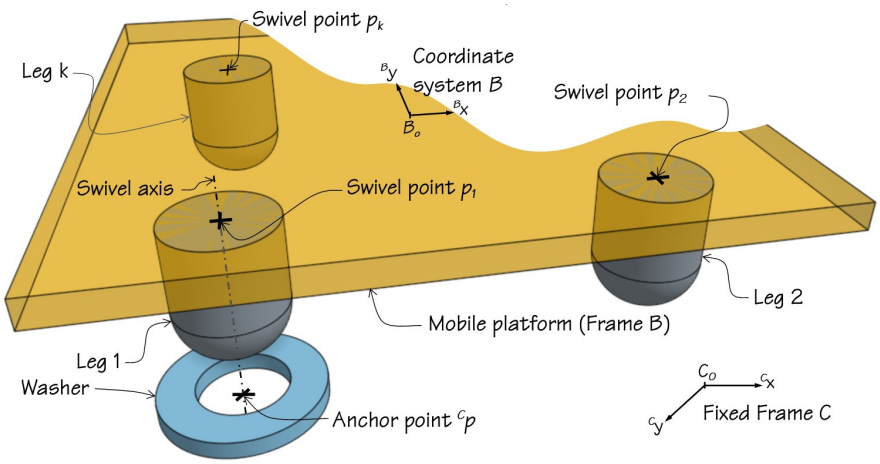

Figure 3.3: *Illustration of anchor point ${}^Cp$, swivel points $p_k, k \in (1, 2, .., n_k)$ and the alignment of ${}^Cp$ and p_1 at the swivel axis.*

on the mobile platform (Frame B) requires the presence of multiple swivel points p_k on the platform. For this purpose the platform used in the present research is equipped with short legs as illustrated in Figure 3.3. The legs act as swivel points $p_k,\ k \in (1, 2, .., n_k)$ of the mobile platform by turning Frame B around the leg held in place in anchor point ${}^Cp$ on a fixed, flat surface C. Surface C is spanned by planar coordinate system C with its origin in C_o. The location of the leg acting as swivel point is referred to as ${}^Bp_k$ in Frame B. When swiveling Frame B around ${}^Bp_k$, the swivel point ${}^Bp_k = {}^B[p_{k,x}\ p_{k,y}]^T$ is aligned with anchor point ${}^Cp$ at the swivel axis in fixed position ${}^Cp = {}^C[p_x\ p_y]^T$, as shown in Figure 3.3 for ${}^Bp_1$. The locations of the swivel points ${}^Bp_k$ and the sensors ${}^Bo_i = {}^B[o_{i,x}\ o_{i,y}]^T$ in Frame B are unknown.

Figure 3.4 depicts the mobile platform in starting position and in a position swiveled around p_k over an angle α_k. Sensor o_i travels the arc-shaped path A_{ki} in the swivel motion between these positions. Path A_{ki} is recorded by o_i as a displacement $\Delta^i o_i = {}^i[\Delta o_{i,x}\ \Delta o_{i,y}]^T$. This displacement can be transformed to coordinates of Frame B as ${}^B\Delta o_i = R_2(-\theta_i)\ \Delta^i o_i$. Path A_{ki} starts off in a direction at an angle β with the ${}^By$-axis. The same angle β occurs between the (radius) vector $\overrightarrow{p_k\, o_i}$ from p_k to o_i, and the ${}^Bx$-axis. The following geometric relations can be observed between these measures:

$$\|A_{ki}\| = \alpha_k\ \|\overrightarrow{p_k\, o_i}\| \tag{3.13}$$

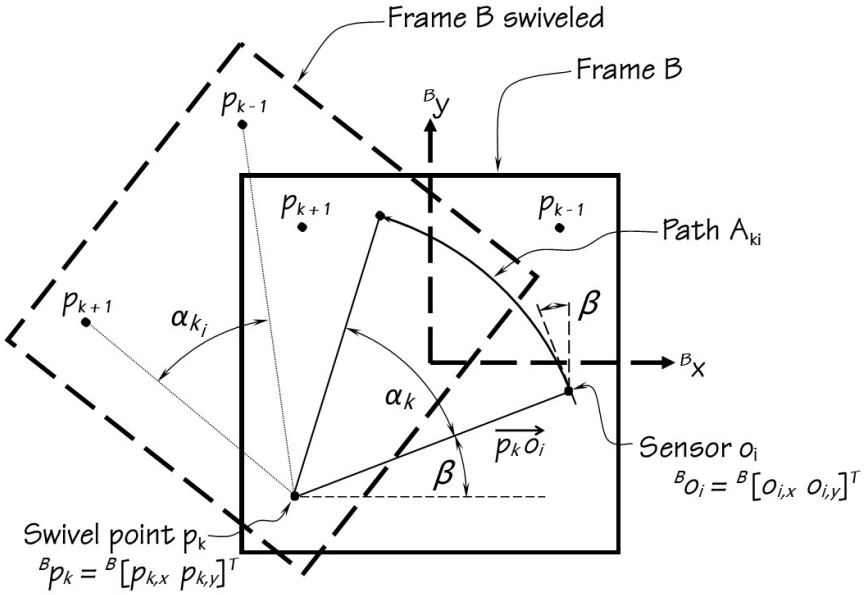

Figure 3.4: *Mobile platform (Frame B) swiveling over angle α_k.*

and:

$$^B\begin{bmatrix}\Delta o_{i,x}\\ \Delta o_{i,y}\end{bmatrix} = \|A_{ki}\| \begin{bmatrix}\sin(\beta)\\ \cos(\beta)\end{bmatrix} \tag{3.14}$$

From Equation (3.13) and (3.14), it follows that:

$$\overrightarrow{p_k\, o_i} = \|\overrightarrow{p_k\, o_i}\| \begin{bmatrix}\cos(\beta)\\ \sin(\beta)\end{bmatrix} = \frac{1}{\alpha_k} R_2(\pi/2 - \theta_i)\Delta^i o_i \tag{3.15}$$

Hence, the location of the sensor o_i can be established as:

$$^B o_i = {}^B[o_{i,x}\ o_{i,y}] = p_k + \overrightarrow{p_k\, o_i} = p_k + \frac{1}{\alpha_k} R_2(\pi/2 - \theta_i)\ \Delta^i o_i \tag{3.16}$$

p_k, α_k and θ_i can be solved by imposing rigid body and matching swivel point conditions on the displacements measured. To apply these conditions the experiment has to be repeated for multiple swivel points $p_k,\ k \in (1, 2, .., n_k)$, with their locations distributed in a polygonal arrangement over the mobile platform. The swivel angle α_k at which the frame is rotated in each swivel experiments should span π minus the internal angle α_{k_i} between lines connecting the actual swivel point p_k with the preceding and following swivel points p_{k-1} and p_{k+1}. Under

this condition, the sum of all swivel angles α_k is equal to $n_k\,\pi$ minus the sum of the internal angles in a n_k-sided polygon: $(n_k - 2)\,\pi$.

$$\sum_{k=1}^{n_k} \alpha_k = n_k\,\pi - (n_k - 2)\,\pi = 2\,\pi \tag{3.17}$$

- **Application of rigid body condition**

  With measurement data acquired for the displacement of all optical flow sensors $\Delta^i o_i, i \in (1, 2, .., n)$, the angles θ_i at which sensors o_i are mounted on Frame B can be estimated by application of the rigid body condition [37]. A consequence of the rigid body condition is that the distance between two points on a rigid body remains the same in any motion of the body. For small displacements $\Delta\, o_i$ and $\Delta\, o_j$ measured by sensors o_i and o_j on the rigid body of a mobile platform, this condition implies that the displacements comply with the following constraint:

$$\Delta\, o_i^T\ \overrightarrow{o_i\, o_j} \approx \Delta\, o_j^T\ \overrightarrow{o_i\, o_j} \tag{3.18}$$

  In practice, there is be a difference ε_{ij} between the left and right hand side of Equation (3.18):

$$\varepsilon_{ij} = (\Delta\, o_i^T\ - \Delta\, o_j^T)\ \overrightarrow{o_i\, o_j} \tag{3.19}$$

  $\overrightarrow{o_i\, o_j}$ can be elaborated in coordinate system B by substitution of o_i and o_j with the expressions for ${}^B o_i$ and ${}^B o_j$ from Equation (3.16):

$${}^B[\overrightarrow{o_i\, o_j}] = {}^B o_j - {}^B o_i = \frac{1}{\alpha_k}\ R_2(\pi/2)\ [R_2(-\theta_j)\ \Delta^j o_j - R_2(-\theta_i)\ \Delta^i o_i] \tag{3.20}$$

  Equation (3.19) can be expanded by insertion of Equation (3.20) for $\overrightarrow{o_i\, o_j}$. The measured displacements $\Delta^i o_i$ and $\Delta^j o_j$ applied in Equation (3.20) to determine $\overrightarrow{o_i\, o_j}$ cannot be the same measurements of displacements Δo_i and Δo_j used in Equation (3.19). Usage of the same measurements results in a trivial solution. The measurement data inserted in Equation (3.20) must originate from a different experiments, using a different swivel point than applied in the experiment to acquire the sensor displacement data for Equation

(3.19):

$$\varepsilon_{ij} = (R_2(-\theta_i)\Delta^i o_{i_2} - R_2(-\theta_j)\Delta^j o_{j_2}) \\ \frac{1}{\alpha_{k_1}} R_2(\pi/2)\,[R_2(-\theta_j)\,\Delta^j o_{j_1} - R_2(-\theta_i)\,\Delta^i o_{i_1}] \tag{3.21}$$

The indexes 1 and 2 in i_1, i_2, j_1, j_2 and k_1 refer to displacement data acquired from sensors o_i and o_j in experiments 1 and 2 using different swivel points k_1 and k_2. Eq. (3.21) can be applied to all tuples of subsets of two pivoting experiments using different pivot points and subsets of two sensors.

The assumption that the sensors are mounted in alignment with the mobile platform coordinate frame (Frame B), expressed at the beginning of this section allows for further simplification of equation (3.21). The assumption implies that the ${}^i y$ and ${}^B y$ axes as well as ${}^i x$ and ${}^B x$ axes have the same direction. Accordingly, angle θ_i is close to zero for all sensors. As a consequence rotation matrix $R_2(\theta_i)$ can be approximated by matrix $\widetilde{R}_2(\theta_i)$, using the limits expressed in Equation (3.2):

$$\widetilde{R}_2(\theta_i) = \lim_{\theta_i \to 0} \begin{bmatrix} \cos(\theta_i) & \sin(\theta_i) \\ -\sin(\theta_i) & \cos(\theta_i) \end{bmatrix} = \begin{bmatrix} 1 & \theta_i \\ -\theta_i & 1 \end{bmatrix}$$

Also higher order terms and multiplications of θ_i and θ_j can be neglected in Equation (3.21), resulting in the following linear equation:

$$\varepsilon_{ij}\,\alpha_k = u \cdot \theta_i + v \cdot \theta_j + w, \quad i \in (1,..,n); j \in (1,..,n); i \neq j \tag{3.22}$$

with :

$$
\begin{aligned}
u = {} & \Delta o_{i_2,x}\Delta o_{j_1,x} - \Delta o_{i_1,x}\Delta o_{j_2,x} + \\
& \Delta o_{i_2,y}\Delta o_{j_1,y} - \Delta o_{i_1,y}\Delta o_{j_2,y} \\
v = {} & -\Delta o_{i_2,x}\Delta o_{j_1,x} + \Delta o_{i_1,x}\Delta o_{j_2,x} - \\
& \Delta o_{i_2,y}\Delta o_{j_1,y} + \Delta o_{i_1,y}\Delta o_{j_2,y} \\
w = {} & \Delta o_{i_2,x}\Delta o_{i_1,y} - \Delta o_{j_2,x}\Delta o_{i_1,y} - \Delta o_{i_1,x}\Delta o_{i_2,y} + \\
& \Delta o_{j_1,x}\Delta o_{i_2,y} - \Delta o_{i_2,x}\Delta o_{j_1,y} + \Delta o_{j_2,x}\Delta o_{j_1,y} + \\
& \Delta o_{i_1,x}\Delta o_{j_2,y} - \Delta o_{j_1,x}\Delta o_{j_2,y}
\end{aligned}
$$

where all terms $\Delta o_{i,x}$ $\Delta o_{i,y}$ and $\Delta o_{j,x}$ $\Delta o_{j,y}$ are displacements measured by the sensors in their ${}^{i}x - {}^{i}y$ and ${}^{j}x - {}^{j}y$ coordinate frames. The superscripts i and j have been omitted for simplicity in the notation. Equation (3.22), is solved by finding values for θ_i and θ_j that minimize ε_{ij}. $\varepsilon_{ij} = 0$ is approximated through linear regression, giving best estimates $\widetilde{\theta}_i$ and $\widetilde{\theta}_j$ for θ_i and θ_j:

$$
[\widetilde{\theta}_i \; \widetilde{\theta}_j]^T = -(\,[\,u \;\; v\,]^T\,[\,u \;\; v\,]\,)^{-1}\,[\,u \;\; v\,]^T\, w \tag{3.23}
$$

- **Application of matching swivel point constraints (MSPC)**

  To derive α_k from the displacements measured by the optical flow sensors, at least three experiments have to be conducted, each with a different swivel point. Under these conditions Equation (3.17) applies, providing one constraint to calculate the value of $\alpha_k,\ k \in (1, .., n_k)$.

  With the orientations of the sensors in the mobile platform θ_i known, more expressions to estimate α_k can be derived from the matching swivel point constraint (MSPC). The principle of MSPC is illustrated in Figure 3.5 and simply states that two different paths between the same pair of swivel points must have the same starting and ending point:

$$
\overrightarrow{p_k\, o_i} - \overrightarrow{p_l\, o_i} = \overrightarrow{p_k\, o_j} - \overrightarrow{p_l\, o_j} \tag{3.24}
$$

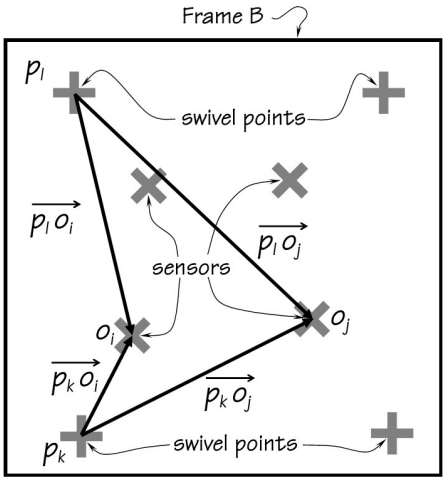

Figure 3.5: *Illustration of the Matching Swivel Point Constraint (MSPC).*

In case of n_k swivel points and n sensors, there are $\binom{n}{2}$ pairs of paths between a pair of swivel points and there are $\binom{n_k}{2}$ different pairs of swivel points. Hence, e_m, the number of MSPC equations (3.24) is:

$$e_m = \binom{n}{2} \cdot \binom{n_k}{2} \tag{3.25}$$

The terms $\overrightarrow{p_k o_i},\ \overrightarrow{p_l o_i},\ \overrightarrow{p_k o_j}$ and $\overrightarrow{p_l o_j}$ are expressed by Equation (3.15) and comprise the unknowns α_k and α_l for the swivel around point p_k and point p_l respectively.

To find the swivel angles α_l and $\alpha_k,\ l \in (1, .., n_k),\ k \in (1, .., n_k),\ l \neq k$, equation (3.24) is expressed in the following compact form:

$$m_c\ \alpha_K^{-1} = 0$$

where:

$$m_c \in \mathbb{R}^{2e_m \times n_k}$$

$$m_c = \begin{array}{c} \begin{array}{ccccc} k=1 & k=2 & \dots & k=i & k=n_k \end{array} \\ \begin{pmatrix} a_{11}-a_{21} & a_{22}-a_{12} & \dots & 0 & 0 \\ a_{11}-a_{21} & 0 & 0 & a_{2i}-a_{1i} & 0 \\ \vdots & \vdots & \vdots & \dots & \vdots \\ 0 & 0 & 0 & a_{ni}-a_{oi} & a_{on_k}-a_{nn_k} \end{pmatrix} \end{array}$$

$$\begin{aligned} a_{ik} &= R_2(\pi/2-\theta_i)\,\Delta^i o_{i,k} \\ \alpha_K^{-1} &= [1/\alpha_1\ 1/\alpha_2\ ..\ 1/\alpha_k\ ..\ 1/\alpha_{n_k}]^T \end{aligned}$$

$\Delta^i o_{i,k}$ is the displacement measured by sensor o_i in the swivel motion around point p_k. After performing the measurements of $\Delta^i o_{i,k}$, α_K^{-1} can be solved by numerical minimization of the norm of $m_c\ \alpha_K^{-1}$ with $\alpha_K = [\alpha_1\ \alpha_2\ ..\ \alpha_{n_k}]^T$ as parameters within constraint (3.17). The solution $\widetilde{\alpha}_K$ producing the minimal norm $\|m_c\ \alpha_K^{-1}\|$ is the optimal estimator for α_K:

$$\widetilde{\alpha}_K = \arg\min_{\alpha_K} \|m_c\ \alpha_K^{-1}\| \tag{3.26}$$

Setting the location of swivel point p_1 to $(p_{1,x}, p_{1,y}) = (0,0)$, the locations of sensors $o_i,\ i \in (1,..,n)$ and the other swivel points $p_k,\ k \in (2,..,n_k)$ relative to p_1, can be calculated from Equation (3.16) and (3.24).

3.4 Setup for odometry using optical flow sensors

To assess the accuracy of odometry using optical flow sensors, a mobile platform is assembled sitting on four legs: $n_k = 4$ and carrying four optical flow sensors: $n = 4$. The platform, depicted in Fig. 3.6 can make hand powered, guided translations and rotations on rounded ends capping the legs at the bottom. Table 3.1 lists the locations of the corners of the platform in the CAD design and according to hand measurements of the actual platform produced by a laser cutter.

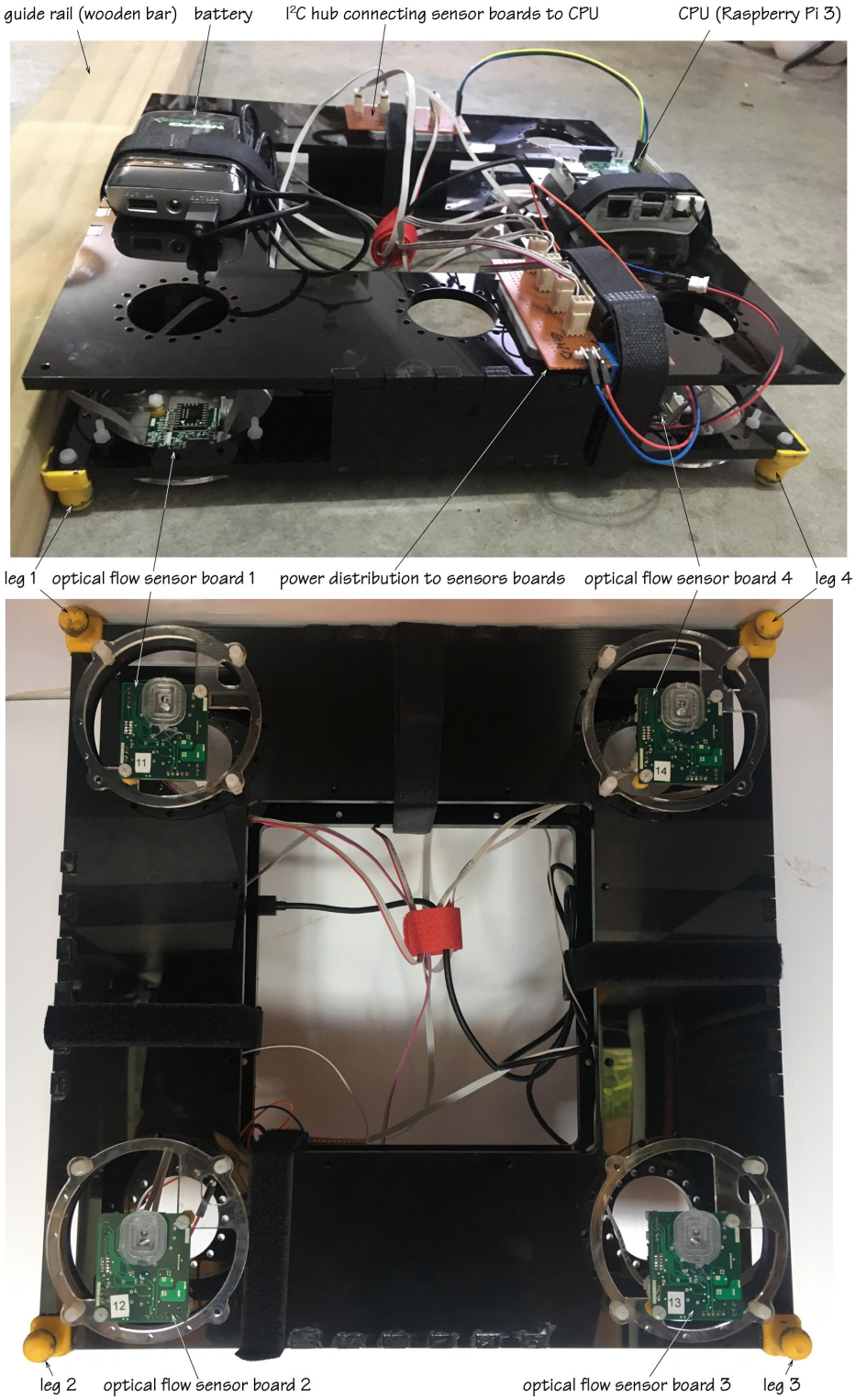

Figure 3.6: *Top and bottom view of the mobile platform.*

Table 3.1: *Location of corners of the mobile platform.*

Location of corners	1	2	3	4
CAD dimensions [mm]	(0.0, 0.0)	(0.0, 326.0)	(326.0, 326.0)	(326.0, 0.0)
Hand measurement [mm]	(0.0, 0.0)	(-2.3, 326.7)	(324.5, 326.6)	(326.9, 0.0)

The square top and bottom panels of the platform were cut on a UNIVERSAL™, 800×450 mm industrial grade flatbed laser cutter, producing a part of which the supposedly square corners were about $0.4°$ (0.4%) off, resulting in a misplacement of over 2 mm of the corners of the frame of 326 mm square. As a consequence, although a CAD design is available, the exact location of the sensors on the mobile platform is unknown. The sensors used are ADNS9800 optical flow sensors from Pixart Imaging Inc. for application in a computer mouse[7]. As can be observed in the bottom view in Figure 3.6, the mobile platform is rigged with four sensors, each mounted on a printed circuit board (PCB). The PCB's are mounted at the bottom side of the frame facing down to allow the sensors to record the optical flow resulted from the relative motion between the platform and the floor. The sensors' apertures are capped with the standard lenses provided by the manufacturer. They sensors are mounted with their top sides at 10.75 mm height over the floor surface, in compliance with the recommendations by the sensor manufacturer[7]. The orientation of the sensors at the bottom side of the mobile platform is in alignment with the mobile platform orientation, meaning that the ${}^{i}y$ and ${}^{B}y$-axes as well as ${}^{i}x$ and ${}^{B}x$-axes have the same direction: $\theta_i \approx 0, \;\; i \in (1, .., n)$.

3.4.1 Data acquisition and synchronization

The static kinematic model presented in Section 3.2 enables easy calculation of the translation and rotation of a mobile platform from the displacement measured in different locations in the platform with optical flow sensors. Since the model is static, the input data retrieved from the sensors must represent the displacement measured between exactly the same two time instances for all sensors used. As concluded in Section 2.5.3 of the literature review, this aspect of timing of the data acquisition is of cardinal importance to the accuracy of odometry.

The setup of the data acquisition system is shown schematically in Fig. 3.7. Each sensor is connected to an AT-Mega 16A micro controller ("μC") acting as bus master at the SPI interface

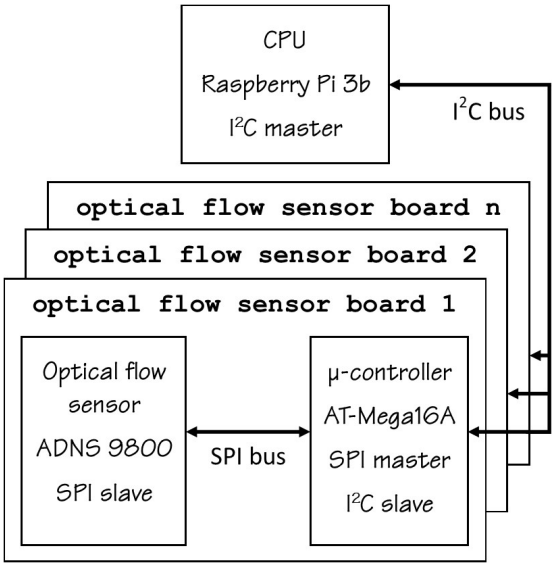

Figure 3.7: *Schematic of the data acquisition system.*

with the sensor. This enables the μC to retrieve the displacement data from the registers of the sensors without interrupting the data recording, preventing jitter. The sensor accumulates the displacement data until it is reset by the data retrieval by the μC. The four AT-Mega μC's are connected as slaves on an I^2C bus to a Raspberry Pi 3b, acting as I^2C bus master and CPU. This implementation allows the data acquisition to be synchronized by a "general call" from the I^2C bus master. A general call is a call to the I^2C address 0^8. It is received by all devices on the bus. For the odometry the general call initiates an interrupt routine at all μC's at exactly the same time to retrieve the displacement data from the connected optical flow sensors. This marks the transition to a new sampling period for the sensors. Subsequently the CPU requests the μC's one by one to pass the retrieved displacement data over the I^2C bus. When all μC's have passed their data to the CPU, it starts the following sampling interval by generating the next "general call" in a schedule of strict coincidence. The sampling frequency is not real time controlled this way but has a fairly constant value of 650 ± 5 Hz in the setup described.

The odometry system can be expanded with additional sensor boards, by simply hooking them up to the I^2C bus and addition of their device addresses to the list of boards that are included in the data retrieval loop of the CPU.

3.5 Experiments

With the setup for the optical flow sensors as described in Section 3.4, displacement data from the four sensors are recorded and stored for off-line processing in the two experiments conducted:

- **Experiment 1**

  In the first experiment introduced in Section 3.3.1, the mobile platform slides 10 times up and down in a straight line as illustrated in Figure 3.2. Stop blocks on either end of the path are set at a mutual distance that allows the mobile platform to travel 1 m. between them. This is the only measurement applied in the complete experimental procedure. The platform is moved by hand between the blocks with one side of the platform kept against a straight wooden bar fixed on a surface. The bar, shown in the picture on top in Figure 3.6, acts as a guide rail for the motion and prevents rotation of the platform. The motion is repeated for four orientations of the mobile platform each time with another side against the bar. This experiment has been conducted on three different surfaces: a cast concrete floor, a PVC tabletop of a folding table and a smooth wooden tabletop with white matte finish, in which over 80 m. of optical flow data was collected on each surface.

- **Experiment 2**

  In the second experiment introduced in Section 3.3.2 the mobile platform is turned around one of its legs acting as swivel point, with the leg held in place in a washer (ring), fixed to the surface. The centre of the washer is the anchor point ${}^{c}p$ shown in Figure 3.3. The washer is of a size that it keeps the rounded cap under the leg centered without play. The suspension in the washer constrains the motion of the swivel point to pure rotation. A bar fixed on the floor acts as a limiter for the swivel motion, as illustrated in Fig. 3.8. The motion starts with legs k and $k-1$ against the bar. With leg k in location p_k acting as swivel point, the mobile platform is manually pushed around p_k until leg $k+1$ touches the bar after which the platform is pushed back to its starting position with legs k and $k-1$ against the bar. The motion is repeated 10 times for each leg acting as swivel point $k \in (1, .., 4)$. This experiment was performed on the tabletop at which optical flow data was collected over a distance of 26.8 meter.

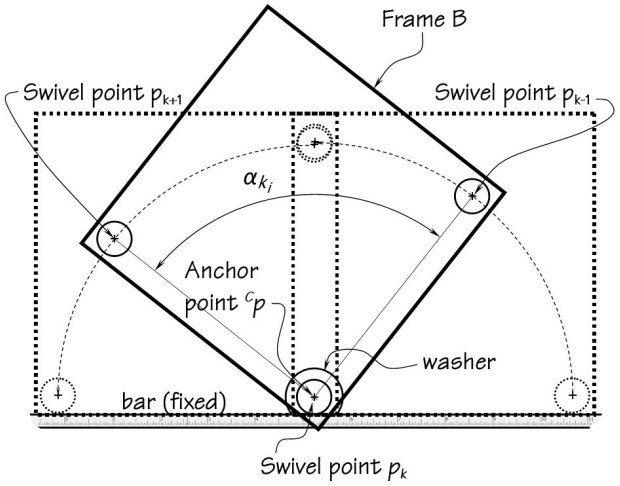

Figure 3.8: *Top view of the swivel motion in experiment 2.*

3.5.1 Calculation of sensitivities

The data collected in the first experiment is processed as expressed by Equation (3.12). The resulting sensitivities are listed in Table 3.2 together with the standard deviation expressed as a percentage of the average value of the sensitivity, in parenthesis. The measurements enable the following observations:

- In spite of placement of the sensor according to the manufacturers instructions, the sensitivities measured exhibit considerable deviation from the nominal sensitivity of 1600 dpi specified, corresponding to 62992 ppm.

- The standard deviation is smaller on rough surfaces, like the concrete floor and the PVC table. This can be explained by considering that rough surfaces produce more features in the image of the sensor. The locations of the features in the image are the observations with which the displacement is established. Increasing the number of observations reduces the standard deviation and makes the measurement more precise.

- The sensitivity is different for each surface. The figure listed for the average sensitivity over all three surfaces in Table 3.2, has a corresponding standard deviation that is much larger than the standard deviation for each surface separately. Using one value for the sensitivity on all surfaces impairs the accuracy of the displacement measurement.

Table 3.2: *Mean values of the sensitivities f_i of the four optical flow sensors o_i measured on different surfaces, $i \in (1,..,n), n = 4$.*

Surface	f_1 [ppm]	f_2 [ppm]	f_3 [ppm]	f_4 [ppm]
Concrete floor	62466 (0.02%)	63174 (0.01%)	72649 (0.03%)	66363 (0.02%)
PVC table top	63672 (0.02%)	64521 (0.01%)	75842 (0.02%)	67967 (0.01%)
Smooth table top	64625 (0.20%)	64282 (0.14%)	74871 (0.34%)	67685 (0.19%)
Average sensitivity.	63588 (1.39%)	63992 (0.92%)	74454 (1.79%)	67338 (1.04%)

The sensitivities are specified in pixels per meter [ppm].
The figure in brackets is the standard deviation of the measured sensitivity values, expressed as a percentage of the mean sensitivity.

Obviously, the standard resolution provided by the manufacturer can not be used to measure the displacements of the sensors accurately, without verification.

3.5.2 Determination of sensor orientation and location

In the second experiment data is acquired from four optical flow sensors in swivel motions around four swivel points: $n = 4, n_k = 4$. The collected optical flow data $\Delta^i o_{p,i}$ [pixels] is converted to displacements $\Delta^i o_i$ [m] using the sensitivities figures f_i listed in Table 3.2, established in experiment 1:

$$\Delta^i o_i = \frac{\Delta^i o_{p,i}}{f_i} \quad [\mathrm{m}]$$

With the dimensional data $\Delta^i o_i$ from experiment 2, sensor orientations θ_i, swivel angles α_k and locations ${}^B o_i$ are determined, $i \in (1,..,n), k \in (1,..,n_k)$. θ_i is estimated using the expression for linear regression in Equation (3.23). The results in Table 3.3 exhibit very small orientation angles, as is to be expected for sensors mounted in alignment with the mobile platform coordinate frame B. The very small values for $\widetilde{\theta}_i$ provide justification for the use of the simplified rotation matrix $\widetilde{R}_2(\widetilde{\theta}_i)$ and elimination of higher order and product terms for $\widetilde{\theta}_i$ and $\widetilde{\theta}_j$ in Equation (3.22).

Subsequently, the swivel angles α_k required for the calculation of the locations of pivot points and sensors can be estimated using the estimated values for $\widetilde{\theta}_i$. α_k, $k \in (1,..,n_k)$ are retrieved from the minimization of the Euclidean norm of $m_c\, \alpha_K^{-1}$, as expressed by Equation (3.26). With $n = 4, n_k = 4$ the number of MSPC equations (3.24) $e_m = 36$ according to Equation

Table 3.3: *Experimental results for sensor orientation θ_i and swivel angle α_k.*

k, i	1	2	3	4
$\widetilde{\theta}_i$ [rad]	$12.63\ 10^{-3}$	$-8.57\ 10^{-3}$	$2.56\ 10^{-3}$	$-6.62\ 10^{-3}$
$\widetilde{\alpha}_k$ [rad]	32.15	31.29	31.10	31.13

(3.25) implying that matrix m_c measures 72 rows by 4 columns over which the $n \times n_k = 4 \times 4 = 16$ experimentally acquired datapoints for ${}^i[\Delta o_{i,x}\ \Delta o_{i,y}]^T$ are distributed.

The result for $\widetilde{\alpha}_K$ is established as listed in Table 3.3. The constraint applied to the minimization according to Equation (3.17) takes into account that the data collected is the accumulation of the displacement data of all 10 swivels of the mobile platform: $\sum_{k=1}^{n_k=4} \alpha_k = 2 \cdot 10 \cdot 2\pi = 40\pi$. The sum of the calculated swivel angles in Table 3.3 matches this amount well. With the figures for $\widetilde{\alpha}_k,\ k \in (1, .., 4)$, the vectors $p_k o_i$ connecting all swivel points p_k with all sensors o_i can be computed using the expression in Equation (3.15).

Defining $p_1 = (0, 0)$ as the point of reference, the locations of all other swivel points $p_k\ k \in (2, .., 4)$ are computed as the average value of the locations determined by the vector additions: $p_k = \overrightarrow{p_1\, o_i} - \overrightarrow{p_k\, o_i}$:

$$p_k = \sum_{i=1}^{n=4} (\overrightarrow{p_1\, o_i} - \overrightarrow{p_k\, o_i})/4,\ k \in (2, .., 4)$$

The sensor locations are calculated as the average values of the vector additions defined by Equation (3.16):

$$o_i = \sum_{k=1}^{n_k=4} (p_k + \overrightarrow{p_k\, o_i})/4,\ i \in (1, .., 4)$$

The geometric center of the mobile platform B_o is defined at the intersection of the diagonal between sensor pairs (o_1, o_3) and (o_2, o_4). Table 3.4 gives an overview of the location of swivel points and sensors relative to B_o as established in the measurement procedure described, compared with the figures from the CAD design and locations estimated from the hand measured figures.

Table 3.4: *Overview of the locations of swivel points (legs) p_k and sensors o_i relative to the center of Frame B, B_o.*

k,i	1	2	3	4
Measured locations				
p_k [meter]	(-0.1530,-0.1518)	(-0.1549,0.1628)	(0.1573,0.1627)	(0.1576,0.1556)
o_i [meter]	(-0.1107,-0.1086)	(-0.1132,0.1140)	(0.1155,0.1133)	(0.1109,0,1117)
CAD locations				
p_k [meter]	(-0.1565,-0.1565)	(-0.1565,0.1565)	(0.1565,0.1565)	(0.1565,-0.1565)
o_i [meter]	(-0.1155,-0.1155)	(-0.1155,0.1155)	(0.1155,0.1155)	(0.1155,-0.1155)
Swivel point locations estimated from hand-measurements				
p_k [meter]	(-0.1558,-0.1569)	(-0.1581,0.1569)	(0.1557,0.1568)	(0.1581,-0.1569)

3.6 Validation of the mobile platform path

The effects of measurement of the sensitivity of the sensors, the locations of the swivel points and the locations and orientations of the sensors in the mobile platform on the localization of the mobile platform displacement can be validated through computation of the path of the mobile platform (Frame B) in fixed Frame C.

The path is reconstructed by first order integration of the incremental displacements of the center of the mobile platform:

$$\Delta^B\Theta_B(t) = {}^B[\Delta B_o(t) \mid \Delta\theta_B(t)]^T = {}^B[\Delta B_{o,x}(t)\ \Delta B_{o,y}(t)\ \Delta\theta_B(t)]^T$$

where t represents the time interval at which the displacement occurs. $\Delta^B\Theta_B(t)$ is estimated through Equation (3.7).

The integration process is computed by:

$$\theta_B(t) = \theta_B(t-1) + \Delta\theta_B(t)$$

$$^C\begin{bmatrix} B_{o,x}(t) \\ B_{o,y}(t) \end{bmatrix} = {}^C\begin{bmatrix} B_{o,x}(t-1) \\ B_{o,y}(t-1) \end{bmatrix} + R_2(\theta_B(t))\ {}^B\begin{bmatrix} \Delta B_{o,x}(t) \\ \Delta B_{o,y}(t) \end{bmatrix}$$

$R_2(\theta_B(t))$ is the transformation matrix for the rotation from Frame B to Frame C.

Fig. 3.9 depicts the computed path of the center of the mobile platform B_o over 10 return sweeps for all four swivel motions in experiment 2. In each run a different leg of the mobile platform is used as swivel point. B_o travels approximately 6.7 [m] over each swivel path, without external correction or resetting of its location. The top picture frame detailing the center of the graph shows the start and return position of the path traveled by B_o. As is to be expected without correction of the location, B_o is slowly drifting away from the starting point with each swivel move, at which it is supposed to return after each sweep. There is no noticeable error in the orientation of any of the paths however. Even after 10 return sweeps the computed orientation of the paths appears to be highly accurate. The leg of the mobile platform acting as swivel point in each experiment is suspended at the anchor point in a washer fixed on the surface as explained in Section 3.5. Physically, no translation of the pivot leg can occur, only rotation. This certainty can be used to rate the accuracy of the mobile platform location as measured with the optical flow sensors, using the parameters in Table 3.4. Any translation of the pivot leg observed from the optical flow data, represents an error that provides an objective measure for the accuracy of the computed displacement of the platform. The location of the swivel point p_k in Frame C, ${}^C p_k = {}^C[p_{k,x}\ p_{k,y}]$ can be derived from the location ${}^C B_o = {}^C[B_{o,x}\ B_{o,y}]$ and orientation θ_B of B_o in Frame C with the expression:

$$ {}^C\begin{bmatrix} p_{k,x}(t) \\ p_{k,y}(t) \end{bmatrix} = {}^C\begin{bmatrix} B_{o,x}(t) \\ B_{o,y}(t) \end{bmatrix} + R_2(\theta_B(t)) \quad {}^B\begin{bmatrix} p_{k,x} \\ p_{k,y} \end{bmatrix} $$

Fig. 3.10 frames the calculated location of the swivel point ${}^C p_k$ at the end of each data sample period, relative to the fixed anchor point ${}^C p$ in the origin of the graph. The figure comprises the graphs for the location of each of the swivel points used in the experiments. Obviously and unavoidably, the swivel point drift away from the pivot point, up to a maximum distance of 0.011 [m], while the center of the mobile platform travels over 6.7 [m] distance. Expressed as a dimensionless figure the drift amounts to $0.011/6.7 \cdot 100\% = 0.16\%$, which is a very satisfactory result for dead reckoning and significantly better than the 0.28% error reported in [37], where double the number of optical flow sensors was used (eight sensors). To evaluate

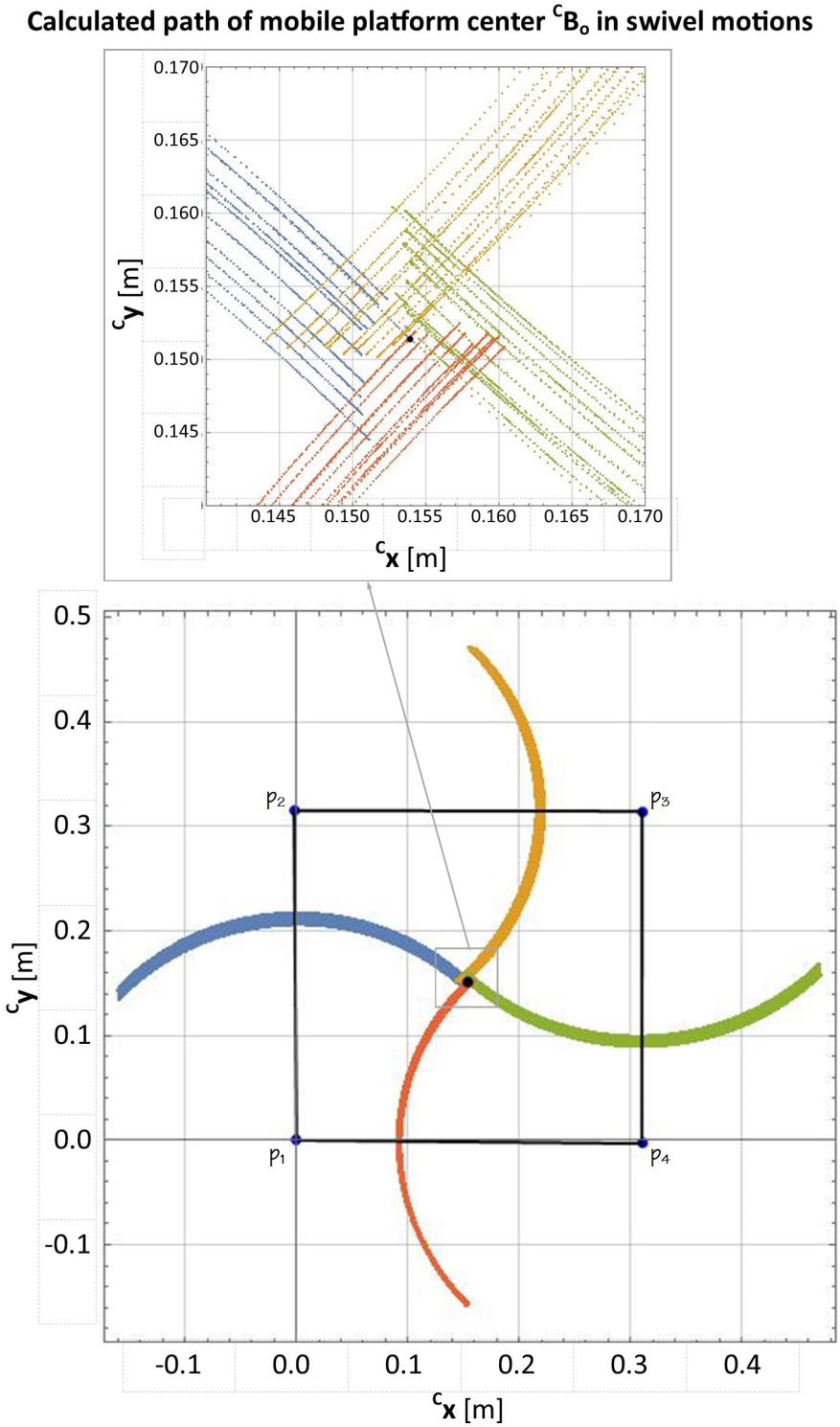

Figure 3.9: *Paths of the centre of the mobile platform in four swivel experiments.*

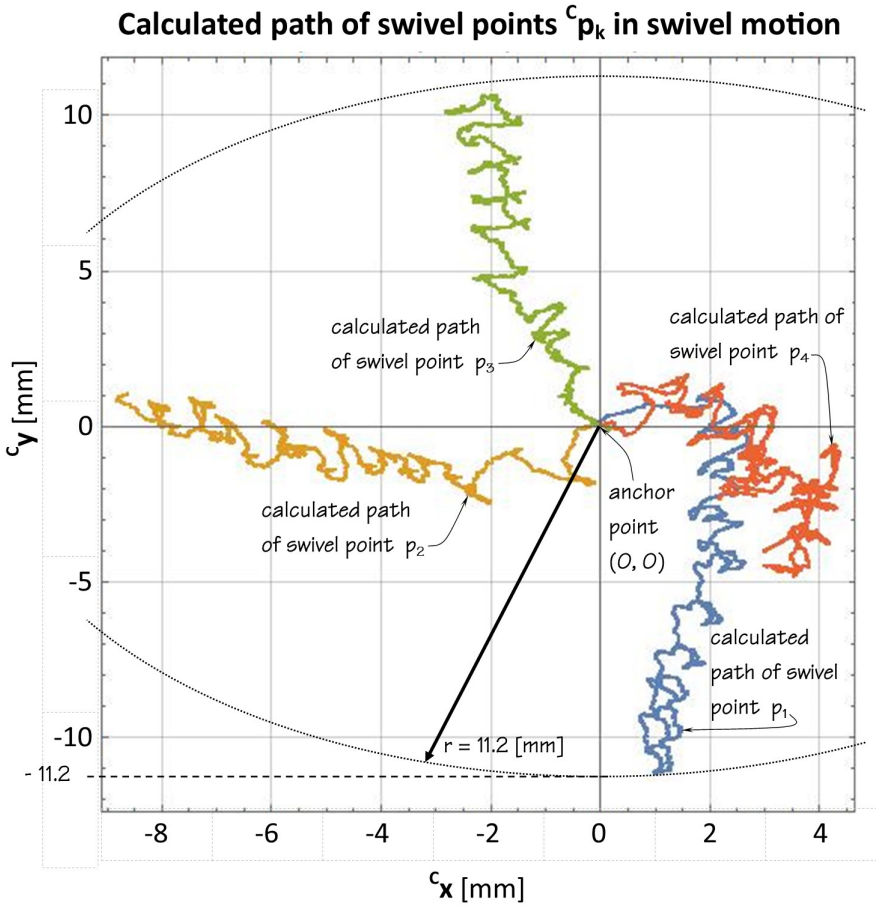

Figure 3.10: *Calculated location ${}^{C}p_k$ of leg k used as swivel point p_k, relative to the fixed anchor point, for each of the four swivel experiments.*

the effectiveness of the measurement procedure applied, the displacement of the swivel point ${}^{C}p_k$ is squared and accumulated over all integration steps t of the experimental procedure for all four swivel runs: $D_p^2 = \sum_{k=1}^{4} \sum_t {}^{C}p_k{}^2$. The variance D_p^2 can be used to compare the accuracy of the location established with optical flow sensors for different sensor parameters and data processing methods. A lower value for D_p^2 indicates a more accurate computation of the mobile platform's location. Table 3.5 lists the deviation D_p^2 for different measurement scenario's, from not calibrated to fully calibrated according to the procedure described in this chapter. Comparison of the measurement scenario's demonstrates that measurement of the sensor sensitivities and in particular measurement of the location of swivel points and sensors strongly reduce the value of D_p^2. These results validate the significance and effectiveness of the measurement procedure presented.

Table 3.5: *Variance D_p^2 computed for different measurement scenario's.*

Included measurement	Scenario:	1	2	3	4
Sensor sensitivity f_s		☐	☑	☑	☑
Locations of swivel points p_k and sensors o_i		☐	☐	☑	☑
Sensor orientation θ_{o_i}		☐	☐	☐	☑
$D_p^2 = \sum_{k=1}^{4} \sum_t {}^C p_k{}^2$ [m^2]		9.63	8.89	2.17	2.17

3.7 Concluding remarks

The new research reported in this chapter focuses on the application of optical flow sensors for odometry. Previous research reports that the sensitivity of optical flow sensors is dependent on multiple factors including the height at which the sensor is mounted over the floor sensor and the optical properties of the floor surface such as reflectiveness and transparency [21, 29, 30]. The present analysis elaborates on these observation in two ways:

1. Scrutiny of the propagation of the error in the sensor sensitivity into the location derived from the sensor data in Section [Section 3.2.1]. The analysis demonstrates that the propagation of a relative error in the sensitivity of the optical flow sensors is constrained to a relative error in the calculated displacement of the mobile platform of the same magnitude.

2. Design of a simple experimental procedure to measure sensitivity of each sensor on each new surface to enable a quick update of the sensor sensitivity [Section 3.3.1].

   Application of the experimental procedure to optical flow sensors installed in compliance with the manufacturers recommendations, confirms the observation that the sensitivities measured on different surfaces exhibit considerable deviation from the nominal sensitivity specified [Section 3.5.1]. Obviously, the standard resolution provided by the manufacturer can not be used to measure the displacements of the sensors accurately, without verification.

   Moreover it is observed that the standard deviation of the measured sensitivity is smaller on rough surfaces, than the standard deviation of the measurements on smooth surfaces. This can be explained by considering that rough surfaces produce more features in the

image of the sensor. The locations of the features in the image are the observations with which the displacement is established. Increasing the number of observations reduces the standard deviation and makes the measurement more precise.

In addition to the sensor sensitivity, the sensor location, orientation and the synchronization of the data acquisition from all sensors are identified as critical parameters to measure the displacement. On these topics the following contributions are made to the existing knowledge of odometry with optical flow sensors:

3. A software solution is proposed and implemented to synchronize the acquisition of displacement data from multiple optical flow sensors that forces the measurements by the sensors in a schedule of strict coincidence [Section3.4.1].

4. A new experiment is designed to measure the locations and orientation of the optical flow sensors on a mobile platform. The measurement method determines the orientation and location of the sensors in separate computations from the same set of data collected by the sensors themselves. The data set comprises of displacement readings from the optical flow sensors acquired in a simple experiment in which the mobile platform is rotated around swivel points. The certainty that the location of the swivel point of the mobile platform is fixed at an anchor point during the experiments is used to validate the obtained sensor locations, without performing additional experiments [Section 3.3.2].

5. Validation of the experimental procedure to measure location and orientation of the optical flow sensors demonstrates its efficacy. After completion of the full measurement procedure, the setup developed using four optical flow sensors exhibits accurate odometry: the computed location of the swivel point of the mobile platform deviated 0.16% of the total distance traveled by the platform (6.7 meter) [Section 3.6]. This is a significant improvement over the next best result of an accuracy of 0.28% published in the open literature [37]. Moreover, the simple experimental procedure and usage of readings from the optical flow sensors only, strongly facilitate implementation of the method in a self-calibration operation.

Chapter 4

Absolute location measurement with a laser lighthouse

4.1 Introduction

As set out in the literature review in Chapter 2 the laser lighthouse is a nearly 40 year old concept that only recently had a practical incarnation with the introduction of the HTC Vive virtual reality gaming kit in 2015, enabling 3D localization of virtual reality (VR) gaming gear for the consumer market[3]. Although it is not strictly the first lighthouse system introduced [64, 67, 81], it is the first consumer electronics lighthouse system that works well. For this reason it has gained popularity amongst researchers in computer vision and the development of VR and augmented reality applications. The HTC Vive VR kit comprises two ”base stations” implementing the laser lighthouse concept. Each base station is put in a stationary position and spins a light sheet around two perpendicular axes, with a fixed frequency similar to that of a lighthouse. A rigid mobile platform equipped with a minimum of three light sensors in different known locations on the platform and with a line of sight (LoS) to the lighthouse, can compute its location and orientation from the time stamps recorded by each light sensor when it is struck by the passing light sheet and by the synchronization pulse generated by the lighthouse. Although the kit comes with two lighthouse base stations and the setup with two stations is recommended for gaming applications, a mobile platform can be located with one

base station as long as a LoS with the lighthouse is maintained. Compared to other localization systems using triangulation based on multiple beacons, the laser lighthouse concept is a wonder of simplicity. For a single lighthouse there is no need for calibration of the location of the beacons relative to each other, or synchronization of the signals emitted by different beacons. The requirement for only one stationary beacon makes deployment of the lighthouse system easier than any other system described in the open literature. The low requirements of the lighthouse system to the conditioning of the workspace makes it an attractive solution to support field deployment of mobile robots. The stationary lighthouse carries the laser emitter, which has the advantage of not exposing it to motions and vibrations as equipment mounted on a vehicle is. No calibration measurement have to be performed to set up a single lighthouse system and no additional data communication is required between the lighthouse and the mobile platform to be tracked. All data processing can be performed "on board" of the mobile platform. Hence the "laser lighthouse" is the most versatile concept to provide absolute location measurements to a mobile platform localization system for precision manufacturing.

The literature review in Chapter 2 already retrieved positive findings on the HTC Vive base stations in perspective of the feasibility case of a mobile platform for precision manufacturing, defined in Chapter 1:

- The noise level in the location of a mobile platform obtained with a single lighthouse is below the maximum allowable manufacturing tolerance. This is a necessary condition to any localization system for a mobile platform for manufacturing.
- An out of the box HTC-Vive kit already demonstrates an accuracy of the required order of magnitude in localizing VR gear.
- The error in the location of a mobile platform obtained with a lighthouse base station is linear with the distance of the platform to the base station.

At the same time no analysis has yet been published on systematic errors in the lighthouse system and their propagation into the location and orientation of a mobile platform using the system.

This is covered in the present chapter, where the lighthouse system is analyzed more rigorously and tested to compare its performance to criteria formulated in the feasibility case in Section 2.2. The structure of Chapter 4 is as follows: Section 4.2 elaborates the operation of a lighthouse and the fundamentals of retrieving a location and orientation from it. The analysis demonstrates the role of the sensor locations in the computation of the location and orientation of the mobile platform. Section 4.3 quantifies the propagation of errors in the sensor locations into an error in the calculated location and orientation of the mobile platform. To minimize errors in sensor locations, a camera calibration method is introduced to design an experiment in Section 4.4 enabling measurement of the sensor locations in the mobile platform, using the lighthouse system. The experiment is demonstrated in Section 4.5, validated in Section 4.6 and concluded in Section 4.7.

4.2 Operation of a laser lighthouse

The lighthouse used for the research described in this section is one of two "base stations", version 1.0 included in the HTC Vive Virtual Reality (VR) kit. Its operation is illustrated in Figure 4.1. The box shaped laser lighthouse "base station" emits two light sheets at the negative ${}^{C}z$ side of the ${}^{C}[x\ y\ z]$ coordinate system of the lighthouse. The light sheets are generated by diffusion of a laser ray through a cylindrical lens. The resulting light sheet fans out at an angle of $^{2}/_{3}\,\pi$ [rad][4]. The coordinate system C spans fixed Frame C connected to the base station, with its origin at the laser lighthouse. A rigid, mobile platform identified as Frame B, carrying a number of n_l light sensors $l_i, i \in (1, .., n_l)$ is moving inside Frame C where the sensors are struck by the passing light sheets. Light sheet "h" rotates around a horizontal ${}^{C}x$-axis perpendicular to the ${}^{C}[y - z]$ plane and sheet "v" around the vertical ${}^{C}z$-axis perpendicular the ${}^{C}[x - y]$ plane, as indicated in Figure 4.1. The origin of coordinate system C, C_o, which coincides with the intersection of the rotation axes of the light sheets is not located exactly in the center of the base station as might be suggested in Figure 4.1. Both light sheets spin in positive direction around their axis of rotation at a frequency of 60 [Hz] corresponding to an angular velocity of $\omega = 120\,\pi$ [rad/sec]. The phases of sheet "h" and "v" are shifted by π [rad],

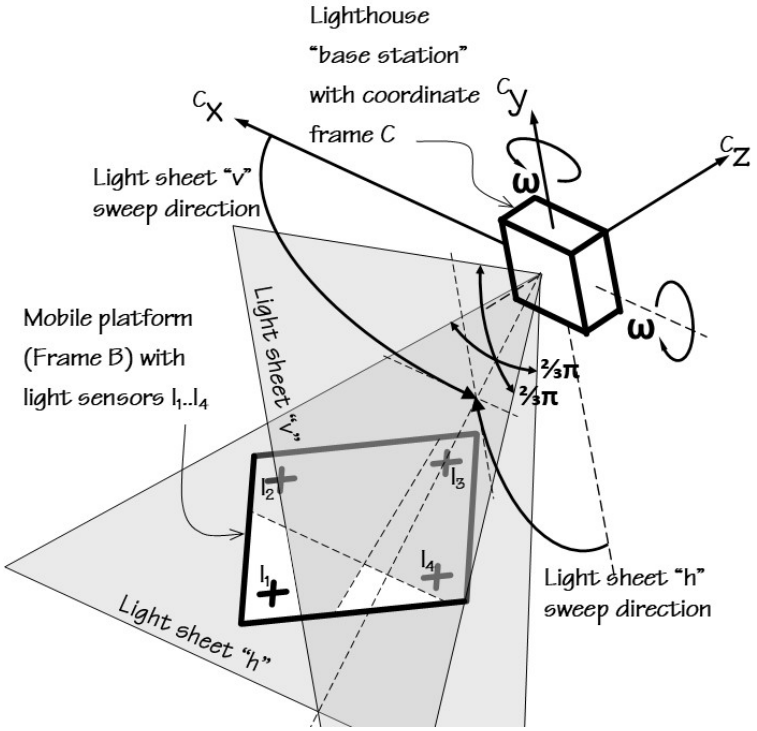

Figure 4.1: *Sweeping of light sheets generated by the lighthouse over a mobile platform (Frame B) with $n_l = 4$ light sensors.*

causing them to swipe alternately through the space at the negative z-side of the lighthouse. Intersection of the light sheets as drawn in Figure 4.1 for illustration purposes, does not occur in practice. In addition to the light sheets, the base station emits omni-directional light flashes for synchronization when either light sheet passes through a fixed orientation in their sweeping motion. A sync pulse is emitted upon light sheet "h" passing through the negative y-axis and a upon light sheet "v" passing through the x-axis. At a rotation frequency of 60 [Hz] for both sheets, the start time of the sync pulses are exactly $1/60 \cdot 1/2 = 8.333$ [msec] apart and mark the "heartbeat" of the lighthouse. The duration of the sync pulses varies between 62.5 and 135 [μsec] which encodes three bit states that identify[9]:

1. The status of the sweep of the second base station; for the research in this chapter only one base station is used, hence the status of this bit is always 0;

2. The light sheet that starts its sweep ("h" or "v");

3. One bit of a sequence broadcasted by the base station, encoding status information.

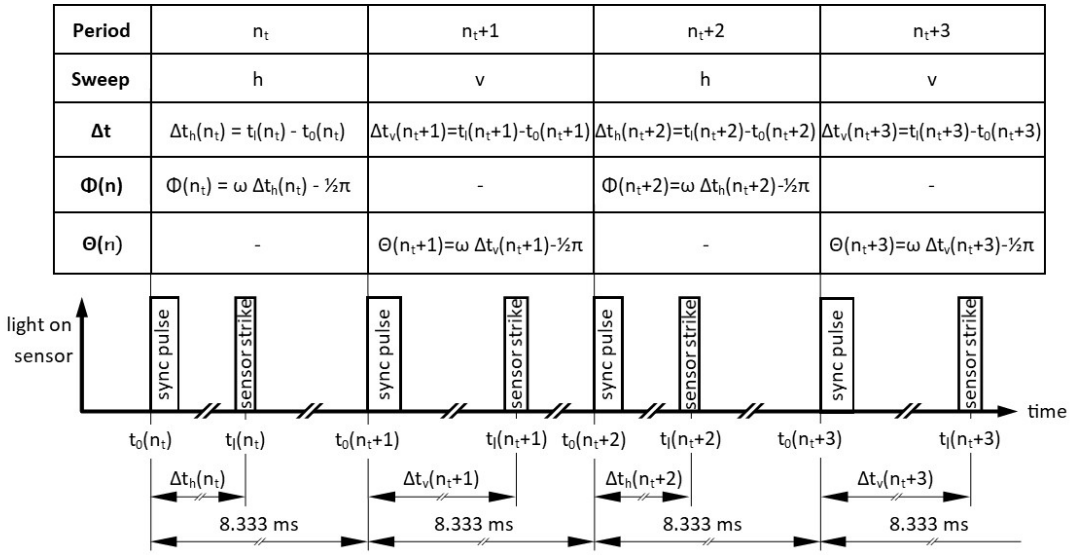

Figure 4.2: *Light pulses observed by a light sensor in exposure range of the lighthouse.*

The sequence of light pulses as observed by a light sensor exposed to the lighthouse is depicted in Figure 4.2. The heartbeat of the base station can be filtered out by the edges 8.33 msec apart. The start of a sync pulse as observed by the rising edge of a heartbeat at all light sensors marks the beginning of a new sweep period n_t and is time-stamped $t_0(n_t), n_t \in \mathbb{N}$. The timing of the first falling edge designates the end of the sync pulse and allows for decoding of the 3 bit code, identifying whether the light sheet coming up is "h"or "v". The subsequent rising and falling edges mark the passing of the light sheet over the sensor. For the purpose of location measurement, the median time between the rising and falling edge is taken as the "time of strike" of the sensor by the light sheet in period n_t. This time is indicated as $t_l(n_t)$ in the table in Figure 4.2. The subsequent rising edge marks the end of the period of the current sweep n_t and the start of the sync pulse for the alternate "v" sweep $n_t + 1$, in which again the time of strike $t_l(n_t + 1)$ is measured. Figure 4.2 is not drawn to scale as in practice the duration of the sync pulses is typically more than one order of magnitude longer than the sensor strikes. Since t_0 is defined by the passing of the light sheet through a fixed orientation, the time of strike t_l allows for calculation of the location of the light sheet at which the strike takes place. The locations are expressed through angles $\phi(n_t)$ and $\theta(n_t)$ for sheets "h" and "v" respectively as defined in the

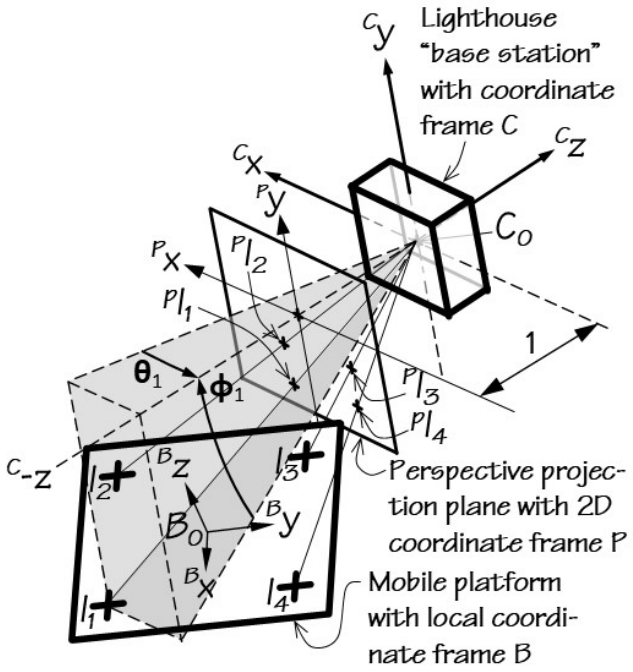

Figure 4.3: *Locations of light sensors $l_i, (i = 1, 2, 3, ..)$ in coordinate systems of the mobile platform (Frame B), the lighthouse (Frame C) and in perspective projection (Frame P).*

table in Figure 4.2 and illustrated in Figure 4.3:

$$\phi(n_t) = \omega(t_l(n_t) - t_0(n_t)) - \frac{1}{2}\pi$$

$$\theta(n_t) = \omega(t_l(n_t) - t_0(n_t)) - \frac{1}{2}\pi$$

The expressions include an offset -1/2 π for both angles ϕ and θ, to align the orientations $\phi = 0$ and $\theta = 0$ of the light sheets with the negative z-axis, normal to front face of the base station.

As the analysis in this chapter applies to any sweep period of the lighthouse, the reference to a particular time frame (n_t) is dropped in the notation.

4.2.1 Location measurement with a laser lighthouse

Frame B has its own ${}^{B}[x\ y]$ coordinate system, with its origin B_o in the geometrical center of B. The location of Frame B in Frame C is defined by the location of B_o in Frame C, indicated as ${}^{C}B_o$ and its orientation by the Euler angles ${}^{C}\psi = {}^{C}[\psi_x\ \psi_y\ \psi_z]$ defining rotational angles around

the ${}^{C}x$, ${}^{C}y$ and ${}^{C}z$ axes of Frame C representing the spatial orientation of Frame B in Frame C. With the setup in place to measure angles ϕ_i and θ_i for all sensors $l_i, i \in (1, .., n_l)$, as shown in Figure 4.3, the location of Frame B in the lighthouse coordinate Frame C can be established through the geometrical relationship between the angles and the perspective projection of the sensors:

$$ {}^{P}l_i^T = {}^{P}[l_{i,x}\ l_{i,y}] = {}^{C}[\frac{l_{i,x}}{l_{i,z}}\ \frac{l_{i,y}}{l_{i,z}}] = [\tan(\theta_i)\ \tan(\phi_i)] \tag{4.1} $$

This relationship is identical to the relationship between an object and its projected image in a pinhole camera with the pinhole located in C_o as illustrated in Figure 4.3 [82]. The ${}^{C}l_{i,z}$ coordinate cannot be established from the angles measured by the lighthouse system for a single sensor. To estimate ${}^{C}l_{i,z}$, sounding angles from the lighthouse are required for at least three sensors of which the locations ${}^{B}l_i^T = {}^{B}[l_{i,x}\ l_{i,y}\ l_{i,z}]$ in Frame B are known.

Islam et al. present a trigonometric solution for this purpose, where the angle ϕ as measured with a lighthouse setup, is interpreted as the elevation (polar) angle in spherical coordinates [81]. This seems incorrect however, as Jansen et al. indicate that ϕ is not the spherical elevation angle, but the projection of the spherical elevation angle on the ${}^{B}[y\text{-}z]$ plane (as used in this chapter) [70] .

Borges et al. and Jansen et al. reconstruct the pose of Frame B by minimization of the difference between the angles at which the sensors are sounded by the lighthouse and the corresponding angles calculated from the body pose, using Expression (4.1) [69, 70]. The body pose is specified by a spatial rotation matrix R_3 and translation vector T of Frame B corresponding to its orientation and location in to Frame C. Formulating this as a space transformation of the sensors locations ${}^{B}l_i$ in homogeneous coordinates, the minimization can be expressed as estimating R_3, T and ${}^{C}l_{i,z}$ from the following equation for all sensors l_i on Frame B:

$$ {}^{C}l_i = {}^{C}\begin{bmatrix} l_{i,x} \\ l_{i,y} \\ l_{i,z} \end{bmatrix} = \left[\begin{array}{c|c} R_3 & T \end{array}\right] {}^{B}\begin{bmatrix} l_i \\ \hline 1 \end{bmatrix} \tag{4.2} $$

Equation (4.2) defines three relationships between ${}^{C}l_i = {}^{C}[l_{i,x}\ l_{i,y}\ l_{i,z}]$ and ${}^{B}l_i = {}^{B}[l_{i,x}\ l_{i,y}\ l_{i,z}]$ for each sensor with which the 6 degrees of freedom represented by R_3 and T have to be estimated, together with ${}^{C}l_{i,z}$. Since R_3 and T are identical for each sensor mounted on the same rigid body, additional sensors only add an unknown ${}^{C}l_{i,z}$ to the system of equations. This implies that with a minimum of three sensors $l_i, i \in (p,q,r)$ on Frame B, a system of nine equations is defined with which R_3, T and ${}^{C}l_{i,z}$, can be estimated with the following procedure: Using a first guess or previous known location of the sensors ${}^{C}l_i, i \in (p,q,r)$ in Frame C as starting values for the iteration of ${}^{C}l_i$, the parameters for R_3 and T and coordinate ${}^{C}l_{i,z}$ are estimated. R_3 is determined by the Euler angles ${}^{C}[\psi_x\ \psi_y\ \psi_z]$ defining rotational angles around subsequently the y, x and z axes of Frame C:

$$R_3 = R_z({}^{C}\psi_z)\ R_x({}^{C}\psi_x)\ R_y({}^{C}\psi_y)$$

T is expressed as:

$$T^T = {}^{C}B_o^T = {}^{C}[B_{o,x}\ B_{o,y}\ B_{o,z}]$$

${}^{C}\psi = {}^{C}[\psi_x\ \psi_y\ \psi_z]$, ${}^{C}B_o$ and ${}^{C}l_{i,z}$ are approximated using the Levenberg-Marquardt algorithm [83] to minimize the difference between ${}^{C}[{}^{l_{i,x}}\!/_{l_{i,z}}\ {}^{l_{i,y}}\!/_{l_{i,z}}]$ and $[\tan(\theta_i)\ \tan(\phi_i)]$, where ${}^{C}l_{i,x}$ and ${}^{C}l_{i,y}$ are computed with Equation (4.2) and θ_i and ϕ_i are the (measured) angles at which the sensors l_i are sounded by the lighthouse system:

$${}^{C}[\widetilde{\psi}\ \widetilde{B}_o\ \tilde{l}_{i,z}]^T = \arg\min_{({}^{C}\psi, {}^{C}B_o, {}^{C}l_{i,z})} \left[\sum_{i=(p,q,r)} \left({}^{C}\begin{bmatrix} \frac{l_{i,x}}{l_{i,z}} \\ \frac{l_{i,y}}{l_{i,z}} \end{bmatrix} - \begin{bmatrix} \tan(\theta_i) \\ \tan(\phi_i) \end{bmatrix} \right)^2 \right]$$

The estimates ${}^{C}[\widetilde{\psi}\ \widetilde{B}_o\ \tilde{l}_{i,z}]$ allow for computation of R_3 and T which establishes the pose of Frame B in Frame C. The procedure is completed by updating the locations of the sensors ${}^{C}l_i$ using Equation (4.2) and the estimated values ${}^{C}[\widetilde{\psi}\ \widetilde{B}_o\ \tilde{l}_{i,z}]^T, i \in (p,q,r)$.

4.3 Error propagation in the lighthouse location measurement

In this section it is assumed that the location of Frame B in Frame C is determined with the minimum number of three sensors: $l_i, i \in (p, q, r)$. Obviously, the locations of these sensors in Frame B are cardinal parameters in the calculation of the location of the mobile platform. Although the location of each sensor is established as part of the design process of the rigid mobile platform, it is subjected to tolerances of manufacturing and assembly tolerances on the physical platform. The introduction of surface applicable sensors will definitely make the requirement for determination of the sensor locations manifest. Measuring the locations directly can be challenging as the consequence of their placement. Moreover, the light sensors have a finite surface area of 7.5 mm^2 of which a "focal point" representative for the timing of detection of the light sheet has to be established[10]. It seems sensible to use the geometric center of the sensor surface for this purpose, but this is no more than a "best guess". The consequential error ${}^C\delta l_i$ in the location of the mobile platform established with a location error ${}^B\delta l_i$ for a light sensor can be estimated by computation of a relative conditions number $\kappa({}^B l)$, which gives the ratio between the relative errors ${}^C\delta l/{}^C l$ and ${}^B\delta l/{}^B l$ for sensors $p,\ q$, and r [80]. $\kappa({}^B l)$ can be derived from the relationship between ${}^C l$ and ${}^B l$, through:

$$\kappa({}^B l) = \frac{||{}^B l||||J({}^C l, {}^B l)||}{||{}^C l||} \tag{4.3}$$

The Jacobian $J({}^C l, {}^B l)$ of the differentiation of ${}^C l$ to ${}^B l$ in Equation (4.3) is not simply the rhs of expression for ${}^C l$ in Equation (4.2) differentiated to ${}^B l$. ${}^C l$ is solved for three sensors s_p, s_q and s_r simultaneously in a two step solution.

Firstly the parameters for rotation $R_3 = R_3({}^C\psi)$ and translation $T = T({}^C B_o)$ are estimated, establishing the pose of Frame B in Frame C. These parameters are the Euler angles ${}^C\psi^T = {}^C[\psi_x\ \psi_y\ \psi_z]$ of rotation $R_3 = [R_z({}^C\psi_z)\ R_x({}^C\psi_x)\ R_y({}^C\psi_y)]$ around subsequently the y, x and z axes of Frame C and the location of the origin of Frame B in Frame C for the translation: $T^T = {}^C B_o^T = {}^C[B_{o,x}\ B_{o,y}\ B_{o,z}]$. ${}^C\psi$ and ${}^C B_o$ are approximated using the Levenberg-Marquardt algorithm [83] until the locations of the sensors in Frame C as computed with Equation (4.2) match the angles ϕ_p, ϕ_q, ϕ_r and $\theta_p, \theta_q, \theta_r$ at which the three sensors are sounded with the

lighthouse system.

Next, with the parameters ${}^{C}\psi$ and ${}^{C}B_o$ known, the locations ${}^{C}l_p$,${}^{C}l_q$ and ${}^{C}l_r$ can be calculated with Equation (4.2). Since the values of ${}^{B}l$ are used to find the estimates for ${}^{C}\psi$ and ${}^{C}B_o$, the latter are (implicit) functions of ${}^{B}l$: ${}^{C}\psi = {}^{C}\psi({}^{B}l)$, ${}^{C}B_o = {}^{C}B_o({}^{B}l)$. As a consequence $J({}^{C}l,{}^{B}l)$ has to be evaluated as:

$$J({}^{C}l,{}^{B}l) = [\frac{\partial {}^{C}l}{\partial {}^{C}\psi}\frac{\partial {}^{C}\psi}{\partial {}^{B}l} + \frac{\partial {}^{C}l}{\partial {}^{C}B_o}\frac{\partial {}^{C}B_o}{\partial {}^{B}l} + \frac{\partial {}^{C}l}{\partial {}^{B}l}] \tag{4.4}$$

The differential quotients $\partial {}^{C}\psi / \partial {}^{B}l$ and $\partial {}^{C}B_o / \partial {}^{B}l$ can be derived from implicit differentiation of Equation (4.1) to ${}^{B}l_i$ for $i \in (p,q,r)$, in which the terms $tan(\phi_i)$ and $tan(\theta_i)$ are constant as they refer to one measurement sample for θ_i and ϕ_i only. This reflects the actual situation in which measured values from one sweep of the lighthouse in both sweeping planes are plugged into θ_i and ϕ_i to compute ${}^{C}\psi$ and ${}^{C}B_o$.

$$\frac{\partial}{\partial {}^{B}l}\left[\ \tan(\theta_i)\ \tan(\phi_i)\ \right] = \left[\ 0\ \ 0\ \right] \tag{4.5}$$

In its form presented here, the relation between ${}^{C}\psi$ and ${}^{C}B_o$ from θ_i and ϕ_i is static as it does not comprise a time dimensions. This implies that the values for θ_i and ϕ_i are assumed to be acquired with Frame B being in exactly the same position in Frame C. Hence Frame B should move as little as possible in the time interval between the time stamps of the sensors involved. The Jacobian $J({}^{C}l,{}^{B}l)$ in Equation (4.4) is elaborated in Appendix B.

Inserting the resulting expressions in Equation (4.3) allows calculation of $\kappa({}^{B}l)$ as a function of ${}^{C}\psi$ and ${}^{C}B_o$. Figure 4.4 presents two graphs of this function, for the intended application scenario of a lighthouse system: $\kappa({}^{B}l)$ is computed over a planar space of 2 by 2 meter, with the lighthouse located at a height of 1 meter over and at 0.5 meter off the side of this space. In Graph A the ${}^{B}[x\ y\ z]$ axes of Frame B (the mobile platform) are aligned with the ${}^{C}[x\ y\ z]$ axes of Frame C. In Graph B, Frame B is offset over an angle of $\psi_z = -\pi/4$ radians compared to its pose in Graph A. In both scenario's $\kappa({}^{B}l)$ rates between 1.4 and 1.6 which means that a relative error of 1% in the location of the sensor translates into a relative error in the range of 1.4 – 1.6% of the computed location of Frame B in Frame C. This is quite a benign propagation

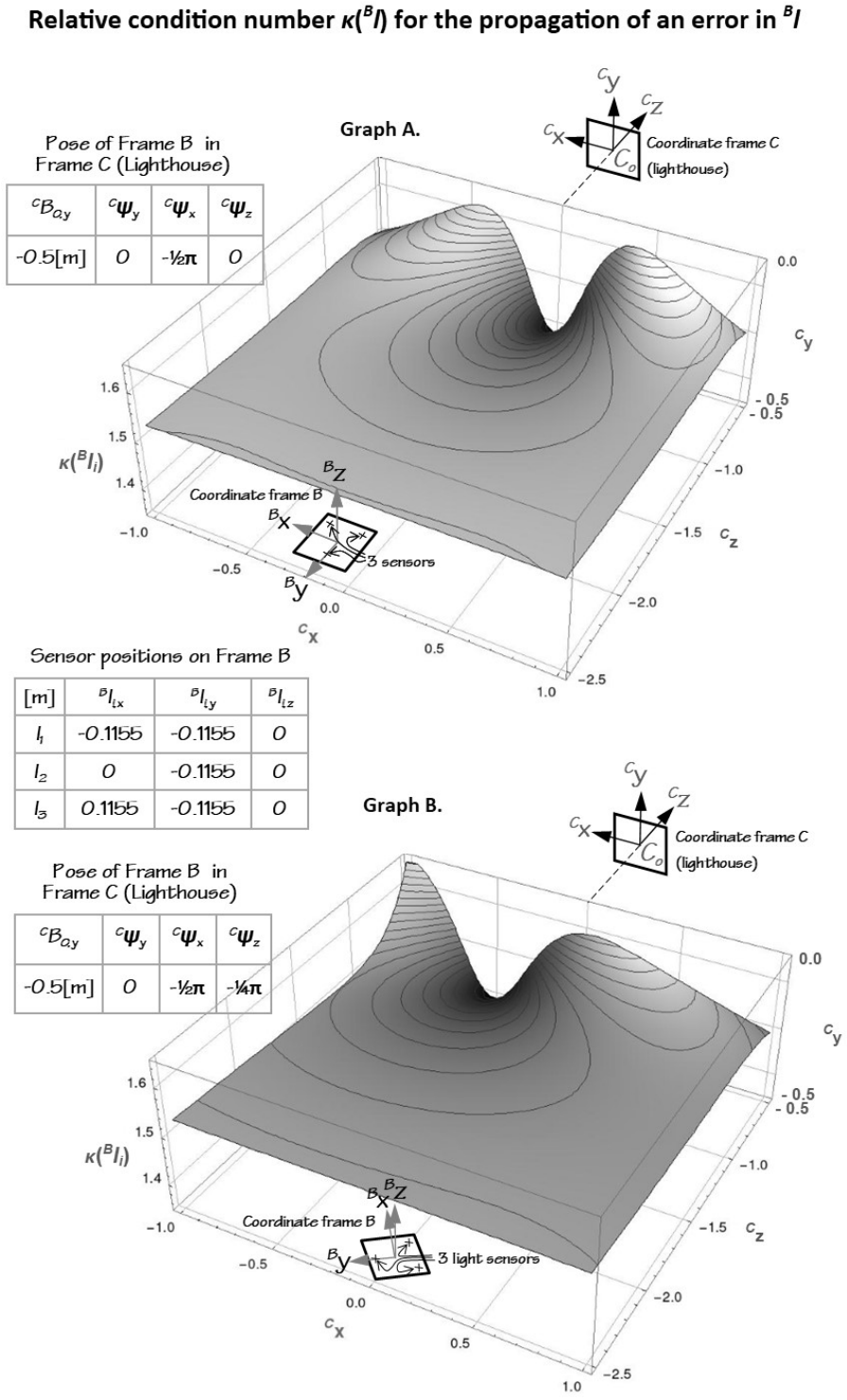

Figure 4.4: *Propagation of an error in the sensor location ${}^{B}l$ into the computed location of Frame B in Frame C, expressed as a relative condition number $\kappa({}^{B}l)$, in a planar workspace ${}^{C}[x\ z]$, for two values of ${}^{C}\psi_z$.*

of this error that shows very good agreement with a previous error propagation analysis based on a 2D analysis [84]. For most of the planar space in Graphs A and B, $\kappa({}^{B}l_i)$ the relative error propagation exhibits a very small, seemingly linear increase with increasing distance to the lighthouse. The increase is minor however and supports the observation that the relative error propagation is nearly constant at a value just above 1.5 at a distance of more than 1 [m] from the lighthouse. A nearly constant propagation of the relative error indicates that the absolute error in the location of ${}^{C}l$ is nearly proportional with the distance of ${}^{C}l$ to C_o. Closer to the lighthouse, $\kappa({}^{B}l)$ decreases as the difference between the sounding angles of the sensors become wider, which improves the conditioning of the location calculation, but at the same time makes the result more sensitive to the orientation of Frame B towards Frame C. This can be seen in Graph A at the higher z-side close to the lighthouse. Directly in front of the lighthouse, $\kappa({}^{B}l)$ has its minimum value, but if Frame B is moved sideways in either x-direction, $\kappa({}^{B}l)$ increases quite steeply as the consequence of the decreasing difference between the sounding angles of the sensors. This observation is supported by Graph B where Frame B is rotated. As a consequence the difference in sounding angles between the sensors now has its maximum off the origin of the x-axis, corresponding to the minimum value of $\kappa({}^{B}l)$ as reflected in the graph. These findings support the recommendation to equip a mobile platform to be operated in a lighthouse frame with more than 3 sensors, so that triplets of sensors with the largest difference in sounding angles can be selected to determine the mobile platform location [84]. This is a subject for further study and optimization. The present analysis indicates that for the intended application here $\kappa({}^{B}l)$ rates between 1.4 and 1.6.

4.4 Measurement of the sensor locations

Nevertheless the constant relative condition number at a fairly benign level, the amplification of absolute errors $\|{}^{C}\delta l_i\|/\|{}^{B}\delta l_i\|$ is still proportional to $\|{}^{C}l_i\|/\|{}^{B}l_i\|$ which is substantial for most lighthouse applications. For a mobile platform with light sensors in a square grid of 20 x 20 cm at 2 m distance of the lighthouse this amplification spans already one order of magnitude. The locations of the light sensors used in the computation of the mobile platform

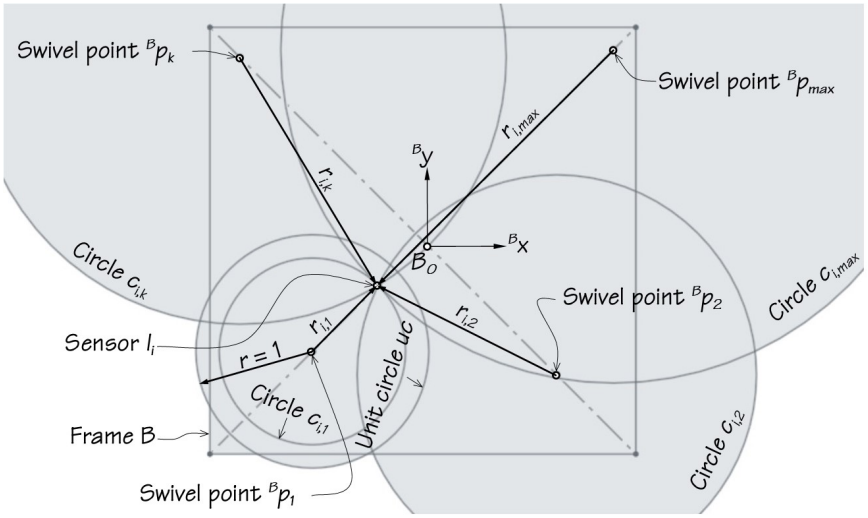

Figure 4.5: *Circular paths $c_{i,j}$ of sensor l_i around swivel points ${}^{B}p_k, k \in (1, 2, .., n_k)$ in Frame B.*

location have to be measured as accurate as possible to minimize errors in the localization. Calculation of the location of Frame B in Frame C is based on the time stamps of triplets of sensors, chosen from the available set of sensors. To obtain the most accurate location for the sensors with the minimum amount of effort, while avoiding use of expensive metrological equipment, the locations are derived from simple length measurements. Length measurements are robust compared to most other measurements and require only simple tools and procedures. Since it is hard to measure distance between any point and a light sensor as argued in Section 4.3, it is performed by the light sensor itself, by turning Frame B around a fixed anchor point ${}^{C}p$ in Frame C on a flat surface. This operation is comparable to the procedure described in Section 3.3.2 to measure the location of optical flow sensors. Similarly the "swivel point" ${}^{B}p_k,\ k \in (1, 2, .., n_k)$ which is the location of the point of rotation in Frame B, is aligned with fixed anchor point ${}^{C}p$ in Frame C at the axis of rotation. The locations of the swivel points relative to each other in Frame B have to be retrieved either from the (CAD) design information, or better, through measurement. Figure 4.5 illustrates the circular paths ${}^{B}c_{i,k}$ traveled by sensor l_i in each swivel motion of the mobile platform around a different swivel point ${}^{B}p_k$. The radii $r_{i,k}$ of circles ${}^{B}c_{i,k}$ drawn in Figure 4.5 are equal to the distance between sensor l_i and swivel point p_k: $r_{i,k} = \|l_i - p_k\|$. The number of light sensors on the mobile platform n_l has to be at least three to establish the location of Frame B in Frame C as explained in Section 4.3: $n_l \geqslant 3$.

Figure 4.5 shows the location of sensor l_i in Frame B at the intersection of circles ${}^{B}c_{i,k}$. ${}^{B}l_i$ is determined unambiguously by the intersection of the paths around at least three different swivel points at known locations in Frame B: $n_k \geqslant 3$.

In Frame C the mobile platform is swiveled around the same fixed anchor point ${}^{C}p$. As a consequence the circles described by sensor l_i occur as concentric circles ${}^{C}c_{i,k}$ around ${}^{C}p$, as depicted in Figure 4.6.

In the recommended setup for the lighthouse[4], the tangent values of the angles at which l_i is sounded by the light sheets on its circular path ${}^{C}c_{i,k}$ around swivel point ${}^{B}p_k$, represent an ellipse ${}^{P}c_{i,k}$ in perspective projection plane P, as expressed by Equation (4.1) and illustrated in Figure 4.6 [85]. Using methods for camera calibration, geometrical parameters can be extracted from the image of each ellipse ${}^{P}c_{i,k}$ and applied to reconstruct the location of the center ${}^{C}ucc_{i,k}$ of a unit circle ${}^{C}uc_{i,k}$ with the same elliptic perspective projection ${}^{P}c_{i,k}$. Appendix C describes the method from Philip to compute orientation and location of the center of the unit circles in the frame of a pinhole camera, which corresponds to Frame C for the present case [86]. Figure 4.6 shows corresponding sets of a unit circle ${}^{C}uc_{i,k}$ sharing the same perspective projection ${}^{P}c_{i,k}$ with circle ${}^{C}c_{i,k}$, drawn up by sensor l_i on its path around anchor point ${}^{C}p$. It can be observed in Figure 4.6 that the distance $\|{}^{C}ucc_{i,k}\|$ from the lighthouse in $C_o = [0\ 0\ 0]$ to the centre of the unit circles ${}^{C}ucc_{i,k}$, is inversely proportional to radius $r_{i,k}$ of the corresponding circle ${}^{C}c_{i,k}$: $\|{}^{C}ucc_{i,k}\| \sim r_{i,k}^{-1}$. This allows for the definition of a ratio $\rho_{i,k}$ that expresses $r_{i,k}$ as a fraction of radius $r_{i,max}$ of circular path ${}^{C}c_{i,max}$, that is traveled by sensor l_i around swivel point ${}^{B}p_{i,max}$ furthest away from l_i:

$$\rho_{i,k} = \frac{r_{i,k}}{r_{i,max}} = \frac{\|{}^{C}ucc_{i,max}\|}{\|{}^{C}ucc_{i,k}\|} \tag{4.6}$$

$$r_{i,max} = \max_{k}(r_{i,k})$$

$$i \in (1, 2, .., n_l)$$

$$k \in (1, 2, .., n_k)$$

$$n_l \geqslant 3 \qquad n_k \geqslant 3$$

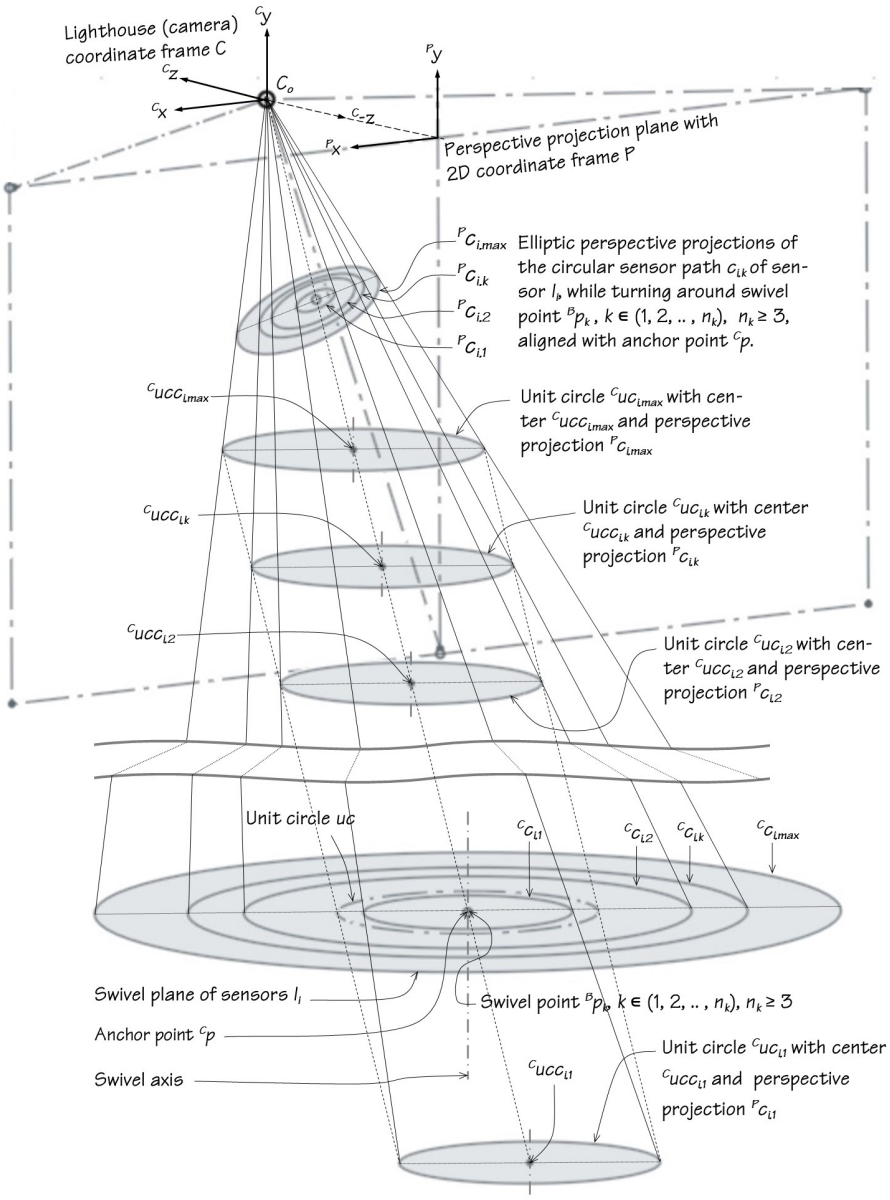

Figure 4.6: *Illustration of the circular paths of the swivel motion of sensor l_i around anchor point ${}^{C}p$ in Frame C using different swivel points $p_k, k \in (1, 2, .., n_k)$ and the unit circles sharing the same perspective projection.*

Obviously ${}^{C}c_{i,max}$ is the circular path with largest radius $r_{i,max}$ of the paths traveled by l_i around all swivel points ${}^{B}p_k$, as can be observed in Figure 4.5. $r_{i,k}$ can now be expressed as:

$$r_{i,k} = \rho_{i,k} \left\| {}^{B}p_{max} - {}^{B}l_i \right\|$$

The location of sensor ${}^{B}l_i$ is at the intersection of circles ${}^{B}c_{i,k}$, $i \in (1, 2, .., n_l)$, $n_l \geqslant 3$, in Frame

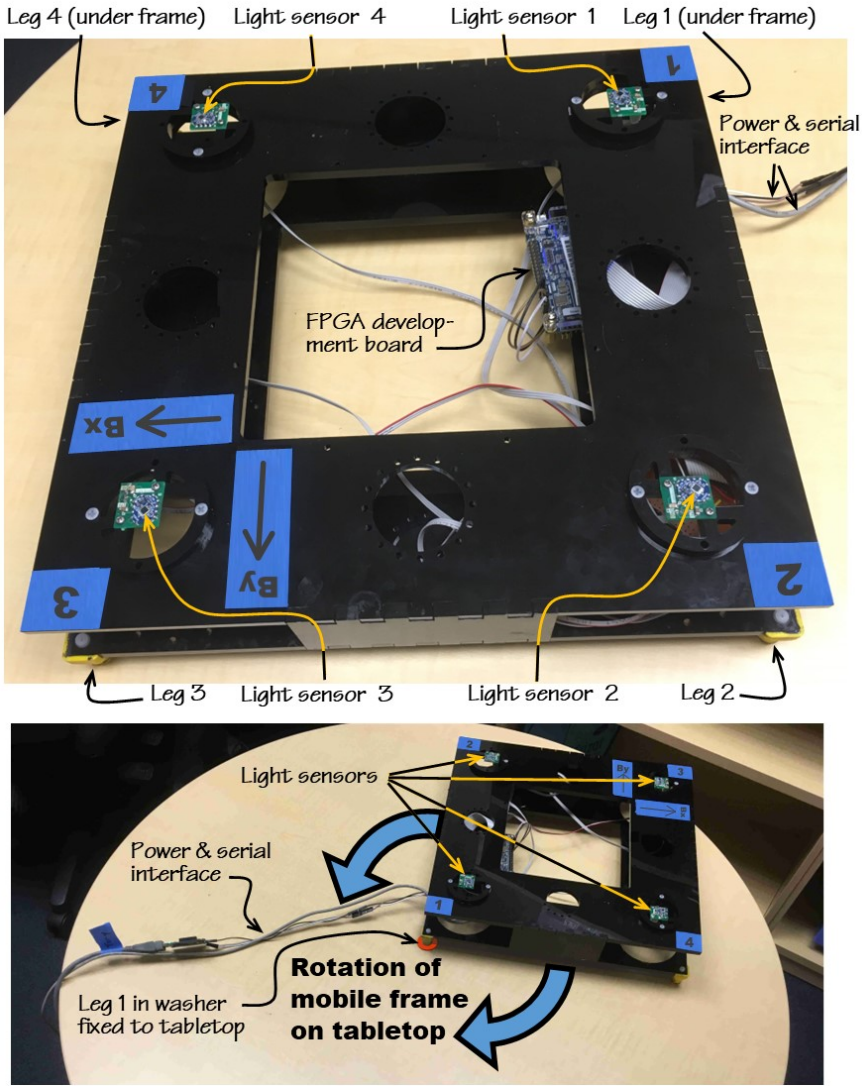

Figure 4.7: *Details of the mobile platform (top) and its operation on a tabletop (bottom).*

B, for which an estimate ${}^{B}\tilde{l}_i$ can be found by the following minimization:

$$ {}^{B}\tilde{l}_i = \arg\min_{{}^{B}l_i} \left[\sum_k (\| {}^{B}p_k - {}^{B}l_i \| - \rho_{i,k} \| {}^{B}p_{max} - {}^{B}l_i \|)^2 \right] \tag{4.7} $$

The sensor locations from the CAD file can serve here as a good starting point for the minimization.

4.5 Setup and experiments

4.5.1 Setup

To test the proposed approach to measure the light sensor locations, a mobile platform has been assembled sitting on legs with spherical caps at the bottom in each corner. Photos of the platform are shown in Figure 4.7. The platform was designed to be 326 mm square, but came out of the industrial grade laser cutter with hand measurable deviations of over 2 mm at the corners. This emphasizes the need for measurement of sensor locations even when using CAM parts. Four legs under the platform act as swivel points $p_k, k \in (1, .., 4)$ in the experiments.

The accuracy of the locations of the legs in the assembled platform is critical to the accuracy of the location of the sensors established in the experiments. Since these locations could deviate from their location in the CAD design as a consequence of the manufacturing tolerances observed, the mutual distance of the legs was measured and processed into locations using least square regression. The legs are numbered as indicated in Figure 4.7 and have locations ${}^B p_k = [{}^B p_{k,x}\ {}^B p_{k,y}]$ in Frame B. There are $\binom{4}{2} = 6$ distances $d_{(k_1,k_2)}$ between each pair of legs (p_{k_1}, p_{k_2}), $(k_1, k_2) \in (1, .., 4),\ k_1 < k_2$, as listed in Table 4.1. To estimate the locations of the legs, three coordinates of the four legs have to be fixed to prevent kinematic solutions to occur: ${}^B p_1 = [0\ 0],\ {}^B p_{4,y} = 0$. Estimates for the remaining locations ${}^B\tilde{p}_k,\ k \in (2, 3, 4)$ can be found through:

$$ {}^B\tilde{p_k} = \arg\min_{{}^B p_k} \left[\sum_{k_1,k_2} (||{}^B p_{k_2} - {}^B p_{k_1}|| - ||d_{k_1,k_2}||)^2 \right] $$
$$ k_1, k_2 \in (1, .., 4),\ k_1 < k_2 $$

The results of the estimate of ${}^B\tilde{p}_k$ as listed in Table 4.1 are used as the locations of the swivel points ${}^B p_k$ in the measurements of the sensor locations.

For the actual location measurement with the lighthouse, the mobile platform is equipped with four light sensors on top, designed to be at the same height, sharing the same plane in Frame B. The sensors share the same number with the leg it is closest to. The light sensitive part of the sensors is a BPW34S photo diode[10] integrated in a Triad TS3633-CM1 Light to Digital

Table 4.1: *Location of legs under the mobile platform.*

Measured distances $d_{(k_1,k_2)}$ [mm], between leg p_{k_1} and leg p_{k_2}					
$d_{(1,2)}$= 314	$d_{(1,3)}$ = 443	$d_{(1,4)}$= 314	$d_{(2,3)}$= 313.5	$d_{(2,4)}$ = 445	$d_{(3,4)}$= 313.5

CAD locations [mm]			**Estimated locations [mm]**		
$\boldsymbol{p_k}$	${}^B\boldsymbol{p}_{k,x}$:	${}^B\boldsymbol{p}_{k,y}$	$\boldsymbol{p_k}$	${}^B\tilde{\boldsymbol{p}}_{k,x}$	${}^B\tilde{\boldsymbol{p}}_{k,y}$
p_1	0	0	p_1	0	0
p_2	0	314	p_2	- 0.9	314.1
p_3	314	314	p_3	312.7	313.6
p_4	314	0	p_4	314.1	0

Converter[11], that is connected to a digital input of a DE0-Nano Development board[12]. The signals of the sensors are identified by their port address. The development board carries an Altera Cyclone IV FPGA running at 50 MHz, allowing simultaneous detection of the edges generated by the passing of the light sheet over the sensor, with a temporal resolution of 20 ns. The time stamps recorded by the FPGA are transmitted continuously through a serial connection over a USB port to a PC and stored for off-line processing.

4.5.2 Experiments

In the experiments, the mobile platform is moved over a table top as depicted in Figure 4.7, with a lighthouse base station installed in a cabinet adjacent to the table, facing the platform. The lighthouse is located at about 40 to 60 cm vertical distance over the tabletop and at about 80 to 90 cm radial distance from the anchor point at the center of the table. The location of the lighthouse is given as a range as adjustments are made in between the experiments to prepare for the next run. During the experiments the location of the lighthouse relative to the tabletop is fixed. In the experiments the platform is rotated around one of its legs, turning in a washer fixed in the center of the table top. The washer serves as the anchor point for the swivel motion. The spherical cap under the leg has a diameter slightly exceeding the inside diameter of the washer, creating a self centering swivel of the cap in the washer. During the experiments the mobile platform is weighed with some ballast over the swivel point securing the leg in its centered position. Data communication occurs over a serial wired connection between the FPGA board and a PC. To prevent the power and data cables to become entangled, the platform is pushed forth and backwards around the swivel point completing a full circle. This operation is repeated

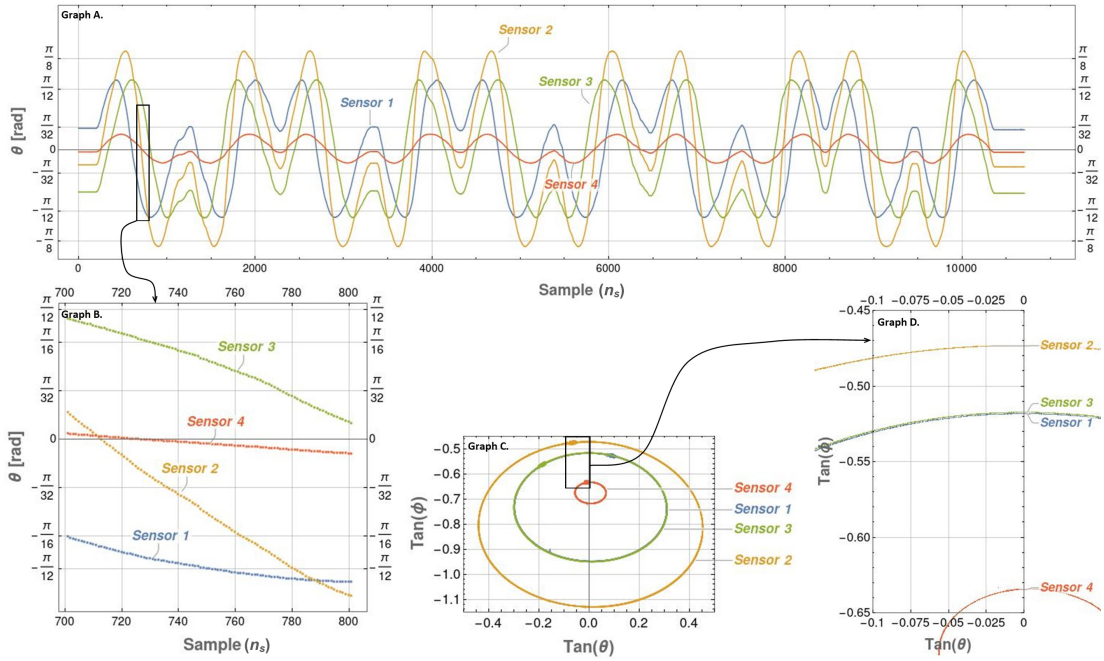

Figure 4.8: *Overview of the results from the swivel experiments using leg 4 of the mobile platform.*

10 times for all four legs, during which the time stamps are collected of the falling and rising edges of light pulses as explained in Section 4.2. Data of the swivel experiment with leg 3 were lost in the handling unfortunately, so that post processing was applied to the data of the experiments with legs 1, 2 and 4. Measurement of the sensor locations can be executed with data of three swivel points on the mobile platform minimally.

4.5.3 Results

The off-line post processing of the recorded time stamps starts with identification of the "heart beat" generated by the sync pulses of the lighthouse. These pulses are detected by multiple sensors simultaneously, have the same duration on all sensors and a period of 8.333 msec, which makes them generally not hard to find. Once the heartbeat has been established identification of the light sheet and associated angle as well as calculation of the magnitude of the angle at which the sensor is sounded is conducted according to the description in Section 4.2. Graph A in Figure 4.8 illustrates the horizontal sounding angle (θ) for four sensors in one experiment. It can be observed that the range of sounding angles is smallest for sensor 4, indicating leg 4

was used as the swivel point in this experiment. Consequently sensor 2, located at the diagonal opposite side on the mobile platform, swivels with the largest radius around leg 4, as reflected by the largest range in sounding angles. The periodicity of the graphs reveals the number of turns that the mobile platform has made (10) and the sample where the rotation was reversed, which is where the graphs of all sensors have a local extreme simultaneously. It can also be observed that during each turn about 1000 soundings were taken, translating to a rotation angle of the platform of $2\,\pi/1000$ radians per sample. In the close up of the graph, depicted in Graph B the separate samples can be identified and the absence of visible noise in the sounding angles observed. This last finding concurs with the observation from Niehorster et al., Greiff et al. and Bauer et al. that the level of jitter in the location measurements with the lighthouse system is very low [71, 73, 76].

Plotting the values of the measured data for $\tan\theta_{n_s}$ and $\tan\phi_{n_s}$ for each sweep n_s against each other, the predicted ellipses as the outcome of the perspective projection of the circular paths of the sensors occur in Graph C. In the close up of the ellipses in Graph D, it can be observed once more how clean the data is and how precise the samples of the 10 turns of the mobile platform fit on top of each other. There is hardly any deviation between the ten ellipses. The coordinate pairs ${}^{P}c_{n_s} = {}^{P}[c_{n_s,x}\ c_{n_s,y}] = [\tan(\theta)\ \ \tan(\phi)]$ obtained for each sensor in each sweep n_s, can now be used to compute the ellipse coefficients $(a_1, .., a_6)$ in Equation (C.2), introduced in Appendix C. Equation (C.2) applies to each point ${}^{P}c_{n_s}$ on the ellipse which enables the composition of a system of equations:

$$X\ a = 0 \tag{4.8}$$

where:

$$X = \begin{bmatrix} {}^{P}c_{1,x}^2 & {}^{P}c_{1,x}\,{}^{P}c_{1,y} & {}^{P}c_{1,y}^2 & {}^{P}c_{1,x} & {}^{P}c_{1,y} & 1 \\ & & \vdots & & & \\ {}^{P}c_{N_s,x}^2 & {}^{P}c_{N_s,x}\,{}^{P}c_{N_s,y} & {}^{P}c_{N_s,y}^2 & {}^{P}c_{N_s,x} & {}^{P}c_{N_s,y} & 1 \end{bmatrix}$$

and

$$a = \begin{bmatrix} a_1 & a_2 & a_3 & a_4 & a_5 & a_6 \end{bmatrix}^T$$

where N_s is the number of positions sampled.

Since Equation (4.8) is homogeneous in the coefficients a, the solution needs to be normalized to be unique: $||a|| = 1$. Under this constraint a can be solved by numerical minimization of $||X\ a||$ [87]. A more elegant and generally faster solution can be obtained from the Singular Value Decomposition (SVD) of $X = U_X \Sigma_X V_X^T$, with U_X and V_X orthogonal matrices spanned by the left-singular and right-singular vectors of $m \times n$ matrix X. Σ_X a diagonal matrix with the singular values $[\sigma_1 \dots \sigma_m]$ of X, arranged in descending order. The SVD of X is applied as follows to minimize $||X\ a\ ||$:

$$\begin{aligned} &\min_{||a||=1} ||X\ a\ || = \min_{||a||=1} ||\ U_X \Sigma_X V_X^T\ a\ || \\ &= \min_{||a||=1} ||\ U_X \Sigma_X (V_X^T\ a)\ || = \min_{||y||=1} ||\Sigma_X\ y\ || \\ &= \min_{||y||=1} (\sigma_1\, y_1 + \cdots + \sigma_m\, y_m) \geq \sigma_m \end{aligned}$$

where $V_X^T a = y$. Hence, the minimum value for $||X\ a\ ||$ is σ_m which is attained for $y = [\ 0\ 0\ \dots\ 0\ 1\ ]^T$. This implies that $a = V_X y = v_m$, the last right singular vector of X, corresponding to the smallest singular value [88]. With the ellipse coefficients $(a_1, .., a_6)$, matrix Q can be assembled according to Equation (C.4) introduced in Appendix C and the location ${}^C ccu$ and orientation ${}^C nc$ of the unit circles determined following Expressions (C.7) and (C.6) in Appendix C. The solution obtained for ${}^C ccu$ enables computation of $\rho_{i,k}$ using Equation (4.6) with which the location ${}^B l_i$ of the sensors in Frame B can be estimated with Equation (4.7). For the general case, Equation (4.7) is meant to be solved for each light sensor l_i separately. Since the light sensors in the present experiment are all mounted on the same height on top of the mobile platform and share the same the plane for all circles as a consequence, Expression (4.7) can be solved for all combinations of light sensors and swivel points simultaneously. The resulting sensor locations of this computation are listed in Table 4.2 next to the locations according to the CAD file.

Table 4.2: *Measured ratio of sensor circle radii and sensor locations calculated from measurements and design (CAD) specifications.*

	Radii ratio $\rho_{i,k}$			**Measured location [m]**		**CAD location [m]**	
p_k / l_i	p_1	p_2	p_4	${}^{B}l_{i,x}$	${}^{B}l_{i,y}$	${}^{B}l_{i,x}$	${}^{B}l_{y,i}$
l_1	0.1514	0.7143	0.7127	-0.115073	-0.115619	-0.115375	-0.114918
l_2	0.7154	0.1503	1	-0.116556	0.115984	-0.115375	0.116082
l_3	1	0.7131	0.7158	0.115112	0.116721	0.115625	0.116082
l_4	0.7157	1	0.1515	0.116342	-0.115441	0.115625	-0.114918

4.6 Validation of the mobile platform path

The accuracy of the locations of the sensors determined with the procedure described in Section 4.5, is investigated though reconstruction of the path of the mobile platform in the experiments and the path of the leg used as swivel point in particular. This leg only turns around its axis and does not translate in the experiments. Its stationary position in the turns with the mobile platform should be reflected in the reconstructed poses of the platform. In fact the deviation of the swivel point from its "mean" position in the reconstructed poses is not only a good measure for the precision of the lighthouse localization system but also of its accuracy as it is known that the true deviation is zero. The path of Frame B in Frame C is simulated by reconstruction of the pose of the mobile platform for each sweep n_s of the lighthouse according to the procedure described in Section 4.3:

- Firstly the angles ${}^{C}\psi(n_s)$ and location ${}^{C}B_o(n_s)$ are estimated for all possible triplet combinations out of the available set of sensors. Out of the locations calculated for each of these triplets a trimmed mean location ${}^{C}\overline{B}_o(n_s)$ is established in which the triplet locations with the largest deviation to the calculated mean location are dropped. In this case with time stamps of four sensors available, the worst 25% locations (being 1 location out of four triplets) is dropped.

- Then, applying the coordinate transformation of Equation (4.2), the location of swivel point p_k in Frame C is found by: ${}^{C}p_k = [\, R_3 \,|\, T \,]\, {}^{B}p_k$, where $k \in (1, 2, 4)$ is the number of the leg used as swivel point.

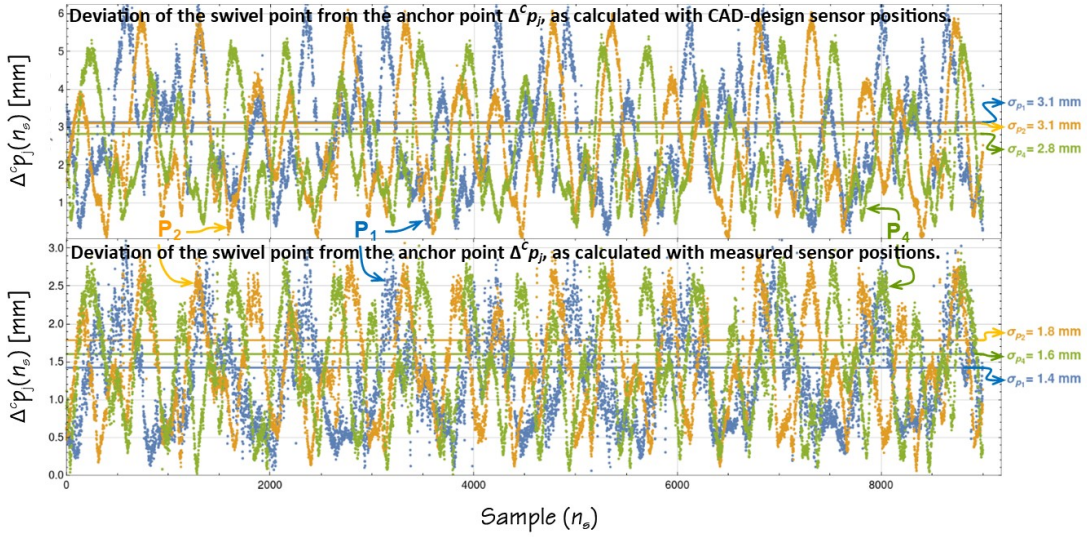

Figure 4.9: *Deviation of the calculated location of the swivel points from the stationary anchor point in the swivel experiments.*

The movement of the swivel point p_k is expressed as the standard deviation σ_{p_k} of all positions sampled in an experiment with swivel point $k \in (1, 2, 4)$, comprising of about $N_s = 10,000$ samples:

$$
\begin{aligned}
{}^C\overline{p}_k &= \frac{1}{N_s} \sum_{n_s=1}^{N_s} {}^C p_k(n_s) \\
\Delta^C p_k(n_s) &= \| {}^C p_k(n_s) - {}^C \overline{p}_k \| \\
\sigma_{p_k} &= \sqrt{\frac{1}{N_s} \sum_{n_s=1}^{N_s} ({}^C p_k(n_s) - {}^C \overline{p}_k)^2}
\end{aligned}
$$

$\Delta^C p_k(n_s)$ is plotted in Figure 4.9 for the three swivel experiments with legs 1, 2 and 4, for the two cases simulated: with sensors in design location according to the CAD file and with sensors in the measured locations. Table 4.3 summarizes the results. The error in the location of the swivel point is expressed as a relative error $\sigma_{p_k} / \| {}^C\overline{p}_k \|$ which makes it independent of the distance from the sensors to the lighthouse. This allows for easier comparison of the different results. It can be observed that measurement of the sensor locations has reduced σ_{p_k} by 40%, which is a significant improvement of the precision of the localization of a rigid body with a lighthouse system. Since it is known that the location of the anchor point is stationary in the

Table 4.3: *Comparison of the deviation of the reconstructed location of the swivel point for the sensors in measured and design (CAD) location.*

Swivel point	Estimated location of anchor point: ${}^{C}\overline{p}_k$				Sensors in measured location		Sensors in CAD location	
k	${}^{C}\overline{p}_{k,x}$	${}^{C}\overline{p}_{k,y}$	${}^{C}\overline{p}_{k,z}$	$\|{}^{C}\overline{p}_k\|$	σ_{p_k}	$\sigma_{p_k}/\|{}^{C}\overline{p}_k\|$	σ_{p_k}	$\sigma_{p_k}/\|{}^{C}\overline{p}_k\|$
1	0.01034	-0.6398	0.9489	1.1445	0.001425	0.12%	0.003138	0.28%
2	-0.0355	-0.3859	0.7723	0.8641	0.001789	0.21%	0.003109	0.36%
4	-0.0356	-0.3849	0.7723	0.8637	0.001605	0.19%	0.002827	0.33%

All locations and standard deviations in meter.

swivel motion, the measured improvement of the precision of the location of Frame B in Frame C for different poses of Frame B, also expresses improvement of the accuracy of the location established with the lighthouse system. This is demonstrated by the graphs in Figure 4.9 that exhibit periodicity of $\Delta^{C}p_k(n_s)$, in sync with the turns of the mobile platform. The periodicity reveals a systematic error in the localization of the anchor point, dominating the magnitude of $\Delta^{C}p_k(n_s)$, that is most likely caused by remaining inaccuracies of the locations of sensors and swivel points. Hence $\Delta^{C}p_k(n_s)$ can be used as a cost function to identify and further minimize systematic errors in the localization with a lighthouse system.

Under the assumption that the periodicity of the graph is caused by systematic errors, the noise level, superimposed on the systematic error in the graphs in Figure 4.9 is estimated by visual inspection to be about an order of magnitude smaller than the systematic error in the location in the top graph. This rates the noise level at a magnitude of about 3 $[10^{-4}\,\text{rad}]$, just above the top of the range measured by Bauer et al. for one lighthouse base station (5.5 – 27.8 $[10^{-5}\,\text{rad}]$) using a tracker with 22 light sensors.

The result of the present research to measure the locations of the sensors on the mobile platform, is a reduction of the relative localization error of the lighthouse system from over 0.3% to below 0.2% using one lighthouse base station.

4.7 Concluding remarks

The findings in the present chapter can be summarized in the following conclusions:

- The tangent values of the horizontal and vertical angles θ and ϕ respectively at which light sensors are sounded by the lighthouse system coincide with the horizontal and vertical coordinate of the perspective projection of the light sensors [Section 4.2.1].
- Based on this principle a new experiment is designed in which the light sensors are moved in a circle by swiveling the mobile platform around an anchor point. The circular paths of the light sensors are recorded by the lighthouse system as perspective projections of concentric circles around the anchor point. Using camera calibration methods enables computation of the ratio of radii of the circular paths from the elliptic projections with which the location of the sensors in the mobile platform can be established [Section 4.4].
- The certainty that the location of the swivel point of the mobile platform is fixed at an anchor point during the experiments is used to validate the obtained sensor locations, without performing additional experiments [Section 4.6].
- The approach to use camera calibration techniques is an effective way to improve the accuracy of the location measurement with the lighthouse system without using external measurement instruments for calibration [Section 4.4]. After measuring the sensor locations on the experimental mobile platform with the present procedure, the relative error of the location of the mobile platform established with one lighthouse base station, dropped from over 0.3% to below 0.2% (meter error per meter distance) [Section 4.6].
- The relative condition number for the propagation of errors in the location of the light sensors into the calculated location of a mobile platform rates between 1.4 and 1.6 for the HTC Vive lighthouse system base station [Section 4.3].
- The nearly constant value of the relative condition number over most of the operating range of the lighthouse implies that the error in the calculated location of a mobile platform is about linear with the distance to the lighthouse base-station [Section 4.3]. This observation is backed up by the measurements by Bauer et al. [76].

- The noise level in the angles at which the light sensors are scanned in the experiments reported is estimated at a magnitude of $3\ [10^{-4}\,\text{rad}]$ [Section 4.6]. This noise level is just above the top of the noise range measured by Bauer for one lighthouse base station (5.5 – $27.8\ [10^{-5}\,\text{rad}]$) using a tracker with 22 light sensors [76].

Chapter 5

Discussion and conclusions

The introduction of a mobile platform that can cut and engrave sheet material with a laser beam dramatically increases the capability and versatility of desktop manufacturing technology and empower the professional and semi-professional maker with small machines that can do big things. It will not only make a significant addition to the tool set for the maker community, but potentially also a useful contribution to the development of mobile devices for manufacturing in general, which has been earmarked as one of the spearheads of the Industry 4.0 R&D program.

Accurate localization is cardinal in the design of mobile platforms for manufacturing as argued in Section 2.3. The present thesis contributes to the development of a localization system by researching methods to measure location, orientation and displacement of a mobile platform.

To judge the feasibility of application of the methods researched, a benchmark is compiled from design practices for parts cut from sheet material with a laser cutter as reported in Table 2.1 in Section 2.2. The benchmark states that the maximum allowable manufacturing tolerance of a part is 0.1% of the maximum dimension of the part to be cut. The mobile platform carrying the laser cutter has to localize itself with a better accuracy by some margin to be able to cut a part within this tolerance [Section 2.3].

The experience with laser cutting parts for the mobile platform used in the present research project demonstrates that the benchmark is no trivial condition: the square bottom and top panels of the mobile platform of the experimental setup shown in Figures 3.6 and 4.7, that were cut on an industrial grade flatbed laser cutter using a gantry to move the toolhead, were

off-spec according to the design codes of all industries consulted [Section 2.2]. Thanks to their dimensional failures however, the panels contributed greatly to the project by raising the awareness that although CAD-CAM is used to produce the panels, the locations of the mounting holes for the sensors in the panels can not be assumed to be in close agreement with the designed location. Analysis of the propagation of errors in the location of sensors in the mobile platform in Section 4.3 underscores the importance of accuracy of the sensor locations and expresses the necessity to measure the sensor locations. This was a crucial finding for the course of the research as the requirement to measure the location and orientation of the optical flow sensors and the location of the light sensors occurs for any mobile platform equipped with multiple sensors for the purpose of measuring its location and orientation. Measurement of the location of the sensors will be certainly required when after market surface applicable sensors become available that can turn any rigid body into an object that can be spatially tracked with a lighthouse.

In this context the present research project focuses on the design of a localization system for mobile platforms that is easily calibrated and validated to be fit for its purpose: measuring the location and orientation of a mobile platform to enable it to support manufacturing operations within the allowable manufacturing tolerances.

5.1 Discussion

5.1.1 Experimental design

In all models used to compute the displacement, location and orientation of a mobile platform from measurement by multiple optical flow sensors or multiple light sensors, the relative location of the sensors towards each other in the mobile platform coordinate system is a highly critical parameter. Errors in the locations of the sensors are amplified in the calculation of the displacement and location of the mobile platform. Accuracy of the sensor location and orientation is cardinal for an accurate estimate of the location and orientation of the mobile platform as argued in both Chapters 3 and 4. In the models describing the kinematic relationship between the displacement of the optical flow sensors and the displacement of the mobile platform

as well as the model describing the geometric relationship between the position of the projection of the light sensors and the location of the mobile platform, the locations of the sensors are represented by a point in the coordinate frame of the mobile platform (Frame B). Since the physical sensors are by no means points however, a ”focal point” has to be identified on the sensor’s radiant sensitive area to properly represent the sensor location in the model. There is no physical basis why this point would coincide necessarily with the geometrical center of the sensor. Moreover the sensors sit on a surface somewhere in a rigid platform that has manufacturing tolerances which makes their location even more unlikely to comply with their designed locations. The only way to beat these odds is by measuring the sensor location and orientation with the sensors themselves.

For this purpose an experimental procedure is designed that forces the mobile platform to swivel over a circular path around a fixed ”anchor point”. The circular motion of the mobile platform imposes an additional constraint on the kinematic and geometric model that enables calculation of the sensor location from the displacements and locations measured by the sensors themselves. Consequently the location of each sensor calculated from these measurements is the position of the ”focal point” of the sensor.

The use of the fixed anchor point in the experiments also allows the same measurement data to be used for validation of the measured sensor locations. The displacements and positions measured with the sensors in the swivel motion are used as input in the kinematic and geometric models with the sensors in their measured location, to calculate the displacement and location of the mobile platform without imposing the constraint of the fixed anchor point. If the sensors are in the correct locations in the model, the simulated displacement and location of the platform reflect the circular path with which the displacements and locations were recorded by the sensors. Ideally, the ”swivel point”, of the mobile platform which is the point on the mobile platform aligned with the anchor point in the swivel motion does not translate linearly. Any translation of the swivel point of the mobile platform in the simulation can be considered to be caused by measurement noise or an error in the sensor locations. Since the systematic errors in the experiments are recognizable by their periodicity in synchronization with the swivel motion, it is fairly easy to recognize that the sensor locations are still somewhat off in the validations of

both optical flows sensors in Section 3.6 and light sensors in Section 4.6. At the same time the deviations of the swivel point can be used as a cost function to further improve the locations of the sensors, but in that case new measurements have to be conducted for validation.

As a consequence of a shared design for the experiment to measure the location and orientation of the optical flow sensors and the experiment to measure the location of the light sensors, the procedure to swivel the mobile platform around an anchor point is similar in both experiments and can be combined in one procedure to measure the location of both types of sensors. The swivel motion is constrained by a condition to the angle over which the mobile platform swivels for the measurement with the optical flow sensors, but that does not prevent determination of the location of the light sensors from their readings in the same procedure. There is no requirement to swivel the mobile platform over a full circle to compute the locations of the light sensors. A partial circle around each swivel point as used for the measurement of the measurement of the optical flow sensors is adequate to determine the locations of the light sensors as well.

An additional advantage of combining the experimental procedures to measure the orientation and locations of the optical flow sensors and the locations of the light sensors is that the location of the swivel points can be established from the readings of the optical flow sensors when the sensitivity of the optical flow sensors is measured first. In that case the hand measurements of the distance between the swivel points as used in Section 4.4 can be avoided with more accurate results. All advantages of the experimental design to measure the locations of the optical flow sensors mentioned in Section 3.7 will extend to the measurement of the light sensors as well: it requires only one measurement to set the length of a straight path to measure the optical flow sensor sensitivities. Orientations and locations of all sensors on the mobile platform can be derived subsequently from the displacements measured by the optical flow sensors and bearing angles measured by the light sensors on the mobile platform in the swivel experiments. This makes design of the experiments highly suitable to be implemented as a self-calibration procedure.

5.1.2 Sensor timing and sensor fusion

In addition to the accuracy of the location of the sensors on the mobile platform, the accuracy of the location of the mobile platform computed from the displacements and locations measured by the optical flow and light sensors depends on the timing of the sensor readings. The odometry model introduced in Section 3.2 is a purely static (algebraic) model to compute the displacement of the mobile platform from the displacement data measured by the optical flow sensors. Since the model has no time dimension, the displacement data is assumed to be collected between exactly the same time instances for all sensors. This is the principal condition of the design of the data acquisition system that synchronizes the collection of displacement data from the optical flow sensors in a schedule of strict coincidence, as explained in Section 3.4.1. The lighthouse system described in Section 4.2.1 reconstructs the location of the mobile platform from the locations of the light sensors in perspective projection as acquired with the sweeps of the lighthouse. The geometric relationship between the location of the mobile platform and location of the light sensors in perspective projection is also purely static. The issue here is that by design of the lighthouse system the locations of the different light sensors cannot be acquired coincidentally. The locations in perspective projection are calculated by the length of the time interval between the sync pulse from the lighthouse and the passing of the light sheet over the sensor as explained in Section 4.2.1. By principle this can not be scheduled coincidentally for multiple sensors in different locations. If the mobile platform is not moving the sensors are not moving and the measurement is exact. If the platform is moving, the sensors change position in the lighthouse coordinate frame between the instances of the light sheet sweeping over each light sensor. The sensor is recorded in the wrong location as a consequence of which the error propagation has been elaborated in Section 4.3. To make this tangible with an example it is presumed that the mobile platform moves straight at a modest speed of 6 cm/sec while the lighthouse system scans its position with the fixed frequency of 60 Hz. The platform moves over 1 mm between each scan which is the worst case order of magnitude of an error in the measurement of the location of a light sensor. Assuming that the sensors are placed about 20 cm apart on the mobile platform a misplacement of 1 mm represents a relative error of 0.5% in the location of the sensor. According to the analysis in Section 4.3 the relative condition

number of the lighthouse system in its recommended setup rates between 1.4 to 1.6, which means that the relative error in the location of the mobile platform is amplified from 0.5% to a range between 0.7% to 0.8%. The absolute misplacement of the mobile platform is 0.7% to 0.8% of the distance from the platform to the lighthouse. This is a fatal error in perspective of the benchmark set for the mobile platform of a location accuracy of 0.1%.
The situation can be improved by the use of a dynamic model describing the motion of the mobile platform and a Kalman filter that compares the location of the platform as predicted by the model using input from the light sensors with the location as derived by integration of the displacements measured with the optical flow sensors.

5.2 Observations and conclusions

5.2.1 Odometry with optical flow sensors

Previous research established that the precision of the odometry of a mobile platform using optical flow sensors depends on the sensitivity of the sensors used and is inversely proportional to the number of sensors installed [Section 2.5.3]. The accuracy of the displacement of a mobile platform measured with optical flow sensors depends on the accuracy of the sensor location and the timing of the data acquisition with the sensors [Section 2.5.3]. The best distribution of the sensors is in a regular polygonal arrangement of maximum possible size on the mobile platform [31, 39]. The orientation of the sensors has no consequences for the sensibility of the odometry system with optical flow sensors [39].

In addition, the present research has determined that the propagation of a relative error in the sensitivity of the optical flow sensors is constrained to a relative error in the calculated displacement of the mobile platform of the same magnitude [Section 3.2.1]. The noise in the measured sensitivity on rough surfaces is smaller than the noise in the sensitivity measured on smooth surfaces [Section 3.7].

The research conducted has produced designs of the following system and experiments:

- A data acquisition system that executes the data collection with the optical flow sensors in a schedule of strict coincidence;

- A simple experiment to measure sensitivities of optical flow sensors;
- An experiment to measure location and orientation of the optical flow sensors on the mobile platform using readings from the sensors itself.

In the latter experiment orientation and location of the sensors are determined in independent computations from the same set of measurement data acquired with the optical flow sensors while swiveling the mobile platform around a fixed anchor point, without any prior knowledge of the location of the sensors or the anchor point. Since the anchor point is stationary in each experiment, its displacement as calculated with the measured values for the orientation and location of the optical flow sensors directly reflects the measurement error of the location of the mobile platform and can serve as a validation, without performing additional experiments [Section 3.3.2]. After establishing the location and orientation of the optical flow sensors on the experimental setup with the method designed in the present research, the accuracy of the odometry performed with the setup using four optical flow sensors exhibits considerable improvement. The computed location of the swivel point of the mobile platform deviated 0.16% of the total distance (6.7 meter) traveled by the mobile platform [Section 3.6]. The simple experimental procedure and usage of readings from the optical flow sensors only, strongly facilitate implementation of the method in a self-calibration operation.

5.2.2 Absolute location measurement with a laser lighthouse

The research conducted on absolute location measurement of a mobile platform with the lighthouse system comprises analysis of the propagation of errors in the location of the light sensors on the mobile platform in the computation of the absolute location and orientation of the mobile platform. In the recommended setup of the HTC Vive lighthouse base station, the relative condition number for the propagation of errors in the location of sensor into the calculated location of a mobile platform rates between 1.4 and 1.6. The nearly constant value of the relative condition number over most of the operating range of the lighthouse implies that the error in the calculated location of a mobile platform is about linear with the distance to the lighthouse base-station [Section 4.3]. This observation complies with the observation that

the noise in the bearing angles at which the sensors on the mobile platform are sounded, are independent from the distance to the lighthouse [76].

Additionally an experimental design is derived from a camera calibration method, to measure the location of the light sensors on the mobile platform using readings from the sensors itself [Section 4.4]. In the experiment the mobile platform is swiveled around a fixed anchor point similar to the experiment to measure the location and orientation of optical flow sensors in a mobile platform. Since the anchor point is stationary in this experiment too, its displacement as calculated with the measured values for the location of the light sensors directly reflects the measurement error of the location and orientation of the platform and can serve as a validation again, without performing additional experiments. Validation of the designed method to measure location and orientation of the light sensors demonstrates its efficacy. The relative error (meter error per meter distance) of the location of the mobile platform, computed under the assumption that the sensors are in their designed (CAD) location on the mobile platform, amounted to 0.3%. This error dropped to below 0.2% when using locations of the sensors on the mobile platform as measured with the experimental method designed in the present research [Sections 4.4 and 4.6]. The level of angular noise observed in the experiments is of the same order of magnitude as the noise level reported in the open literature. The simple experimental procedure and usage of readings from the light sensors only, strongly facilitate implementation of the method in a self-calibration operation.

Further observations reported in the open literature, relevant for future work are:

- The noise in the location obtained from the measurement with a single lighthouse is non-isotropic and is strongest in the direction of the line of sight between the lighthouse and the tracked object. In the direction perpendicular to the line of sight, the magnitude of the noise is two to three times smaller [76].

- The angular noise correlates inversely to the number of light sensors mounted on the tracked object [76].

5.3 Feasibility

The main question to be addressed after conducting the research reported in the present thesis is whether it is feasible to measure the location and orientation of a mobile platform within the allowable manufacturing tolerances to enable it to manufacturing parts of the required quality. In Chapter 2 the feasibility question has been quantified by the formulation of a benchmark for the allowable manufacturing tolerances at 0.1% of the maximum dimension of the part. Assuming that the location measurement system can be arranged in such a way that the maximum distance of the mobile platform to the navigation beacon(s) is of the same magnitude as the maximum dimension of the part, the benchmark implies that the location of the platform has to be measured with a combined accuracy and precision better than 0.1% of the distance to the navigation beacon to make this possible. The following observation and conclusions of the research conducted give some perspective to this challenge:

1. The noise level in the angles at which the light sensors are sounded in the experiments, where the mobile platform is moving slowly, is estimated at an order of magnitude lower than the allowable manufacturing tolerance level [Section 4.6]. This observation is backed up by measurements reported in the open literature in which both noise level and accuracy of the localization of a stationary tracker equipped with 22 light sensors meet the benchmark requirements [76].

2. The location of the swivel point of the mobile platform computed from the displacements measured with the optical flow sensors deviates 0.16% of the total distance (6.7 meter) traveled by the mobile platform in the swivel experiments [Section 3.6]. Although this figure seems to exceed the benchmark value, it has to be considered that the absolute error in the displacement of the mobile platform measured with optical flow sensor can be reduced by using a sampling interval for the displacement that is shorter in time and as a consequence shorter in absolute distance traveled by the mobile platform. Since the sampling frequency was about 650 Hz in the experiments, at the maximum speed of the mobile platform of 100 [10^{-3} m/sec], the displacement of the platform is 100/650 = 0.15 [10^{-3} m/sample]. The expected value of the error of the measurement with optical flow

sensors is $0.16\% \times 0.15$ = 2.4 [10^{-7} m/sample]. The conclusion from this estimate is that the length of the sampling interval can easily be tuned to keep the error of the odometry with optical flow sensors within the margins of the allowable manufacturing tolerances as long as there is a sufficiently accurate measurement of the location of the mobile platform in the absolute (lighthouse) reference frame to reset the odometry.

3. After measuring the locations of the sensors on the mobile platform with the procedure introduced in Section 4.4, the relative error of the location of the mobile platform established with one lighthouse base station, dropped below 0.2%.

The conclusion is that the lighthouse system can locate the mobile platform within the required tolerances at 0.1% when it is stationary as the precision of localization with the HTC-Vive laser lighthouse base station is an order of magnitude better than the benchmark. When moving however, the location of the mobile platform can not be measured within the required tolerances with the present lighthouse setup due to a lack in accuracy. Since the mobile platform is supposed to perform laser cutting at a speed up to 10 cm/sec further development of the localizations is required. The present research has identified many leads for continued research and improvement of the localization system that will be discussed in in the next section.

5.4 Future work

In addition to experimental designs to measure the locations and orientations of optical flow sensors and light sensors in the coordinate system of a mobile platform, the present research has identified and opened up many opportunities for further research and improvement of the accuracy of the localization of a mobile platform applying incremental odometry with optical flow sensors and localization with a laser lighthouse:

- **Improve accuracy of estimated location and orientation of the sensors**

  As suggested earlier in Section 5.1.1, the deviation of the swivel point on the mobile platform from the anchor point as computed from the measurement data from the sensors can be used to improve the accuracy of the estimated location and orientation of both

optical flow sensors and light sensors on the platform. A new independent measurements data set has to be acquired in that case to validate the updated locations of the sensors.

- **Increase of the number of sensors on the mobile platform**

  Bauer et al. observe an inverse correlation between the angular noise of the lighthouse system and the number of light sensors mounted on the tracked object [76], but lack the data to characterize the correlation. According to the analysis made for optical flow sensors in Section 2.5.3, the precision of the displacement of a tracked object computed from the displacement measured by multiple sensors on the object is inversely proportional to the number of sensors used, as expressed by Equation (2.4). It is expected that a similar relation exists for number of light sensors on a tracked object. As the experimental mobile platform used in the present research carried only four optical flow sensors and four light sensors, substantial improvement of the precision of the localization can be expected from increasing the number of sensors on the platform.

- **Selection of subsets of sensors from the sensors available on the mobile platform**

  An analysis by Paijens et al. of the error propagation in a 2D version of the lighthouse system demonstrates a strong dependency of the relative condition number on the orientation of the sensor triplet used to localize the mobile platform, towards the lighthouse [84]. The observation is that the larger the difference between the angles at which the sensors in the triplet are sounded, the lower the condition number of the computation of the location of the triplet and the more precise the location of the mobile platform is. This observation can be compiled in an algorithm that picks the sensors used for the location measurement of the mobile platform to obtain the highest accuracy and precision of the computed location. Hu et al. demonstrate that a similar strategy to calculate the displacement of a mobile platform as a trimmed mean of displacements measured by optical flow sensors can be applied to increase the accuracy and precision of incremental odometry [37].

- **Location of the lighthouse**

  Bauer reports significant more accurate results for the localization of trackers that move

in directions perpendicular to the line of sight between the tracker and the lighthouse than of trackers moving in the direction of the line of sight [76]. As mentioned in Section 2.6.1 this corresponds to the notion that movements of objects perpendicular to the line of sight are easier to spot than movements in the direction of the line of sight. Following this line of thought, to monitor the movements of a mobile platform over a plane, the best location for a lighthouse is overhead facing downward at the plane. Although this setup requires some rigging of the lighthouse and limits its flexible deployment to a certain extent, it also reduces the maximum distance between lighthouse and light sensors on the mobile platform and could significantly improve accuracy and precision of the localization of the platform. Analysis of the error propagation for this setup is strongly recommended.

- **Sensor fusion**

  The measurements of the optical flow sensors and the light sensors can be fused by through the use of a dynamic model of the motion of the mobile platform and a Kalman filter. The Kalman filter compares the position of the platform as predicted by the dynamic model taking input from the light sensors with the position as derived from the measurements of the optical flow sensors and computes the Kalman gain introduced in Equation 2.4 in Section 2.4 to establish an weighed mean location of the platform. An interesting alternative to the definition of the position and orientation of the mobile platform as the state variable for the Kalman filter is the use of the angles at which the light sensors are sounded as state variables in an extended Kalman filter. A similar model is proposed by Font and Battle for the localization of a mobile robot by triangulation using multiple beacons [89] and appears to improve the accuracy of the location estimate of the robot effectively.

Appendix A

List of symbols

General

subscripts right: $\_i$, $\_j$	ordinals in sequential numberings
superscripts left: ${}^{B}\_$, ${}^{C}\_$, ${}^{P}\_$	applicable coordinate system, B for Frame B (mobile platform), C for Frame C (fixed coordinate system from the lighthouse) and P for Frame P (perspective projection plane) respectively
σ^2	variance
σ	standard deviation
$\mu-$	micro [10^{-6}]
$\widetilde{x}$	least square estimate of variable x

Chapter 1

d	dimension of a part
d_d	dimension of a part according to the design
μ_d	mean value for dimension d measured amongst the parts manufactured

List of symbols continued from previous page

σ_d^2	variance of the dimension d measured amongst the parts manufactured
σ_d	standard deviation of the dimension d measured amongst the parts manufactured
Δ_{max}	allowable manufacturing tolerance
ϵ_{max}	allowable tolerance expressed as a dimensionless number: $\epsilon_{max} = \Delta_{max}/d_{max}$
d_{max}	largest dimension of a part
Δ_{mp}	abolute error in the measurement of its own position (localization)
Δ_{mg}	absolute error caused by fine adjustment of the toolhead position with mini gantry
Δ_t	Total deviation of toolhead position on mobile platform
Δ_{fb}	Total deviation of toolhead position for a full size flatbed laser cutter with a gantry that envelopes the complete sheet
ϵ_{mp}	Δ_{mp} expressed as a fraction of the maximum dimension d_{max} of the part being cut: $\epsilon_{mm} = \Delta_{mp}/d_{max}$
d_{mmin}	minimum value for the largest dimension of a part for which $\epsilon_{mm} < \epsilon_{max}$

Chapter 2

k_k	Kalman gain
σ_1, σ_2	standard deviation of location information from source 1 (sensor 1) and source 2 (sensor 2) respectively
σ_1^2, σ_2^2	variance of location information from source 1 (sensor 1) and source 2 (sensor 2) respectively

List of symbols continued from previous page

σ_f^2	variance of fused location information
μ_1, μ_2	mean value of location information from source 1 (sensor 1) and source 2 (sensor 2) respectively
μ_f	mean value of fused location information
f	sensitivity of optical flows sensor expressed in pixels per meter
Δsp	displacement measured by optical flow sensor expressed in pixels
Δs	displacement of optical flow sensor expressed in meter

Chapter 3

B_o	origin of the coordinate system of Frame B
${}^B x, {}^B y$	x and y-axis of the coordinate system of Frame B respectively
C_o	origin of coordinate system of Frame C
${}^C x, {}^C y, {}^C z$	x, y and z-axis of frame C respectively
${}^C B_o$	position of B_o in Frame C
θ_B	orientation of frame B in Frame C
n	number of optical flow sensors on mobile platform (Frame B)
o_i	optical flow sensor i, $i \in (1, 2..n)$
${}^B o_i = {}^B[o_{i,x}\ o_{i,y}]^T$	position of aperture of sensor o_i in frame B
${}^B o_i'$	position of aperture of sensor o_i in frame B at the end of a sample time interval
$\Delta {}^B o_i$	displacement of sensor o_i in a sample time interval expressed in coordinates of Frame B

List of symbols continued from previous page

θ_i	orientation of sensor o_i in Frame B
^{i}	coordinate system of optical flow sensor o_i
$^ix, ^iy$	x and y-axis of coordinate system ^{i} of optical flow sensor o_i
$\Delta B_o = {}^B[\Delta B_{o,x}\ \Delta B_{o,y}]^T$	translation of frame B in a sample time interval
$\Delta\theta_B$	rotation of frame B in sample time interval
$R_2(\theta)$	planar rotation matrix transforming the coordinates of a fixed object when the coordinate system rotates over angle θ
$\Delta^i o_i = {}^i[\Delta o_{i,x}\ \Delta o_{i,y}]^T$	displacement of sensor o_i in a sample interval as recorded by the sensor itself
$\Delta^B o_i(\Delta\theta_B)$	displacement of sensor o_i as the consequence of the rotation of Frame B over angle $\Delta\theta_B$
I_n	n-dimensional identity matrix
$\Delta\Theta_B$	union of ΔB and $\Delta\theta_B$: $[\Delta B\|\Delta\theta_B]$
${}^BA_{o_i}$	transformation matrix transforming $\Delta^B\Theta_B$ into $\Delta^{o_i}s_{o_i}$
ΔO_n	vector aggregating the displacements registered by all sensors each in their own coordinate system
A_n	matrix aggregating all matrices ${}^BA_{o_i}$. The ^{B} superscript is dropped in the notation in Section 3.2.
$R_{2n}(\theta_n)$	diagonal matrix of rotation matrices $R_2(\theta_i)$, $i \in (1, 2..n)$
A_n^+	pseudoinverse of A_n
$\Delta^i o_{p,i} = {}^i[\Delta o_{p,i,x}\ \Delta o_{p,i,y}]^T$	displacement of sensor o_i in a sample interval expressed in pixels in the image of the sensor
f_i	sensitivity of sensor o_i [pixels/meter]
d_f	distance traveled by the mobile platform to measure the sensitivity of the optical flow sensors
f_O	array of sensitivities f_i of all sensors o_i

List of symbols continued from previous page

δf_i	error in value of sensivity f_i
$\delta[\widetilde{\Theta}_B]$	error in $\widetilde{\Theta}_B$
$\kappa(\widetilde{\Theta}_B, f_O)$	relative condition number κ for the propagation of errors δf_i into an error $\delta[\Delta\widetilde{\Theta}_B]$, $i \in (1, 2..n)$
J	Jacobian matrix
w_n	largest singular value of matrix A_n
w_1	smallest singular value of matrix A_n
n_k	number swivel points on mobile platform
p_k	swivel point k, $k \in (1, 2..n_k)$
${}^B p_k = {}^B[p_{k,x}\ p_{k,y}]^T$	position of swivel point in Frame B (mobile platform)
${}^C p$	fixed anchor point
${}^C p = {}^C[p_x\ p_y]^T$	position of fixed anchor point in Frame C
α_k	turning angle of sensor o_i in swivel motion around swivel point p_k
A_{ki}	path (arc) traveled by sensor o_i in swivel motion around swivel point p_k
β	angle between path A_{ki} and the the ${}^B y$-axis at start of the swivel motion around swivel point p_k
$\overrightarrow{p_k\, o_i}$	vector from swivel point p_k to sensor o_i, representing the radius of path A_{ki}
$\overrightarrow{o_i\, o_j}$	vector connecting sensor o_i to sensor o_j
ε_{ij}	difference between expression at lhs and expression at rhs of equation, subject to minimization to equate the expressions
e_m	number of equations defining the matching swivel point constraint

List of symbols continued from previous page

m_c	matrix of distances between optical flow sensors o_i and o_j, $i \in (1, 2..n)$, $j \in (1, 2..n)$ measured in swivel motion around swivel points p_k, $k \in (1, 2..n_k)$
$a_{i\,k}$	displacement measured by optical flow sensors o_i in swivel motion around swivel point p_k expressed in coordinates of Frame B (mobile platform)
α_K	matrix aggregating all turning angles α_k of the swivel motion around swivel point p_k, $k \in (1, 2..n_k)$
$\Delta^i o_{i,k}$	displacement measured by sensor o_i in the swivel motion around point p_k

Chapter 4

n_l	number of light sensors on mobile platform (Frame B)
l_i	light sensors i on mobile platform (Frame B), $i \in (1, 2..n_l)$
ω	angular velocity at which the light sheets are swept by the HTC Vive laser lighthouse base stations: $\omega = 120\,\pi$ [rad/sec]
h	identifier of light sheet that rotates around axis parallel to the ${}^C x$-axis
v	identifier of light sheet that rotates around axis parallel to the ${}^C y$-axis
n_t	index number for time interval
ω	rotation speed of light sheet emitted by laser lighthouse [rad/sec]
t_0	start time of new sweep period of lighthouse, coincides with start of synchronization pulse

List of symbols continued from previous page

t_l	time at which light sheet strikes light sensor
θ	actual angle of light sheet "v"
ϕ	actual angle of light sheet "h"
${}^P x, {}^P y$	x and y-axis of coordinate system P respectively
$l_i = [l_{i,x}\ l_{i,y}\ l_{i,z}]^T$	position of light sensor l_i in frame B
${}^C\psi_x, {}^C\psi_y, {}^C\psi_z$	rotation angles (Euler angles) around ${}^C x, {}^C y$ and ${}^C z$ axis respectively
$R_x({}^C\psi_x), R_y({}^C\psi_y), R_z({}^C\psi_z)$	rotation matrices transforming the coordinates of a point in the C-frame for a rotation around the ${}^C_x, {}^C_y$ and ${}^C_z$ axis over angles of ${}^C\psi_x, {}^C\psi_y$ or ${}^C\psi_z$ respectively
$R_3 = R_z({}^C\psi_z)\ R_x({}^C\psi_x)\ R_y({}^C\psi_y)$	spatial (3D) rotation matrix of Frame B in Frame C
T	Translation vector of Frame B in Frame C, $T = {}^C B_o = {}^C[B_{o,x}\ B_{o,y}\ B_{o,z}]^T$
p, q, r	indexes of three light sensors selected to localize the mobile platform with the lighthouse
δl_i	error in position of sensor l_i, $i \in (1, 2..n)$
$\kappa({}^B l)$	relative condition number κ for the propagation of errors ${}^B\delta l_i$ in the location of sensor l_i in Frame B into errors ${}^C\delta l_i$ in the position of sensor l_i in Frame C, $i \in (1, 2..n)$
${}^B c_{i,k}, {}^C c_{i,k}$	circular path traveled by sensor l_i in swivel motion around swivel point p_k, in Frame B and Frame C respectively
$r_{i,k}$	radius of circle $c_{i,k}$
${}^P c_{i,k}$	perspective projection of circle $c_{i,k}$ on perspective projection plane P
${}^C uc_{i,k}$	unit circle in Frame C reconstructed from ${}^P c_{i,k}$
${}^C ucc_{i,k}$	location of center of unit circle ${}^C uc_{i,k}$ in Frame C
$p_{i,max}$	swivel point furthest away from light sensor l_i

List of symbols continued from previous page

$r_{i,max}$	radius between $p_{i,max}$ and light sensor l_i
$\rho_{i,k}$	$\rho_{i,k}$ expresses $r_{i,k}$ as a fraction of radius $r_{i,max}$: $\rho_{i,k} = r_{i,k}/r_{i,max}$
$d_{(k_1,k_2)}$	distance between swivel points p_{k_1} and p_{k_2}
${}^P c_{n_s} = {}^P[c_{n_s,x}\ c_{n_s,y}]$	point on ellipse in perspective projection of circular path of sensor in a swivel motion
$a = (a_1, .., a_6)$	ellipse coefficients
X	data set of ellipse coefficients obtained from measurements in matrix form
U_X, V_X	matrices with left-singular and right-singular vectors of matrix X respectively
Σ_X	diagonal matrix with the singular values of matrix X
$[\sigma_1 \dots \sigma_m]$	singular values of matrix X in descending order
v_m	last right singular vector of X, corresponding to the smallest singular value σ_m
n_s	ordinal in sequential numbering of lighthouse sweeps $n_s = (1, .., N_s)$
N_s	total number of lighthouse sweeps in experiment
${}^C\overline{p}_k$	mean value of measured positions for the swivel point ${}^C p_k$
$\Delta {}^C p_k(n_s)$	absolute deviation between actually measured position for the swivel point ${}^C p_k(n_s)$ and ${}^C\overline{p}_k$
σ_{p_k}	standard deviation of the measured values for the position of the swivel point ${}^C p_k$

Appendix B

Elaboration of the Jacobian $J(^{C}l,^{B}l)$

For all expressions applies that the index i refers to any triplet of three light sensors l_p, l_q and l_r of all available sensors. A triplet is the minimum of three sensors that is required to obtain a position of Frame B in Frame C. It implies that the Jacobian $\partial\, ^{C}l_i/\partial ^{B}l_i$ has 9 x 9 = 81 elements. Plugging the expressions for $^{P}l_i$ from Equation (4.1) in Equation (4.5) yields:

$$\frac{\partial\, ^{P}l_i^T}{\partial\, ^{B}l_i} = \left[\frac{\partial\, (^{C}l_{i,x}/^{C}l_{i,z})}{\partial\, ^{B}l_i} \; \frac{\partial\, (^{C}l_{i,y}/^{C}l_{i,z})}{\partial\, ^{B}l_i} \right] = \begin{bmatrix} 0 & 0 \end{bmatrix} \tag{B.1}$$

Application of the chain rule for differentiation expands the elements in vector $\frac{\partial\, ^{P}l_i^T}{\partial\, ^{B}l_i}$ as shown here for the first element $^{P}l_{i,x} = \frac{^{C}l_{i,x}}{^{C}l_{i,z}}$:

$$\frac{\partial\, (^{C}l_{i,x}/^{C}l_{i,z})}{\partial\, ^{B}l} = \left(^{C}l_{i,z} \frac{\partial\, ^{C}l_{i,x}}{\partial\, ^{B}l} - ^{C}l_{i,x} \frac{\partial\, ^{C}l_{i,z}}{\partial\, ^{B}l} \right) \frac{1}{^{C}l_{i,z}^2} \tag{B.2}$$

Since the z-coordinate $^{C}l_{i,z}$ of any sensor on the mobile frame will never be zero in the lighthouse coordinate system, Equation (B.1) can be solved by finding the roots of the numerator in Equation (B.2):

$$^{C}l_{i,z}\left(\frac{\partial\, ^{C}l_{i,x}}{\partial\, ^{B}l}\right) - ^{C}l_{i,x}\left(\frac{\partial\, ^{C}l_{i,z}}{\partial\, ^{B}l}\right) = 0 \tag{B.3}$$

The two terms of this equation can be elaborated further by plugging into Equation (B.3), the transformation of ${}^{B}l_i$ into ${}^{C}l_i$ according to Equation (4.2) :

$$ {}^{C}l_i = \left[R_3({}^{C}\psi({}^{B}l)) \;\middle|\; T({}^{C}B_o({}^{B}l)) \right] \left[{}^{B}l_i \;\middle|\; 1 \right]^T \tag{B.4} $$

For compactness of writing, the transformation matrix $\left[R_3({}^{C}\psi({}^{B}l)) \;\middle|\; T({}^{C}B_o({}^{B}l)) \right]$ will be further referred to as TR. The rows in this transformation matrix willl be identified by a subscript, hence:

$$ {}^{C}l_{i,x} = TR_1 \left[{}^{B}l_i \;\middle|\; 1 \right]^T \tag{B.5} $$

Differentiating Equation (B.5) to ${}^{B}l$ yields:

$$ \begin{aligned} \frac{\partial\, {}^{C}l_{i,x}}{\partial\, {}^{B}l} = & \left[{}^{B}l_i \;\middle|\; 1 \right] \left[\frac{\partial TR_1}{\partial {}^{C}\psi} \;\middle|\; \frac{\partial TR_1}{\partial {}^{C}B_o} \right] \begin{bmatrix} \frac{\partial {}^{C}\psi}{\partial {}^{B}l} \\ \hline \frac{\partial {}^{C}B_o}{\partial {}^{B}l} \end{bmatrix} \\ & + TR_1 \frac{d}{d\, {}^{B}l} \begin{bmatrix} {}^{B}l_i \\ \hline 1 \end{bmatrix} \end{aligned} \tag{B.6} $$

Plugging Equation (B.6) into (B.3), together with the equivalent expression for $\frac{\partial\, {}^{C}l_{i,z}}{\partial\, {}^{B}l}$, the following relationship is obtained for $\frac{\partial\, ({}^{C}l_{i,x}/{}^{C}l_{i,z})}{\partial\, {}^{B}l}$:

$$ \begin{aligned} & \frac{\partial\, ({}^{C}l_{i,x}/{}^{C}l_{i,z})}{\partial\, {}^{B}l} = \\ & \left[{}^{B}l_i \;\middle|\; 1 \right] \left({}^{C}l_{i,z} \left[\frac{\partial TR_1}{\partial {}^{C}\psi} \;\middle|\; \frac{\partial TR_1}{\partial {}^{C}B_o} \right] - {}^{C}l_{i,x} \left[\frac{\partial TR_3}{\partial {}^{C}\psi} \;\middle|\; \frac{\partial TR_3}{\partial {}^{C}B_o} \right] \right) \begin{bmatrix} \frac{\partial {}^{C}\psi}{\partial {}^{B}l} \\ \hline \frac{\partial {}^{C}B_o}{\partial {}^{B}l} \end{bmatrix} \\ & + \left({}^{C}l_{i,z}\, TR_1 - {}^{C}l_{i,x}\, TR_3 \right) \frac{d}{d\, {}^{B}l} \begin{bmatrix} {}^{B}l_i \\ \hline 1 \end{bmatrix} \end{aligned} \tag{B.7} $$

An equation similar to (B.7) can be formulated for $\frac{\partial\, ({}^{C}l_{i,y}/{}^{C}l_{i,z})}{\partial\, {}^{B}l}$ by substitution of ${}^{C}l_{i,y}$ and TR_2 for ${}^{C}l_{i,x}$ and TR_1, respectively. For the three sensors used to locate the mobile frame in the lighthouse coordinate system this provides three pairs of equations spanning a system of

linear equations of the form:

$$A \begin{bmatrix} \frac{\partial {}^{C}\psi}{\partial {}^{B}l} \\ \hline \frac{\partial {}^{C}B_o}{\partial {}^{B}l} \end{bmatrix} = b \tag{B.8}$$

with:

$$A = \begin{bmatrix} \left[{}^{B}l_1 \;\middle|\; 1 \right] \left({}^{C}l_{1,z} \left[\frac{\partial TR_1}{\partial {}^{C}\psi} \middle| \frac{\partial TR_1}{\partial {}^{C}B_o} \right] - {}^{C}l_{1,x} \left[\frac{\partial TR_3}{\partial {}^{C}\psi} \middle| \frac{\partial TR_3}{\partial {}^{C}B_o} \right] \right) \\ \left[{}^{B}l_1 \;\middle|\; 1 \right] \left({}^{C}l_{1,z} \left[\frac{\partial TR_2}{\partial {}^{C}\psi} \middle| \frac{\partial TR_2}{\partial {}^{C}B_o} \right] - {}^{C}l_{1,y} \left[\frac{\partial TR_3}{\partial {}^{C}\psi} \middle| \frac{\partial TR_3}{\partial {}^{C}B_o} \right] \right) \\ \vdots \\ \left[{}^{B}l_3 \;\middle|\; 1 \right] \left({}^{C}l_{3,z} \left[\frac{\partial TR_2}{\partial {}^{C}\psi} \middle| \frac{\partial TR_2}{\partial {}^{C}B_o} \right] - {}^{C}l_{3,y} \left[\frac{\partial TR_3}{\partial {}^{C}\psi} \middle| \frac{\partial TR_3}{\partial {}^{C}B_o} \right] \right) \end{bmatrix}$$

and:

$$b = \begin{bmatrix} \left({}^{C}l_{1,x}\, TR_3 - {}^{C}l_{1,z}\, TR_1 \right) \frac{d}{d\,{}^{B}l} \begin{bmatrix} {}^{B}l_1 \\ \hline 1 \end{bmatrix} \\ \left({}^{C}l_{1,y}\, TR_3 - {}^{C}l_{1,z}\, TR_2 \right) \frac{d}{d\,{}^{B}s} \begin{bmatrix} {}^{B}l_1 \\ \hline 1 \end{bmatrix} \\ \vdots \\ \left({}^{C}l_{3,y}\, TR_3 - {}^{C}l_{3,z}\, TR_2 \right) \frac{d}{d\,{}^{B}l} \begin{bmatrix} {}^{B}l_3 \\ \hline 1 \end{bmatrix} \end{bmatrix}$$

Using the Mathematica™ function "LinearSolve" the 27 elements of each of the Jacobian matrices $\frac{\partial {}^{C}\psi}{\partial {}^{B}l}$ and $\frac{\partial {}^{C}B_o}{\partial {}^{B}l}$ are computed by solving Equation (B.8). Plugging the resulting matrices into Equation (4.4) completes the calculation of $J({}^{C}l,{}^{B}l)$ as shown in Figure 4.4.

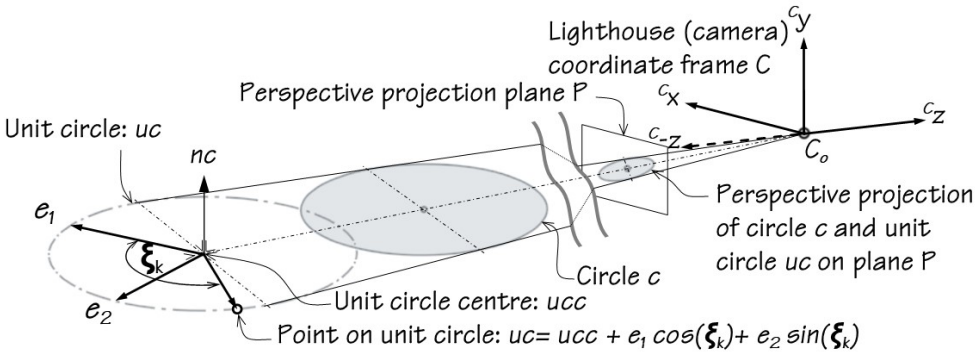

Figure C.1: *Reconstruction of the position of a unit circle from its elliptic perspective projection.*

Appendix C

Reconstruction of the position of a unit circle from its perspective projection

Camera projections of circular features have been researched extensively to develop methods to reconstruct the position and orientation of circles relative to the camera. The approach by Philip [86], illustrated in Figure C.1, starts with the parametric definition of the points uc_j on a unit circle uc: ${}^{C}uc_j = {}^{C}[uc_{j,x}\ uc_{j,y}\ uc_{j,z}]^T$ in the camera space, Frame C:

$$\begin{aligned} {}^{C}uc_j &= {}^{C}[uc_{j,x}\ uc_{j,y}\ uc_{j,z}]^T \\ &= {}^{C}ucc + {}^{C}e_1\cos(\xi_j) + {}^{C}e_2\sin(\xi_j) \\ & j = 1, 2, ..; \quad 0 \leqslant \xi_j \leqslant 2\pi \end{aligned} \tag{C.1}$$

ucc is the circle centre and ${}^{C}e_1$ and ${}^{C}e_2$ are orthonormal vectors spanning the circle plane in Frame C. As the consequence of the perspective projection, this circle will be recorded as an ellipse on the projection plane P. Points ${}^{P}c = {}^{P}[c_x\ c_y]^T$ on the same ellipse in the projection plane have the following relationship:

$$a_1\,{}^{P}c_x^2 + a_2\,{}^{P}c_x\,{}^{P}c_y + a_3\,{}^{P}c_y^2 + a_4\,{}^{P}c_x + a_5\,{}^{P}c_y + a_6 = 0 \tag{C.2}$$

Inserting the expression for perspective projection from Equation (4.1) in Equation (C.2), the ellipse can be formulated in matrix form in coordinates of the C-frame, as:

$${}^{C}c^{T}Q\,{}^{C}c = 0 \tag{C.3}$$

where:

$$Q = \frac{1}{2}\begin{bmatrix} 2a_1 & a_2 & a_4 \\ a_2 & 2a_3 & a_5 \\ a_4 & a_5 & 2a_6 \end{bmatrix}$$

Matrix Q can be scaled as appropriate, as Equation (C.3) is homogeneous. Since Q is a symmetrical matrix with real elements, its singular value decomposition (SVD) $U_Q\Sigma_Q V_Q^T$ coincides with its eigenvalue decomposition $V_Q\Lambda_Q V_Q^T$: $U_Q\Sigma_Q V_Q^T = V_Q\Lambda_Q V_Q^T$ [90]. This implies that the diagonal matrices Σ_Q and Λ_Q, with respectively the singular values and eigenvalues of Q, both in descending order, are the same: $\Sigma_Q = \Lambda_Q$. The matrix with left-singular vectors U_Q and the matrix of eigenvectors V_Q of Q are also the same for a symmetrical matrix with real elements: $U_Q = V_Q$. The left-singular vectors/eigenvectors in U_Q and V_Q are arranged in the same order as the corresponding singular values/eigenvalues in Σ_Q and Λ_Q.

By insertion of Equation (C.1) in Equation (C.3), together with the eigenvalue decomposition of $Q = V_Q\Lambda_Q V_Q^T$ (retrieved from the SVD of $Q = U_Q\Sigma_Q V_Q^T$), while substituting $\Pi = V_Q^T\,{}^{C}ucc$, $f_1 = V_Q\,{}^{C}e_1$ and $f_2 = V_Q\,{}^{C}e_2$, the following conditions can be extracted that have to be met in

order for Equation (C.3) to be true for all ξ_j:

$$f_1^T \Lambda f_1 = f_2^T \Lambda f_2 = \Pi^T \Lambda \Pi \tag{C.4}$$

$$f_1^T \Lambda f_2 = \Pi^T \Lambda f_1 = \Pi^T \Lambda f_2 = 0 \tag{C.5}$$

Conditions (C.4) and (C.5) do not fully define Π, f_1 and f_2, as the circle can be rotated around the normal vector through the circle centre ucc, without changing the circle definition. f_1 and f_2 can therefore be freely chosen in the circle plane within the constraint that they have to be orthogonal. Philip proposes to use as unit vectors [86]:

$$\begin{aligned} f_1 &= [\ \cos(\varphi) \quad 1 \quad \sin(\varphi)\ ]^T \\ f_2 &= [\ -\cos(\varphi) \quad 1 \quad -\sin(\varphi)\ ]^T \end{aligned}$$

which meets the conditions for f_1 and f_2 in Equation (C.4). The first condition of Equation (C.5) to f_1 and f_2 translates into:

$$\cos(\varphi)^2 = \frac{\lambda_2 - \lambda_3}{\lambda_1 - \lambda_3}$$

This establishes the normal vector ${}^C nc$ of the circle plane:

$${}^C nc = {}^C e_1 \times {}^C e_2 = \pm V_Q\,(f_1 \times f_2) = \pm V_Q\,[-\sin(\varphi)\ \ 0\ \ cos(\varphi)]^T \tag{C.6}$$

Π can be determined from the condition of Equation (C.5) that it is orthogonal to f_1 and f_2:

$$\Pi = c_\Pi\,(f_1 \times f_2) = c_\Pi\,\lambda_2[-\lambda_3 \sin(\varphi)\ \ 0\ \ \lambda_2 \cos(\varphi)]^T$$

Constant c_Π can be deduced from the conditions imposed by Equation (C.5). With Π resolved, the location of the circle centre in Frame C, ${}^C ucc$, can be be expressed as:

$${}^C ucc = V\,\Pi = \pm V_Q \left[-\sqrt{\frac{-\lambda_3}{\lambda_1}} \sin(\varphi)\ \ 0\ \ \sqrt{\frac{-\lambda_1}{\lambda_3}} \cos(\varphi) \right]^T \tag{C.7}$$

The sign for V_Q in Equation (C.7) is easily recognized through comparison of the calculation of ${}^{C}ucc$ with the location of the anchor point ${}^{C}c_p$ in the physical setup.

This completes the computation of the centre and orientation of the unit circle according to Philip [86].

References and notes

[1] C. Anderson, *Makers: The New Industrial Revolution*. Random House, 2012.

[2] J. J. Dong, *Rapid Response Manufacturing: Contemporary methodologies, tools and technologies*. Springer Science & Business Media, 1997.

[3] Y. Koren, *The global manufacturing revolution: product-process-business integration and reconfigurable systems*. John Wiley & Sons, 2010, vol. 80.

[4] P. Markillie, *A third industrial revolution: Special report manufacturing and innovation*. Economist Newspaper, 2012.

[5] M. Shneier and R. Bostelman, "Literature review of mobile robots for manufacturing," NIST, Tech. Rep., May 2015.

[6] B. Goodno and J. Gere, *Mechanics of Materials, SI Edition*. Boston, MA: Cengage Learning, 2018.

[7] "The international vocabulary of metrology—basic and general concepts and associated terms (vim), 3rd edn." BIPM, IEC, IFCC, ILAC, IUPAC, IUPAP, ISO, OIML (2012), Tech. Rep., 2012.

[8] American Bureau of Shipping, *Shipbuilding and repair quality standard for hull structures during construction*. American Bureau of Shipping, New York, 2007.

[9] A. Paijens, L. Huang, and A. Al-Jumaily, "Implementation and calibration of an odometry system for mobile robots, based on optical computer mouse sensors," *Sensors and Actuators A: Physical*, vol. 301, p. 111731, jan 2020.

[10] D. K. Ballast, *Handbook of construction tolerances*. John Wiley & Sons, 2007.

[11] D. Whitbread, *The Design Manual*. UNSW Press, 2009.

[12] J. Borenstein, H. R. Everett, L. Feng, and D. Wehe, "Mobile robot positioning: Sensors and techniques," *Journal of Robotic Systems*, vol. 14, no. 4, pp. 231–249, apr 1997.

[13] K. S. Chong and L. Kleeman, "Accurate odometry and error modelling for a mobile robot," in *IEEE International Conference on Robotics and Automation*, vol. 4. IEEE, 1997, pp. 2783–2788.

[14] J. Borenstein, H. Everett, L. Feng *et al.*, "Where am I? sensors and methods for mobile robot positioning," *University of Michigan*, vol. 119, no. 120, p. 27, 1996.

[15] R. Faragher, "Understanding the basis of the kalman filter via a simple and intuitive derivation," *IEEE Signal Processing Magazine*, vol. 29, no. 5, pp. 128–132, sep 2012.

[16] E. Eitel, "Basics of rotary encoders: Overview and new technologies," *Machine Design Magazine*, vol. 7, 2014.

[17] J. Zhou and L. Huang, "Experimental study on sensor fusion to improve real time indoor localization of a mobile robot," in *2011 IEEE 5th International Conference on Robotics, Automation and Mechatronics (RAM)*, 2011.

[18] A. Martinelli and R. Siegwart, "Estimating the odometry error of a mobile robot during navigation," in *Proceedings of European Conference on Mobile Robots (ECMR'03) 2003 Sep.* ZTUREK Research-Scientific Inst, 2003.

[19] J. Borenstein and L. Feng, "UMBmark: a benchmark test for measuring odometry errors in mobile robots," in *Mobile Robots X*, W. J. Wolfe and C. H. Kenyon, Eds. SPIE, dec 1995.

[20] J. Borenstein and L. Feng, "Correction of systematic odometry errors in mobile robots," in *Proceedings 1995 IEEE/RSJ International Conference on Intelligent Robots and Systems. Human Robot Interaction and Cooperative Robots*. IEEE Comput. Soc. Press.

[21] T. Ng, "The optical mouse as a two-dimensional displacement sensor," *Sensors and Actuators A: Physical*, vol. 107, no. 1, pp. 21–25, oct 2003.

[22] M. R. Andrea Bonarini, Matteo Matteucci, "A kinematic-independent dead-reckoning sensor for indoor mobile robotics," *Proceedings of 2004 IEEEIRSJ International Conference on Intelligent Robots and Systems September 28 - October 2,2004, Sendai, Japan*, 2004.

[23] D. Sekimori and F. Miyazaki, "Precise dead-reckoning for mobile robots using multiple optical mouse sensors," in *Informatics in Control, Automation and Robotics II*. Springer, 2007, pp. 145–151.

[24] M. Tresanchez, T. Pallejà, M. Teixidó, and J. Palacín, "The optical mouse sensor as an incremental rotary encoder," *Sensors and Actuators A: Physical*, vol. 155, no. 1, pp. 73–81, oct 2009.

[25] J. Cooney, W. Xu, and G. Bright, "Visual dead-reckoning for motion control of a mecanum-wheeled mobile robot," *Mechatronics*, vol. 14, no. 6, pp. 623–637, jul 2004.

[26] J. D. Jackson, D. W. Callahan, and J. Marstrander, "A rationale for the use of optical mice chips for economic and accurate vehicle tracking," in *2007 IEEE International Conference on Automation Science and Engineering*. IEEE, sep 2007.

[27] D. H. Yi, T. J. Lee, and D. I. Cho, "A new localization system for indoor service robots in low luminance and slippery indoor environment using afocal optical flow sensor based sensor fusion," *Sensors*, vol. 18, no. 2, p. 171, jan 2018.

[28] T. Ng and K. Ang, "The optical mouse for vibratory motion sensing," *Sensors and Actuators A: Physical*, vol. 116, no. 2, pp. 205–208, oct 2004.

[29] U. Minoni and A. Signorini, "Low-cost optical motion sensors: An experimental characterization," *Sensors and Actuators A: Physical*, vol. 128, no. 2, pp. 402–408, apr 2006.

[30] J. Palacin, I. Valgañon, and R. Pernia, "The optical mouse for indoor mobile robot odometry measurement," *Sensors and Actuators A: Physical*, vol. 126, no. 1, pp. 141–147, jan 2006.

[31] S. Kim and H. Kim, "Optimal optical mouse array for accurate mobile robot velocity estimation," in *2013 10th IEEE International Conference on Networking , Sensing and Control(ICNSC)*. IEEE, 2013, pp. 83–88.

[32] P. L. Wu, S. L. Jeng, and W. H. Chieng, "Least squares approach to odometry based on multiple optical mouse sensors," in *2010 5th IEEE Conference on Industrial Electronics and Applications*. IEEE, jun 2010.

[33] D. H. Yi, T. J. Lee, and D. I. Cho, "Afocal optical flow sensor for reducing vertical height sensitivity in indoor robot localization and navigation," *Sensors*, vol. 15, no. 5, pp. 11 208–11 221, may 2015.

[34] D. Hyun, H. S. Yang, H. R. Park, and H.-S. Park, "Differential optical navigation sensor for mobile robots," *Sensors and Actuators A: Physical*, vol. 156, no. 2, pp. 296–301, dec 2009.

[35] D. Sekimori and F. Miyazaki, "Self-localization for indoor mobile robots based on optical mouse sensor values and simple global camera information," in *2005 IEEE International Conference on Robotics and Biomimetics-ROBIO*. IEEE, 2005, pp. 605–610.

[36] S. Bell, "High-precision robot odometry using an array of optical mice," in *2011 IEEE Reg. 5 Student Paper Contest*. Oklahoma Christian University, 24 March 2011.

[37] J. S. Hu, Y. J. Chang, and Y. L. Hsu, "Calibration and on-line data selection of multiple optical flow sensors for odometry applications," *Sensors and Actuators A: Physical*, vol. 149, no. 1, pp. 74–80, jan 2009.

[38] S. Kim and H. Kim, "Systematic robustness analysis of least squares mobile robot velocity estimation using a regular polygonal optical mouse array," *Asian Journal of Control*, vol. 14, no. 2, pp. 348–358, March 2012.

[39] M. Cimino and P. R. Pagilla, "Optimal location of mouse sensors on mobile robots for position sensing," *Automatica*, vol. 47, no. 10, pp. 2267–2272, oct 2011.

[40] S. Kim, "Isotropic optical mouse placement for mobile robot velocity estimation," in *IEEE/ASME International Conference on Advanced Intelligent Mechatronics (AIM)*. IEEE, July 9-12 2013.

[41] S. Kim and H. Kim, "Optimal placement of optical mice for accurate mobile robot velocity estimation," *International Journal of Control, Automation, and Systems (2014) 12(4):861-869*, vol. 12, no. 4, pp. 861–869, July 2014.

[42] H. Liu, H. Darabi, P. Banerjee, and J. Liu, "Survey of wireless indoor positioning techniques and systems," *IEEE Transactions on Systems, Man, and Cybernetics, Part C (Applications and Reviews)*, vol. 37, no. 6, pp. 1067–1080, nov 2007.

[43] R. Mautz, *Indoor Positioning Technologies*. Habilitation thesis, ETH Zurich, Department of Civil, Environmental and Geomatic Engineering, Institute of Geodesy and Photogrammetry Zurich, 2012.

[44] L. Mainetti, L. Patrono, and I. Sergi, "A survey on indoor positioning systems," in *2014 22nd international conference on software, telecommunications and computer networks (SoftCOM)*. IEEE, 2014, pp. 111–120.

[45] F. Gustafsson and F. Gunnarsson, "Mobile positioning using wireless networks: possibilities and fundamental limitations based on available wireless network measurements," *IEEE Signal processing magazine*, vol. 22, no. 4, pp. 41–53, 2005.

[46] C. Peng, G. Shen, Y. Zhang, Y. Li, and K. Tan, "Beepbeep: a high accuracy acoustic ranging system using cots mobile devices," in *Proceedings of the 5th international conference on Embedded networked sensor systems*. ACM, 2007, pp. 1–14.

[47] H. W. Wehn and P. R. Belanger, "Ultrasound-based robot position estimation," *IEEE transactions on Robotics and Automation*, vol. 13, no. 5, pp. 682–692, 1997.

[48] R. Horaud, B. Conio, O. Leboulleux, and B. Lacolle, "An analytic solution for the perspective 4-point problem," *Computer Vision, Graphics, and Image Processing*, vol. 47, no. 1, pp. 33–44, 1989.

[49] D. DeMenthon and L. S. Davis, "Exact and approximate solutions of the perspective-three-point problem," *IEEE Transactions on Pattern Analysis & Machine Intelligence*, no. 11, pp. 1100–1105, 1992.

[50] D. Eberli, D. Scaramuzza, S. Weiss, and R. Siegwart, "Vision based position control for MAVs using one single circular landmark," in *Unmanned Aerial Vehicles*. Springer Netherlands, 2010, pp. 495–512.

[51] J. E. D. Williams, *From sails to satellites : the origin and development of navigational science*. Oxford University Press, 1992.

[52] B. Sorensen, M. Donath, G.-B. Yang, and R. Starr, "The minnesota scanner: a prototype sensor for three-dimensional tracking of moving body segments," *IEEE Transactions on Robotics and Automation*, vol. 5, no. 4, pp. 499–509, 1989.

[53] E. Hughes, A. Forbes, W. Sun, P. G. Maropoulos, J. E. Muelaner, J. Jamshidi, and Z. Wang, "iGPS capability study," National Physical Laboratory, 2010.

[54] M. M. Simi, "A real-time positioning system for mobile robots based on laser triangulation," Master's thesis, Northwestern University, 2000.

[55] S. Linga, "A novel positioning system for accurate tracking in indoor environments," Master's thesis, Massachusetts Institute of Technology, 2007.

[56] G. Alenya, J. Escoda, A. Martinez, and C. Torras, "Using laser and vision to locate a robot in an industrial environment: A practical experience," in *Proceedings of the 2005 IEEE International Conference on Robotics and Automation*. IEEE.

[57] W. Gao, S. Kim, H. Bosse, H. Haitjema, Y. Chen, X. Lu, W. Knapp, A. Weckenmann, W. Estler, and H. Kunzmann, "Measurement technologies for precision positioning," *CIRP Annals-Manufacturing Technology*, vol. 64, no. 2, pp. 773–796, 2015.

[58] W. Murphy and W. Hereman, "Determination of a position in three dimensions using trilateration and approximate distances," Department of Mathematical and Computer Sciences, Colorado School of Mines, Golden, CO 808401-1887, USA, Tech. Rep. MSC-95-07, Oct 1995.

[59] J. A. B. Josep M. Font-Llagunes, "Consistent triangulation for mobile robot localization using discontinuous angular measurements," *Robotics and Autonomous Systems Volume 57, Issue 9, 30 September 2009, Pages 931-942*, 2009.

[60] J. Font-Llagunes and J. Batlle, "Mobile robot localization. revisiting the triangulation methods," *Proc. IFAC Int. Symp. Robot Control, vol. 8, Santa Cristina Convent, Univ. Bologna, Bologna, Italy, Sep. 2006, pp. 340-345.*, 2006.

[61] M. Betke and L. Gurvits, "Mobile robot localization using landmarks," *IEEE transactions on robotics and automation*, vol. 13, no. 2, pp. 251–263, 1997.

[62] T. Tsumura, N. Fujiwara, T. Shirakawa, and M. Okazaki, "A system for measuring current position and/or heading of vehicles," *Bulletin of JSME*, vol. 25, no. 203, pp. 821–826, 1982.

[63] T. Tsumura, N. Fujiwara, M. Hashimoto, and T. Tang, "Low-cost localization device for autonomous robots has portable computer that outputs localization and orientation data after making final calculation," International patent JP2008525811, 1984.

[64] T. Tsumura, N. Fujiwara, M. Hashimoto, T. Tang, "A new method of vehicle position and heading measurment by use of a laser-beacon," *Journal of the Robotics Society of Japan*, vol. 2, no. 6, pp. 557–565, 1984.

[65] T. Tsumura, "Survey of automated guided vehicle in a japanese factory," in *Robotics and Automation. Proceedings. 1986 IEEE International Conference on*, vol. 3. IEEE, 1986, pp. 1329–1334.

[66] C. J. Romanik Jr, "Optical system for accurate monitoring of the position and orientation of an object," US Patent 5,729,475, 1999.

[67] S. Hernández, J. Torres, C. Morales, and L. Acosta, "A new low cost system for autonomous robot heading and position localization in a closed area," *Autonomous Robots*, vol. 15, no. 2, pp. 99–110, 2003.

[68] C. J. Cohen and F. V. Koss, "Comprehensive study of three-object triangulation," in *Mobile Robots VII*, vol. 1831. International Society for Optics and Photonics, pp. 95–106.

[69] M. Borges, A. Symington, B. Coltin, T. Smith, and R. Ventura, "HTC vive: Analysis and accuracy improvement," in *2018 IEEE/RSJ International Conference on Intelligent Robots and Systems (IROS)*. IEEE, oct 2018.

[70] W. Jansen, D. Laurijssen, W. Daems, and J. Steckel, "Automatic calibration of a six-degrees-of-freedom pose estimation system," *IEEE Sensors Journal*, vol. 19, pp. 8824–8831, 2019.

[71] D. C. Niehorster, L. Li, and M. Lappe, "The accuracy and precision of position and orientation tracking in the htc vive virtual reality system for scientific research," *i-Perception*, vol. 8, no. 3, p. 23, 2017.

[72] E. Luckett, "A quantitative evaluation of the htc vive for virtual reality research," Master's thesis, The University of Mississippi, 2018.

[73] M. Greiff, A. Robertsson, and K. Berntorp, "Performance bounds in positioning with the vive lighthouse system," in *2019 22th International Conference on Information Fusion (FUSION)*, 2019, pp. 1–8.

[74] K. Sletten, "Automated testing of industrial robots using htc vive for motion tracking," Master's thesis, University of Stavanger, Norway, 2017.

[75] B. Kilberg, F. Campos, F. Maksimovic, T. Watteyne, and K. Pister, "Accurate 3d lighthouse localization of a low-power crystal-free single-chip mote," *Journal of Microelectromechanical Systems*, vol. 29, pp. 818–824, 2020.

[76] P. Bauer, W. Lienhart, and S. Jost, "Accuracy investigation of the pose determination of a VR system," *Sensors*, vol. 21, no. 5, p. 1622.

[77] V. Holzwarth, J. Gisler, C. Hirt, and A. Kunz, "Comparing the accuracy and precision of steamvr tracking 2.0 and oculus quest 2 in a room scale setup," in *ICVARS 2021*, Melbourne, VIC, Australia, 2021.

[78] S. van der Veen, M. Bordeleau, P. Pidcoe, C. France, and J. Thomas, "Agreement analysis between vive and vicon systems to monitor lumbar postural changes," *Sensors*, vol. 19, no. 17, p. 3632, 2019.

[79] A. C. Rencher and W. F. Christensen, "Methods of multivariate analysis," *Wiley*, 2012.

[80] L. Trefethen and D. Bau, *Numerical Linear Algebra*, ser. Other Titles in Applied Mathematics. Society for Industrial and Applied Mathematics (SIAM), 1997.

[81] S. Islam, B. Ionescu, C. Gadea, and D. Ionescu, "Indoor positional tracking using dual-axis rotating laser sweeps," in *2016 IEEE International Instrumentation and Measurement Technology Conference Proceedings*, IEEE. IEEE, may 2016, pp. 1–6.

[82] R. Klette, *Concise Computer Vision*. Springer London.

[83] A. Ranganathan, "The Levenberg-Marquardt Algorithm, Lecture notes," Georgia Institute of Technology, Georgia, USA, June 2004.

[84] A. Paijens, L. Huang, and A. Al-Jumaily, "Analysis of sensor arrangements to localize mobile robots with one laser lighthouse," in *2017 24th International Conference on Mechatronics and Machine Vision in Practice (M2VIP)*. IEEE, nov 2017.

[85] D. Salomon, *The Computer Graphics Manual*, ser. Texts in Computer Science. Springer London, 2011.

[86] J. Philip, *An algorithm for determining the position of a circle in 3D from its perspective 2D projection*. Department of Mathematics, Royal Institute of Technology, 1997.

[87] A. Fitzgibbon, M. Pilu, and R. Fisher, "Direct least square fitting of ellipses," *IEEE Transactions on Pattern Analysis and Machine Intelligence*, vol. 21, no. 5, pp. 476–480, may 1999.

[88] W. Gander, "The Singular Value Decomposition, Lecture Notes," ETH Zurich, December 2008.

[89] J. M. Font and J. A. Batlle, "Dynamic triangulation for mobile robot localization using an angular state kalman filter," in *Proc. of the 2nd European Conference on Mobile Robots*, 2005, pp. 20–25.

[90] G. Strang, *Introduction to Linear Algebra*. Cambridge University Press, 2016.

Notes

[1] "Optical mouse sensors", PixArt Imaging Inc.,https://www.pixart.com/products-comparison/7/Optical_Mouse_Sensor

[2]"HTC Vive lighthouse chaperone tracking system explained" - YouTube, https://www.youtube.com/watch?v=J54dotTt7k0

[3]"HTC reveals virtual reality headset with Valve at MWC", https://www.bbc.com/news/technology-31664948

[4] HTC VIVE user guide (2017)

[5]Oliver Kreylos, "Lighthouse tracking examined", http://doc-ok.org/?p=1478

[6] Metris, "iGPS Data Sheet v1.3. 2007", http://www.nucleon.com.br/upload/26.pdf

[7] Pixart Imaging Inc. Taiwan, "ADNS 9800 Data Sheet"

[8]telos Systementwicklung GmbH, "I^2C – What's That?", https://www.i2c-bus.org/addressing/general-call-address/

[9]A. Yates, Nairol, "LighthouseRedox - lighthouse reverse-engineered documentation", https://github.com/nairol/LighthouseRedox

[10]BPW34 BPW34S Silicon PIN Photodiode Data sheet, https://www.vishay.com/docs/81521/bpw34.pdf

[11]TS3633-CM1 Light to Digital Converter. Castellated Module Product Datasheet, rev. B

[12]Terasic Technologies, "DE0-Nano User Manual", http://DE0-Nano.terasic.com